Uncovering the Genetic and Functional Diversity of Midbrain Dopamine Neurons

By

Daniel J Kramer

A thesis submitted in partial satisfaction of the

Requirements for the degree of

Doctor of Philosophy

in

Molecular and Cell Biology

in the

Graduate Division

of the

University of California, Berkeley

Committee in Charge:

Professor Helen Bateup, Chair
Professor John Ngai
Professor Stephan Lammel
Professor Mark D'Esposito

Summer 2020

Abstract

Uncovering the Genetic and Functional Diversity of Midbrain Dopamine Neurons

by

Daniel Joseph Kramer

Doctor of Philosophy in Molecular and Cell Biology

University of California, Berkeley

Professor Helen Bateup, Chair

Midbrain dopamine (DA) neurons in the substantia nigra pars compacta (SNc) and ventral tegmental area (VTA) project throughout the brain to modulate a diverse set of behaviors and brain states. Although their effects are widespread, they represent a very small fraction of neurons. Dopamine neurons rely on their diverse inputs, outputs, physiology, and gene expression in order to maintain their broad behavioral influence. To better understand the different roles dopaminergic projections play in the brain, the circuits need to be studied in isolation as adjacent neurons and circuits often mediate distinct behaviors. Because of their close anatomical proximity, novel tools and methods must be devised in order to precisely dissect dopaminergic sub-circuits. New tool development will depend on identifying the underlying genetic signature of dopaminergic subpopulations to allow consistent, reproducible labeling of distinct populations. Gene expression analysis will also reveal unique genes expressed in DA neurons that could lend functional importance to already established dopaminergic circuits.

Here we used single-cell RNA-sequencing to determine the unique gene expression signature of DA neurons and identify genes that define distinct dopaminergic subpopulations. We used retrograde tracing, electrophysiology, and disease models to show that genetically defined populations are functionally distinct with defined projections, unique physiological characteristics, and selective sparing in a Parkinson's disease model. Through this work, we defined two circuits that arise from populations in the ventromedial VTA marked by their expression of *Neurod6* and *Grp* and determined that single genes are not sufficient to label dopaminergic subtypes. Because of this, we developed a Flp-recombinase dopaminergic reporter mouse (DAT-Flp). Using this mouse, we were able to use intersectional genetic tools to selectively label Neurod6-DA neurons to enable future investigations into the role that these neurons play in dopaminergic functions.

Acknowledgements

To Helen – My full gratitude can't be contained in such a short acknowledgement. Suffice to say, I could not have hoped for a better boss, mentor, sounding board, or coach. You were constantly available with a wealth of knowledge and experience. I always felt you were in my corner, championing my cause and I could never thank you enough for the help and support.

To my family: Mom - Thank you for making me feel like everything I did was special. From publishing a paper to scrambling eggs, you were never short of enthusiasm and encouragement. You were always all ears for my work and that was so refreshing. Dad, thank you for asking so many insightful questions. Even without a neuroscience background, you consistently pushed the limits of what I knew. Liz, thank you for making me feel like scientist. I could always count on you to provide a stable ground to stand on and making me feel like what I did had an impact on the world. To all of you, I never felt anything but unconditional love and a sense pride. I love with all of my heart.

To my lab – John, you became such a close friend. I could depend on you to listen to my whining and eat wings. I'll miss you a ton now that you'll be in NY. Polina, you deserve at least half of this degree. In the literal sense, I have honestly no clue what I would have done without your guidance and help. You will forever be 'my postdoc'. Erin, you have been wonderful to work with and I can't wait to see how far you'll go. Villy, Katie, Kamran, and Jillian, I have seen you all more than my family for the past 5 years that you have become a second family. I will always feel a deep respect and love for you all. Thank you for sitting through my lab meetings and providing true insight and ideas. I'm looking forward to keeping close tabs on all of your successes.

To Kelsey – Thank you for being my biggest fan and a constant source of stability. You always give me the benefit of the doubt and that has been instrumental in keeping my head above water. I'm excited to join you on your own Ph.D. journey so I can begin to pay you back for your unwavering support. I love you so much.

To Colin – You may have been far away, but you understood what I was going through and have the highest emotional intelligence of anyone I know. Every day I miss living close to you. Your perspective on the brain and the human condition is unparalleled.

To Max – I brag about you whenever I get the opportunity. You have been an emotional support for the decade we've known each other. Already looking forward to our next out 'n back.

To David – I'm glad to have found a brother across the country. I admire and look up to

you. You are just a great person through and through. I'm glad our friendship will live on through Follies until the end of time.

To Franzi – I've never met someone that was so eager to be in your corner. You may be the most loyal person I've met. I will pick blackberries and make jam or gelato in your honor whenever I can.

To Beach House – Amy, Janice, and Orestes, how fortunate I was to have lived with you for 2 years. Words can do justice for how fondly I look back to our time together. It felt so cozy waking up knowing you would be there in the morning. I feel deeply connected to each of you, with a unique kinship that will never go away. You allowed me to let my guard down and became a real family. I love you all. Beach House for life means for life.

To Movie Night – Franzi, Tim, Eva, George, Lydia, and John, the world that we created just through hanging out every couple of weeks and watching movies provided such a perfect space to air grievances, be heard, take a deep breath, and relax. I will never watch movies the same way again. I will miss you all as we each go our separate ways. I couldn't have done it without you all.

To BOSS – What a wonderful thing we pulled out of thin air. Eva, your unbridled enthusiasm for the work that we did, and your ability to guide a group of rowdy children to be excited by science is something I will always admire. I'm sad I may never tag-team a classroom with you again. You have always been a beacon of happiness and hope. Dom, it was fun to learn how truly different the world works outside of the university system. Beyond BOSS, you have been a rock of a friend, always there to listen and provide perspective. I'm so happy you'll be staying and I'll be able to keep seeing you.

To BCBA – To everyone I worked with, you provided an outlet and a vision of what the future would look like. These projects forged such unique and strong relationships with likeminded people. I could not have gotten through this without you all. Justin, playing ping-pong with you while fantasizing about our futures is something I look back on with a huge smile. Amanda, brainstorming and editing with you until the wee hours, surprisingly, is something I wouldn't change for the world.

I fear COVID-19 will color our memories of graduate school. The same way I look back to my undergraduate days with rose colored glasses, glossing over the 25 minute walk to campus in -10˚C I had to do every day. Hopefully we can ignore the final months when things fell off the truck-bed and caused a chaotic pileup. It was truly a wonderful ride and I will miss it dearly.

Table of Contents

Chapter 1: Untangling the diversity of midbrain dopamine neurons

Daniel Joseph Kramer

Department of Molecular and Cell Biology
University of California Berkeley

To many neuroscientists one pyramidal cell is just like another. I, on the contrary, believe that it is important to distinguish the many types of pyramidal cells.
        F. Crick 1999[1]

The foundational concepts of neuronal heterogeneity
Even at their most nascent, the earliest foundational principals of the neuronal brain began to underscore how mysterious and heterogeneous this organ was. The first hypotheses by Wilhem von Waldeyer and Wilhem His Sr., which were expanded upon with the elegant hand of Santiago Ramon y Cajal[2], outlined the neuron doctrine, "the nervous system is made up of innumerable nerve units (neurons) which are anatomically and genetically independent of each other[3]." The beauty of the word, that even at its very inception, contained in it the idea that each neuron was an independent and unique entity. Cajal's careful drawings succeeded in bringing to life the unique characteristics of neurons and postulated the direction of information flow[2]. Not only did this make clear that each neuron had a different architectural make-up, but because of their polarity it made sense then that any given neuron will receive inputs from specific subsets of neurons and send processes to distinct anatomical nuclei. Even Golgi, who believed the brain was a reticular network, defined at least two populations: spiny and aspiny cells[3]. It is in these drawings and ideas made over 100 years ago that we see the birth of neuronal heterogeneity principles.

Decades after the basic tenants of the neuron doctrine transformed neuroscience, the expansion of neuronal heterogeneity began. The 'one neuron, one transmitter' hypothesis, while only recently shown to not be universal, underscored that neurons are specialized with different neurotransmitters that have different downstream effects[4-6]. It was around this time when Dale and Eccles were formulating their theories that early staining methods began to illustrate these ideas. As an example, new methods using formaldehyde fixation allowed for the staining of dopamine (DA) neurons in the rat brain stem[7] showing, one, that DA did in fact exist in the mammalian central nervous system and two, that there are specialized neurons that release DA. With the further advent of labeling techniques from *in situ* hybridization and immunohistochemistry[8,9], neuroscientists were able to start labeling neurons throughout the brain based on their neurotransmitter identify. While assumed previously, it was now definitive that there was both local (within brain regions) and global (across brain region) segregation of neurons based on their type.

Even with widespread agreement that the brain holds an array of varying cell types, the question could arise - why the focus on neuronal heterogeneity? If one wants to understand the brain completely, which at its core is the fundamental goal of any basic neuroscientist, there needs to be a neuronal parts list. We can't completely know a machine without knowing how it is built. First, a parts list will provide essential access to cells of interest so tools can be developed. Second, access to defined cell types will generate more reproducibility. Investigators can consistently target their cell populations of interest, and the field can unambiguously refer to them. Third, given that numerous

neuronal disorders affect specific neuronal populations or manifest more severely in some populations, having defined groups can help provide information about which neurons need intervention. In addition, their definition can also provide clues or a platform to explore why they are more at risk than their neighbors.

Now, two decades later, it would appear Francis Crick's call to action is being put to the test and the field is making major strides exploring neuronal heterogeneity[1]. There is a vast array of different neuronal types described in the brain with many experiments underway to parse of the genetic signatures that define them. Countless seemingly homogenous neuronal populations have been genetically dissected using recent advances in molecular biology. Single-cell RNA sequencing (scRNAseq) has allowed researchers to separate any neuronal population and find distinct genetic subclasses of neurons throughout the brain.

Single-cell RNA sequencing and the height of neuronal heterogeneity exploration

All neurons in the central nervous system can likely point to a single nerve cell evolved eons before as their origin[10,11]. From those original neurons and circuits, there has been built an elegantly organized structure in the mammalian brain with similar yet specialized cells. There are many traits one could use to segregate and define the different classes of neurons that have developed; inputs, outputs, physiology, morphology, neurotransmitter release, and response to disease. At the heart of each of these characteristics, however, lies the neurons' underlying gene expression. The set of genes that is expressed by a given neuron from birth through maturity can define all of these baseline, fundamental features and the functional differences between groups. As an example, ephrins and their receptors, among many other gene families, help define axon guidance and projection targets[12]. Expression of these guidance genes forms a foundation for circuit building. In addition to this, a neuron's innate physiological properties are defined by the makeup of their ion channels which in turn is defined by the genes they express. These properties have been used, in concert with morphology, to start defining pyramidal and interneurons before gene expression analysis became ubiqitous[13,14]. Furthermore, often the neurotransmitter identify of a neuron is easily defined by the machinery expressed by that neuron for synthesis, packaging, and uptake of a given neurotransmitter. Thus, defining a neuronal subpopulation based on its fundamental gene expression is a valid and effective way to cluster groups with functional relevance and similarity[15-17].

Recognizing that a neuron's gene expression could define its properties was a simple first step. The difficulty comes in executing on that goal. Early neuronal sequencing studies used micro-arrays which relied on high quantities of RNA. This meant that the majority of work used heterogeneous populations that were pooled and treated as homogenous groups[16]. Single-cell expression analysis became more vital as it was revealed neurons were heterogeneous and difficult to tease apart. This started in earnest in 1992 when RNA was isolated from single neurons through patch pipettes, amplified, and blotted for specific genes using a northern blot[18]. However, because

northern blots weren't sensitive enough for some genes, *in situ* hybridization didn't allow for multiplexing genes, and even following amplification there wasn't sufficient mRNA[19,20], these weren't sufficient techniques to truly uncover the diversity of neurons. The following years, however, major strides were made to improve the methods behind amplification[19,21-23]. By the late 2000s, cDNA amplification and micro-arrays became powerful enough to allow for in depth sequencing of single neurons[24,25]. Using these techniques, scientists were able to uncover significant heterogeneity in dorsal root ganglion cells (DRGs), Hippocampal C1 neurons, and neural progenitors[22,24-26]. Following this, there was a drastic improvement of sequencing methods and increases in web resources which led to a rush to start defining the gene expression of neurons throughout the brain[27-29]. Together, these provided a foundation for an explosion in neuronal single-cell studies.

By the beginning of the 2010s, single cell sequencing techniques started an era of exponential growth[23]. What began at laser-dissection and micromanipulations was now advanced microfluidic devices and next-generation sequencing[23,30]. The most popular methods that capitalized on this wave was the commercial Fluidigm C1 system and DropSeq[30]. There are some key caveats to consider that come with these methods that rest on the dissociation of neural tissue that is required for both techniques. During processing, there is substantial cell damage, the potential exclusion of sensitive populations, and changes in RNA expression or processing due to stress or cell state changes. In addition to the biological changes, scRNAseq analysis can be confounded by low expressed genes dropping out, over indexing highly expressed genes, and, perhaps most importantly, an imperfect correlation between gene expression and protein levels[31-33]. Even with these caveats, given the relative simplicity with which these populations can be verified post-hoc, it is still the definitive way to genetically define large numbers of neurons quickly and accurately.

Improved scRNAseq methods vastly streamlined the process and increased throughput which has facilitated its use for many labs. To date, there have been numerous single-cell studies on almost every neuronal population, and several large-scale undertakings to identify nearly every neuron throughout the mouse brain[34-36] simultaneously. However, we now stand in an important transitionary period. While we could continue to break down neuronal populations further and further, we don't have a complete grasp on what it means to be a subpopulation. More importantly, it is unclear what, if any, functional relevance being a distinct genetic class ascribes. It is now up to researchers to determine what roles these novel cell populations play, and whether they are functionally relevant or just artifacts of too much digging.

What it means to be a neuronal subpopulation

> *There is, however, a general sense that understanding all this information*
> *has lagged far behind its accumulation…*
>   Sydney Brenner[37]

Even with nearly 100 billion neurons in the human brain[38], it is almost certain every

neuron is truly unique. Between adjacent neurons, with their variability between gene expression, morphology, and circuitry, it is unlikely there are any two identical neurons. With this understanding, we know it would be impossible to find functional relevance at the scale of billions of neuronal subgroups. While acknowledging biology doesn't always parse itself in convenient ways, there are clear families of neurons that likely represent a compromise at which we can draw a line at a subpopulation[39]. Earlier successful attempts at defining neuronal populations used combinations of morphology, physiology, and anatomy[40,41]. As single-cell gene expression becomes more high-throughput, however, we can start to use multiple characteristics to find groups.

At its most basic, a subset of neurons could be defined as a group of cells that perform the same function within the same circuit[13]. However, neurons can perform multiple functions, or could perform the same function *sometimes* depending on extrinsic factors. As an example, two neurons in the same circuit could, when activated, trigger movement. However, one neuron could possess an opioid receptor which will alter its activation depending on the status of opioid release at that time. These two neurons fall into the same circuit, have the same function, but respond differently to some factors. For single-cell sequencing, at its foundation, a neuronal subpopulation is defined simply as a cluster of neurons that share a similar genetic signature as defined by the specific algorithm that is being used[32,42]. While methods are getting more robust, there are still some pitfalls with these analyses. First, depending on the parameters used, different numbers of subpopulations can be 'discovered'. Clustering depends inherently on the assumption that there are biologically discrete neuronal populations. Avoiding the creation of the incorrect amount of subtypes necessitates multiple labs attempting to cluster to find coherence[33]. Secondly, the varying- and high-dimensionality of scRNAseq data can sometimes confound what clustering methods are most appropriate for driving relevant results. Sometimes this can be avoided by ascribing *a priori* knowledge to aide clustering analyses, but this removes unbiased clustering and can lead to circular logic[43]. Most importantly, at its foundation, scRNAseq follows the assumption that classifying by gene expression positively defines a population. While shown to be the most robust method we have, it still needs substantial confirmation. **Thus, the most stringent definition for a neuronal population will depend on both underlying gene expression and confirmation of functional relevance**. Single-cell sequencing can provide a shared, stable, and molecular "ground state" that helps define its functional capacities[42] which can then be followed up to determine if these clusters define a group of cells that perform a similar function[13].

There has been considerable work in the past few years that elegantly combined sequencing data with functional follow up. A recent single-cell study in serotonin neurons in the raphe nuclei revealed 11 genetically defined populations broadly bucketed into two groups based on cell bodies being present in the dorsal or medial raphe[44]. When the projections of these two populations were explored, it was clear that they had distinct, non-overlapping targets. While this isn't definitive, and doesn't include all the subpopulations the group found, distinct projection targets from neighboring neurons of the same major type is part of the necessary criteria for being a distinct subpopulation. Another good example comes from work in the well-characterized

retina[45]. Due to its organization, limited size, and defined circuitry, the retinal cell types have been studied intensively for years. One large population of retinal neurons, the rod bipolar cell, was found through ssRNAseq to have 15 subpopulations. To confirm these, the researchers explored each group's neuronal morphology. Interestingly, each of the 15 subpopulations has very distinct, conserved morphology. Again, without a strict definition of functional relevance we can't know they are truly distinct. However, conserved morphological characteristics lend credence to these being separate subpopulations. Finally, cortical neuron sequencing from several groups has attempted to match subpopulations with canonical cortical projections[46,47]. Interestingly, the majority of cortical subpopulations had a specific, single projection target, although there were several subpopulations with the same target. Interestingly, similar yet genetically distinct subpopulations did not have distinct projections.

These examples represent the exception, not the norm. More often, subpopulations are genetically defined and there is no follow up. The likely cause for this is because it is far easier and faster to collect and analyze scRNAseq data than it is to verify and validate genetically defined populations. As an example, in a superb undertaking by Saunders *et al.*[34], a novel genetic population of spiny projection neurons (SPNs) was discovered and named 'eccentric' SPNs (eSPNs) based on their unique genetic signature. Canonically, the striatum is almost wholly comprised of two distinct classes of projection neurons; dopamine receptor 1 (D1) expressing, direct pathway SPNs (dSPNs), and dopamine receptor 2 (D2) expressing, indirect pathway SPNs (iSPNs). This third axis of eSPNs represents only 4% of all SPNs and can be broken down further into D1 and D2 expressing eSPNs. Although they differentially express 110 genes relative to canonical dSPNs and iSPNs, eSPNs don't display any known differences in circuitry, physiology, anatomy, or response to disease. While definitely possible, it remains to be determined whether the genetically defined eSPNs are a de-facto neuronal subpopulation.

A large caveat that comes with attempting to define subpopulations by both genetics and function is relying on the assumption that biology has provided clear cut populations. In the dorsal and ventral striatum, a large portion of genes that define clusters of subpopulations of both D1 and D2 SPNs follow gradients of expression including cannabinoid receptors[48,49]. Beyond the striatum, continuous gene expression is found in both cortical pyramidal neurons and hippocampal interneurons[50,51], and intermediate groups of neurons that fall into multiple clusters are found in the cortex[52]. In addition to the gradients of gene expression and intermediate phenotypes, neurons can lose marker genes as they develop and even change their neurotransmitter identity during development or due to activity[53]. Because clustering will depend on finite gene expression boundaries, having continuous gradients of expression of various genes makes it difficult to define subgroups. While previous examples have shown that some genetically defined populations are functionally relevant and distinct, gradient gene expression, changes in gene expression, and changes in identity throughout maturation highlights the necessity for following up genetic clustering with confirmation of functional relevance.

ScRNAseq depends on an unbiased approach to finding subpopulations which

assumes there are underlying gene expression differences that aren't readily clear. There is, however, an equally as valid approach to finding subpopulations. The opposite approach, one that is more *ad hoc*, is to choose a gene with a known functional role. Whether it's a receptor or ion channel, applying this gene expression criterion to the population of interest will generate a functional group. As an example, oxytocin receptors (*Oxtr*) are expressed in ~55% of VTA DA neurons and ~25% of SNc DA neurons. Oxytocin released from neurons in the hypothalamus increase excitability in *Oxtr*-expressing VTA DA neurons due to receptor activation and decrease excitability in SNc DA neurons because of increased inhibitory tone from local *Oxtr*-expressing GABAergic interneurons[54]. In another example, neurotensin receptor 1(*Ntsr1*) is expressed in a small portion of DA neurons in the VTA. Even though they represent a small subset, ablation of Ntsr1-DA neurons led to pronounced changes in energy balance, and sucrose intake[55]. Clearly, OXTR-DA neurons and NTSR-DA neurons are functional subgroups. They respond to neuropeptides and stimuli different from their neighbors. However, *Oxtr* or *Ntsr1* expression is not correlated with any published DA neuron subpopulation[33]. Either these individual genes don't follow the clustering defined by global gene expression, or they aren't expressed highly enough, although the published data indicate that likely isn't the case[54,55]. In either case, it is clear that global, single-cell gene expression is not the only method available to discover relevant neuronal subgroups.

Some additional guidelines should be added to defining a molecular ground state of a neuron. It should exclude certain genes, like those that are activity-dependent or define transient cell states. Neurons, more so than cells outside the CNS, will have a big variance in their gene expression given their need to survive and adapt throughout the lifetime of the organism. This creates additional problems. Are there learning-related long-term gene expression changes that would force a neurons removal from its cluster? The only true way around this is to do multiple experiments on different biological samples to find the consistent ground state. All of these caveats together, we can start to lay out the rules for neuronal populations. First, using scRNAseq is a great first pass to provide a foundation of study. Second, it should ideally be followed up with at least one form of functional confirmation, like projection or physiological analysis. Third, any group can realistically be broken down further using known, functionally relevant genes. Finally, a true necessity for defining a subpopulation depends on replication from multiple biological samples, and hopefully, different labs. It is through this approach that we can hopefully group sets of neurons that have the same role and respond to the same stimuli. With these criteria in place, we can start to explore specific, seemingly homogenous populations to uncover the heterogeneity that exists.

Dopamine's anatomical discovery and heterogeneity

In mice, there are only about 25,000 total DA neurons, representing about 0.03% of all neurons in the brain[56-58]. Even with these small numbers, DA neurons receive numerous diverse inputs[59] and have varied projections throughout the brain[60]. Because they can modulate the activity of a variety of brain regions and, DA neurons are known to play a role in diverse behaviors[61,62]. Most importantly, DA neurons throughout the midbrain have varied responses to disease, most notably, Parkinson's disease[63]. For

these reasons, efforts to parse out the functional differences between DA neurons have made up a significant portion of dopaminergic study since the neurons were discovered in the mid-20th century.

Even after DA had been shown to be present in the rabbit brain[64-66], the scientific majority did not think DA held any functional relevance because it showed no effect when washed on to muscle tissue[7]. It wasn't until a unique formaldehyde vapor based staining and fixing method allowed for the fluorescent visualization of dopaminergic neurons that the paradigm shifted[67,68]. Once this method was discovered, the field quickly took to work to define all of the dopaminergic populations throughout the rodent brain, initially finding 12 groups (named A1-A12)[69]. Old groups were then broken down further, and some new populations were discovered (A13-17) decades later following the advent of immunohistochemistry for tyrosine hydroxylase (TH)[70], the rate limiting step in catecholamine synthesis of which DA is the first step. The vast majority of DA neurons are found in the midbrain, regions A8-A10, corresponding in the mouse to the retrorubral field (RRF), Substantia nigra pars compacta (SNc), and ventral tegmental area (VTA), respectively (Fig. 3A). While midbrain neurons project throughout the brain, projections are broken down in that the SNc neurons project strongly to the dorsal striatum (Fig. 3B) while the VTA neurons represent the rest of DA neurons projections throughout the brain[60]. Considering they represent the vast majority of DA signaling in the brain, midbrain DA neurons have been the focus of the DA field since.

From their earliest discovery, it has been clear that not all DA neurons are alike. First, as previously mentioned, they are found in multiple, distinct anatomical regions throughout the brain. Even if the neurons were identical, disparate brain locations point towards differences in connectivity. Anatomically close populations, like the SNc and VTA, have relatively clear boundaries between their neurons. Beyond their multiple cell body locations, DA neurons vary in size and morphology between the VTA and SNc and even within these regions[69,70]. In addition, both fluorescent formaldehyde staining and TH immunohistochemistry indicated there was a large variability in TH expression and DA concentration between neurons. Perhaps the most striking difference between DA neurons was discovered well before DA was characterized in the brain. In the early 20th century, it was clear a prominent neurodegenerative disorder, Parkinson's disease (PD), resulted from degeneration of a very specific population of neurons in the midbrain, although they hadn't yet been characterized beyond their dark pigment (hence the name, substantia *nigra*). This neuronal response to PD sparked decades of research.

Differential response of DA neurons in Parkinson's disease.

Descriptions of the symptoms of PD have been around for centuries from the bible to Da Vinci[71,72]. The first in depth description and naming of the disease came in 1817 by Dr. James Parkinson[73,74]. Today, at its most basic, PD represents a family of similar disorders characterized by bradykinesia, muscular rigidity, resting tremors, postural instability, and responsiveness to levodopa[71,75]. Anatomical confirmation that can only happen post-mortem, will show a substantial reduction in the numbers of caudal and ventrolateral SNc DA neurons and Lewy body deposits, protein aggregates made primarily of α-synuclein protein, from the remaining DA neurons up to the cortex,

depending on disease severity[71,76]. Early research into PD used reserpine, an antipsychotic drug introduced in the early 1950s, as one of the first models of PD. It caused dyskinesia and muscle rigidity because it blocks monoamine transport, and thus depletes dopamine release. L-Dopa was shown to ameliorate the effects of reserpine, pointing towards DA (or nor-adrenaline) as a root cause for the disease[73]. In addition to these data, early speculation of DAs role in motor control was hypothesized because of its high concentration in the caudate putamen[77]. The gradual accumulation of evidence led scientists to look at DA concentration in diseased brains, and by 1960, it was found that PD patients showed a marked reduction in striatal DA[73,78]. Soon thereafter, L-Dopa (now levodopa) treatment became the gold-standard for PD and dopamine depletion was seen to be the root cause of the disease. Very little has advanced since in terms of functional treatment for PD.

While treatments have essentially stalled since the discovery of levodopa, research into the mechanisms behind DA neuron degeneration has been of major interest for decades. The early recognition that there was selective degeneration of a portion of SNc neurons provided a great starting point for research. One of the first major causative hypotheses was put forward due to evidence that neuromelanized neurons in the midbrain, which are found in the SNc, were selectively degraded as compared to SNc DA neurons without neuromelanin[79]. It was hypothesized that production of neuromelanin leads to the production of toxic free radicals and also binds many drugs[79]. The notion was that over the course of years, neuromelanin continues to build[80], adding the potential for additional stressors, causing progressive degeneration in these cells[79]. While a major step forward, there have been several other hypotheses put forward.

It is unlikely that there is a single smoking gun that causes PD based neuronal degeneration in the SNc[81]. There have been many documented correlations to neuronal death. Lewy pathology (LP), cytoplasmic α-synuclein protein aggregates, is highly associated with clinical PD and LP accumulation can cause neuronal degeneration[75,82]. However, LP is not found in all PD patients, and *is* found in non-PD patients[75,82]. Another major hypothesis points towards mitochondrial dysfunction and oxidative stress[83]. Post-mortem studies often implicate oxidative damage from mitochondrial dysfunction in the pathogenesis of PD[84]. More specifically, reduced mitochondrial complex I activity can lead to decreased ATP production and reactive oxidative species (ROS) leading to cell death[85,86]. ROS may be particularly damaging to SNc neurons because the majority are pacemakers dependent on L-type Ca^{2+} channels, thus increasing their intrinsic calcium levels and oxidation[81,87-89]. VTA neurons on the other hand are less dependent on Ca^{2+} channels for oscillation, and contain more calcium buffering proteins[89,90]. Increased SNc neuron calcium levels and oxidation lead to sustained mitochondrial stress and damage[88,89]. However, this can't alone be the cause of PD specific degeneration because even normal aging results in a significant reduction in SNc DA neurons[80,91]. It is probable that all neurons have and are susceptible to oxidative stress, but the additional effects of pace-making may make SNc neurons more vulnerable[87]. Mitochondrial deficits may affect SNc neurons disproportionately due to channel composition as well. Mitochondrial complex I inhibition activates K-ATP channels in SNc neurons not but VTA neurons, leading to

degeneration of SNc DA neurons that can be rescued when K-ATP channels are knocked out[92]. K-ATP channel activation may be SNc specific due to increased expression of the SUR1 K-ATP subunit[92]. Major evidence for the mitochondrial dysfunction model also comes from two chemical induced dopaminergic lesions. MPTP is a sparse byproduct of MPPP, a synthetic opiate. There were cases in which MPPP users accidentally injected themselves with MPTP, which is converted to MPP^+ in the brain. MPP^+ is taken up by DA transporter (DAT), and shuts down mitochondrial complex 1[87]. The toxic effects of MPTP may also be enhanced or dependent on α-synuclein deposits[87]. 6-hydroxydopamine, 6-OHDA, is synthetic compound that was used starting in the late 1960s to induce degeneration of striatal projecting DA neurons[93]. 6-OHDA leads to dopaminergic degeneration through uptake through DAT and localization to the mitochondria, causing increased ROS and inhibition of mitochondrial complex I[93,94].

While there are far more cases of sporadic PD, the genetic basis also provides clues to the causes and heterogeneity of the disease. About 10% of PD cases are associated with known genetic risk factors[82,83]. The most common genes associated are *SNCA* (α-synuclein gene), *PINK1, PARKIN, DJ-1, and LRRK2* (leucine rich repeat kinase 2)*[82]*. Interestingly, each of these mutations has different disease causing mechanisms. *SNCA* mutations causes high levels of Lewy bodies and early onset of PD symptoms[82,87]. *PINK1* and *DJ-1* cause deficits in mitochondrial function. *PINK1* is a mitochondrial kinase which can protect against mitochondrial dysfunction[87] while *DJ-1* plays a role in regulating oxidant defenses at the mitochondria. Knockout of *Dj-1* in mice increases oxidative load in SNc neurons but not VTA neurons[88]. *PARKIN* plays a role in the unfolded protein response (UPR), and its mutation leads to improper protein degradation and neurotoxic protein accumulation[87]. *For LRRK2*, the most common genetic form of PD at up to 4% of familial cases, there is still no consensus on common mechanistic cause although some evidence shows LRRK2 kinase activity can lead to toxicity[95]. Perhaps unsurprisingly, the genetic underpinnings to PD show a variable and heterogeneous neuronal response. In addition, while these genes are associated with PD, they are also expressed ubiquitously in the brain, so it remains unclear why mutations would lead to selective degeneration in the SNc. Between sporadic and familial PD cases, the best model points towards increased susceptibility of SNc neurons due to higher, calcium dependent pace-making with less calcium buffering. This leads to a higher baseline level of mitochondrial stress and ROS and in turn makes SNc neurons more vulnerable to any additional insult that may occur, including normal aging-associated stressors.

While the debate about differential SNc and VTA has been the major focus of PD research, the VTA alone offers an interesting model to study neuronal susceptibility. In PD, the VTA exhibits roughly 40-70% neuronal death[76,79,96]. Exploring what makes a spared VTA DA neuron different from its susceptible neighbors is a difficult question o answer that is still an open area for investigation. In work presented in Chapter 2 of this these, the presence of the transcription factor *Neurod6* and lack of the neuropeptide gene *Grp* indicated increased resilience to a 6-OHDA mouse model of PD[97]. *Neurod6* has shown to be neuroprotective, maintaining mitochondrial health in cell culture

studies[98,99] which corroborates the evidence that mitochondrial health is a major factor in PD. Earlier work showed that, within the VTA, there may be a selective sparing of DA neurons that were calbindin-positive[90]. Differences could also come from variable DAT expression in the VTA, which leads to less intracellular DA, and thus less oxidative stress[100], although this hasn't been investigated directly. In addition to this, some VTA neurons fire in a pacemaker fashion, while others are more intrinsically silent. Increased pacemaker activity, while not Ca^{2+} based, could still lead to enhanced susceptibility[101]. The connection between spontaneous pacemaker firing in the VTA and PD degeneration has not been examined directly either. So, while many studies have compared the SNc to VTA, there have been very few studies exploring the response within the VTA to PD.

While it isn't completely clear what drives the difference in vulnerability between the SNc and the VTA to PD, and even further, what differentiates susceptible VTA neurons from their spared neighbors, there are some very plausible candidates as discussed above. There are likely many routes that lead to PD and a handful of diseases that have a similar pathophysiology to, and are often misdiagnosed as, PD[71,81]. With these presented studies, what *is* clear is that there are many variables that contribute to neuronal sensitivity to degeneration. Within midbrain dopamine neurons as a population, there are numerous heterogeneous properties that exist that could cause various responses. On this basis alone, what is obvious is that DA neurons represent an extremely diverse neuronal population.

Dopamine neuron functional diversity

Given their differences in anatomy and disease susceptibility, it is no surprise that there are striking differences between DA neurons in terms of their physiology and behavioral roles. The first in depth intracellular physiological characterization of DA neurons came in 1980 by Grace and Bunney[102]. The studies were done in the rat SNc and provided what was, at the time, the definitive physiological profile of a DA neuron[103,104]. The canonical DA neuron is a pacemaker, firing at about 2-5 Hz, with a wide ~3.5 ms action potential (AP)[103,104]. There is also a response to DA via DA receptor 2 (D2) autoreceptors, hyperpolarization that follows action potentials, and an HCN channel mediated SAG component that follows injected hyperpolarizations with a fast return to resting membrane potential (RMP)[92,105,106]. However, almost as soon as this canonical profile was established, it was found that DA neuron physiology couldn't be pinned down that easily. In 1984, it was shown that depending on the projection target of the DA neuron, whether it was the prefrontal, cingulate, or piriform cortex, there were differences in spontaneous firing frequency and in the max firing frequency following current injections[107]. The majority of these neurons were found in the VTA where there is a paucity of striatal-projecting neurons. In addition to this, prefrontal and cingulate cortex-projecting DA neurons showed no response to DA wash-on, indicating they did not have D2 autoreceptors[107]. This was disagreed with for a short time, potentially because researchers assumed non-canonical DA neurons were non-dopaminergic because of their physiology[108], however, it started to become appreciated that some VTA neurons had much different physiological properties than the canonical SNc DA neurons[106,109].

By the early 2000s, there were many examples of the innate heterogeneous properties of DA neurons. First, and most striking, depending on the projection target, a DA neuron will have a different physiological profile. It has increased max firing rates, a slow return to RMP following hyperpolarization, and a larger AP width if it projects to the nucleus accumbens medial shell (NAc MSh) or core, prefrontal cortex (PFC), or amygdala[92,100,107,110-112]. More recently, it was shown there are even subtle differences in SNc DA neurons whether they project to the dorsal medial (DMS) or dorsal lateral striatum (DLS) (Fig. 3A)[113]. Mouse midbrain neurons also have different physiological responses to opioids, with κ-opioids inhibiting NAc-projecting neurons more-so than PFC-projecting neurons[111]. Interestingly, these data aren't applicable to the rat, where NAc-projecting DA neurons see no response to κ-opioid receptor agonists but prefrontal cortex neurons do[114]. DA neuron physiology also varies with gene expression. The typical hyperpolarization activated sag component was shown to depend on whether the neuron expressed calbindin1, no matter if it was in the SNc or VTA[105]. Also, SNc DA neurons exhibit variable physiological properties because of differences in small conductance potassium channels[115]. DA neurons also have varying responses to cocaine depending on their projection target. NAc-projecting DA neurons increase their AMPA/NMDA ratio following cocaine administration whereas PFC- and striatal-projecting DA neurons do not[112]. While the majority of the physiological characterization has happened in brain slices, recent work has elegantly shown the *in vivo* heterogeneity of DA neuron physiology. DA neurons projecting to the DLS have far shorter inter spike intervals in their baseline burst firing rates as compared to DMS-projecting neurons[116]. Further, *adjacent* DMS- and NAc lateral shell (LSh)-projecting DA neurons in the ventral SNc have striking differences in their burst firing patterns[116]. From these data, it is apparent that within this small population of DA neurons exists a vast array of intrinsic physiological properties. In addition, because of their disparate projections, these properties impact the various and sometimes opposing behavioral roles that DA plays within the brain.

DA neurons project throughout the brain and thus play a role in a large set of different behaviors. Projections are broken down into those coming from the SNc and those from the VTA (Fig. 3A). The SNc projects almost exclusively to the dorsal striatum, while the VTA projects to a much larger and diverse subset of regions (Fig. 3B)[60]. Fortunately, DA neurons are somewhat unique as most of them have only a single target region[100,116-118]. DA neurons also have a wide array of inputs, with most coming from the NAc, striatum, amygdala, hypothalamus, midbrain, and cortex[59]. For the VTA and SNc, inputs to a neuron have been studied based on that neurons outputs using cTRIO[118]. This work has shown that most neuronal populations in the VTA receive similar inputs. There are some small subtle differences. LSh-projecting neurons have an increase in LSh and core inputs, and MSh-projecting DA neurons show nearly no dorsal striatum inputs[118]. In the SNc, almost all neurons have identical inputs, except for increases in reciprocal circuitry – there are more DLS inputs to DLS-projecting DA neurons, and more DMS inputs in DMS-projecting DA neurons[113]. Additionally, there is a unique subpopulation in the very lateral SNc that projects to the tail of the striatum[119]. With such a variety of inputs and outputs, DA neurons are well-positioned to integrate various stimuli and have

diverse functional networks.

The behavioral role a DA neuron will play depends heavily on its inputs and outputs. As the majority of SNc neurons project to the dorsal striatum, they affect and drive motor behaviors. This was first evidenced when degeneration of DA neurons led to gross motor impairments in PD patients[77,120]. More definitively, it has been shown that fast, phasic DA neuron activity in the dorsal striatum leads to locomotor onset. In addition, phasic DA activation of SNc DA neuron terminals using channelrhodopsin also initiates locomotor activity[121]. These findings were contrary to the wide-held belief that DA affected movements on slow timescales[122]. Outside of the SNc, there has been evidence that neurons in the VTA also affect motor behavior, as about 30% are active during accelerations in a reward task[62]. However, these findings don't definitively implicate the VTA in driving motor behaviors specifically.

Perhaps the most commonly known behavior associated with DA neurons is reward learning. Early studies recognized rats would self-stimulate in areas with known DA projections in the pre-frontal cortex, however there were additional collaterals from adrenergic and nor-adrenergic projections[123]. It wasn't until precise studies were done using movable electrodes that the tracts coming from midbrain DA neurons (now recognized as the medial forebrain bundle: MFB), specifically VTA neurons, were found to directly influence and drive reward processes[124-126]. While additional work remained to localize other reward hot-spots not necessarily related to DA, this represented a major step forward[123]. In 1997, the model was updated when it was shown DA neuron firing in the monkey midbrain correlated with the onset of an unpredicted reward, or a conditioned stimulus that was associated with a reward[127]. DA neurons fired to represent a 'reward prediction error' - they increased their firing upon an unpredicted reward or conditioned stimulus, or decreased their firing when an expected reward was omitted, thus representing a physical signal for the value of a stimulus relative to the current state[128,129]. DA can be thought of then as representing a *motivational* signal with the goal of moving towards highly rewarding situations. It bursts during a discrete reward or predicted reward, is continually active during persistent rewarding events, and maintains a low, tonic release to enable movement[128]. It also fires in accordance with the likelihood of receiving a reward, allowing for more complex comparisons to be made between multiple awards in order to drive behavior[130].

In more recent years, optogenetics has helped confirm these findings and provide a more nuanced understanding how DA drives motivation, reward, and reinforcement learning. Activation of VTA DA neurons has been causally linked to reward[131], with phasic activation of DA concurrent with an unpredicted reward identified as sufficient to drive reward-seeking behavior and learning[132]. However, adding to the complexity and the innate heterogeneity of DA neurons, there is substantial evidence for both reward *and* aversion triggering DA firing, depending on the neuron. In 1976 it was first shown that stresses caused an increase in DA in the PFC, but not the NAc, in rats[133]. By the 1980s, it was shown more definitively for rats that tail pinch or shock, a traditionally noxious stimuli, excited about 65% of DA neurons projecting to the PFC[134], and caused increased levels of DA in the PFC and NAc[135]. In addition, this response to aversive

stimuli also occurred in the SNc in response to various noxious stimuli[136]. These findings were replicated several times over the next few years using slightly different noxious stimuli and measurements showing there are some differences in location of DA increase that are dependent on the stimuli used[137-140]. Together, this data started to uncover separate types of functional DA neurons in the VTA and SNc and establish a role for DA in measure reward and aversion to drive motivational salience[141].

Beyond the increase in DA in the PFC and NAc in response to aversive stimuli, it was shown that specific cell bodies responded to noxious stimuli. Extracellular recordings found distinct DA neurons, consistently in the ventral VTA, that increase phasic excitation following electric shocks to the hind paw[142]. More dorsal VTA neurons showed the canonical decrease in excitation following shocks[142]. This evidence for two distinct types of neurons even extended to non-human primates[143]. The presence of two distinct responses was further explained when the mesocortical and mesolimbic circuitry was explored more systematically. Aversive stimuli increased synaptic strength onto PFC projecting DA neurons following noxious stimuli, and rewarding stimuli increased synaptic strength in MSh projecting DA neurons[112]. Further, activation of the lateral habenula (LHb) inputs into PFC-projecting VTA neurons led to condition place avoidance[144,145], whereas activation of laterodorsal tegmentum (LDT) inputs into LSh-projecting VTA neurons causes conditioned place preference[145].

All the previous data had outlined a clear role of DA in the PFC in aversive responses, with increases in mesocortical neuron firing and increases in PFC DA concentration following noxious stimuli. However, the NAc had been more difficult to tease apart given that close sub-nuclei have different behavioral roles and incidental activation of adjacent nuclei could confound data[145]. This was clarified when de Jong *et al.* showed using *in vivo* fiber photometry that ventral MSh-projecting DA neurons responded to aversive stimuli, conditioned stimuli for aversive stimuli, and *novel* rewarding stimuli[146]. In addition, neurons projecting to the dorsal MSh, core, and LSh all responded like canonical reward responsive DA neurons[146]. Thus, even for what was thought to be a canonical DA response, there is still heterogeneity in how DA neurons react to rewarding and aversive signals[147]. Using these more comprehensive techniques helped determine the precise role of the various dopaminergic subtypes and their projections to NAc sub-regions in motivated behaviors[141,147-149]. These neurons may not even represent aversive stimuli per se. They may be activated by salient and alerting signals that can help adapt and reorient the animal's behavior towards value learning. This would further solidify DA's role in comparing reward and aversion to drive behavioral motivation, especially because some neurons respond to both aversive and rewarding stimuli[141,143,146]. While the majority of behavioral work in DA circuits centers on reward and motivation, adding to their complexity and heterogeneity, DA neurons play a role in behaviors based on their non-striatal projections.

DA neurons send dense projections to the striatum[60]. However, even with sparse projections to other regions, local circuitry can be modulated by DA. DA neurons project throughout the hippocampus. Through pharmacology and genetic knockouts, DA receptor studies have shown that DA plays a role in spatial memory and recognition

learning in the temporal and dorsal hippocampus through modulation of hippocampal LTP and LTD[150-152]. The canonical response to reward and novelty in the VTA drives DA release in the hippocampus and helps consolidate memories[153]. Interestingly, not only does the hippocampus receive dopaminergic input from the VTA, but also from neurons that co-release noradrenaline and DA in the locus coeruleus (LC)[151,153,154]. Memory persistence, the maintenance and stability of a memory, promoted by projections from the LC was found to be DA dependent and not noradrenaline dependent[154]. Beyond hippocampal memory, DA projections to the amygdala modulate fear memory. The amygdala contains many different DA receptors. Thus, most of the work deciphering how DA contributes to fear memory is through receptor pharmacology studies. DA receptor 1 and 5 (D1 and D5) antagonists in the amygdala attenuates fear memory and agonists potentiate fear memory[155]. D2 antagonists infused into the amygdala during conditioned fear tasks reduced freezing behavior during conditioned stimuli[155]. This corroborates findings that aversive stimuli cause DA release[141], and increase DA concentration in the amygdala[156]. Finally, dopaminergic projections to the anterior cingulate cortex (ACC) show a complex effect on behavioral reversals and decision making[157,158], with VTA DA likely contributing it's measurement of reward prediction error in a feedback loop with the ACC[159]. While there are also clear dopaminergic projections to the lateral septum, bed nucleus stria terminalis (BNST), and perirhinal cortex, among others, the precise role DA may play in these regions is unclear.

Beyond their unique anatomical and disease response heterogeneity, DA neurons have diverse functional properties and behavioral roles. Because of their vast heterogeneity in physiology, behavior, and especially their response to Parkinson's disease, the genetic underpinnings that drive this variance has been of special interest and has generated a lot of investigation. Decades of research have gone into deciphering the genetic makeup of DA neurons and their subpopulations.

Genetic subpopulations of dopamine neurons

As discussed above, a neuronal subpopulation is rarely definable by a single gene. This is certainly true for DA neurons as well. No single gene can define a dopaminergic neuron. There is a checklist from development to maturity that helps define a DA neuron in general, although, even then it is still up to some interpretation. A DA neuron can be defined at its most basic as a neuron that develops from dopaminergic progenitors, and can synthesize, release, and uptake DA. This will depend on a collection of different genes. Some of the most basic genes necessary start with DA synthesis, which will depend on tyrosine hydroxylase (*Th*) and dopa decarboxylase (*Ddc*). DA transporter (*Slc6a3:* DAT) is needed for DA reuptake at the synapse, and vesicular monoamine transporter 2 (*Vmat2*) to package DA into vesicles. Presence of any of these genes doesn't *de facto* define a DA neuron as none of these genes is necessary *and* sufficient for DA release. There are some neurons that express *Th* and not *Slc6a3* in the locus coeruleus, zona incerta, and nucleus raphe[160] and it's not clear whether they can release DA because some *Th*^{+} neurons, including those positive in TH-Cre mice, may not contain much functional TH protein[161]. However, it has been shown some of these neurons in the locus coeruleus do release DA[151]. Thus, while it may exclude a small subset of DA neurons, in recent years DAT expression has been argued to be the best,

most strict marker to identify DA neurons with minimal off-targets[61,161,162].

Part of the genetic DA neuron identity stems from development. There are several transcription factors that define DA neuron lineage, and more specifically, midbrain DA identity. DA neurons originate in the mesodiencephalic floorplate and are pushed into their trajectory in part by *Foxa1/2*[163,164], *Lmx1a/b*[165,166], *Nurr1*[167], and *Ngn2*[33,164,168]. However, these genes alone don't define DA neurons as they are also present and necessary in other neurons that originate in the floorplate. They are expressed in neurons adjacent during development that migrate into the subthalamic nucleus (STN) and premammillary nucleus[169,170]. Midbrain DA neurons can identified from this lineage based on expression of the transcription factor *Pitx3*, a strong marker of midbrain DA neurons[168-170]. Interestingly, genes like *Foxa1/2*, *Lmx1a/b*, and *Nurr1* define *midbrain* DA neurons, as DA neurons outside of the A8-A10 areas don't arise from the same pool of early progenitors[171,172]. Going deeper, some of the fundamental diversity between the SNc and VTA also stems from development. Transcription factors like *Shh* and *En1* along with other factors like retinoic acid and *Aldh1a1* push dopaminergic progenitors towards an earlier developmental, SNc fate[173]. Even with this information, more subtle differences that delineate the complex genetic diversity within the VTA or SNc have yet to be addressed. Based on these definitions, a checklist emerges for midbrain DA neurons. It must contain the majority of the machinery necessary for synthesis, release, and uptake of DA, *and* release dopamine. In addition, it should develop from the mesodiencephalic floorplate and express the transcription factors *Foxa1/2, Lmx1a/b, Nurr1, Ngn2,* and *Pitx3.* With this baseline, one can begin to explore the genetic heterogeneity in midbrain DA neurons.

Because of their unique susceptibility to PD, discovering the genetic underpinnings that cause resistance to disease has been studied extensively. There have been many groups using various methods throughout recent years to decipher the genetic makeup of the different subgroups of DA neurons. The earliest RNA-sequencing studies into dopaminergic genetic heterogeneity compared bulk populations of SNc and VTA neurons with the goal of uncovering the genetic underpinnings of SNc's susceptibility to PD. This consisted of laser microdissection of cells from SNc, and VTA in the mouse[174] and rat[171,175]. Additionally, one study included the DA neurons in the hypothalamus and the LC[171]. Through microarray analysis, a consistent profile of SNc and VTA neurons began to emerge. VTA neurons appeared to have consistently higher levels of *Calb1, Egr1, Grp,* and *Tacr3* while the SNc expressed *Cd24a, Fgf1,Igf1 Sox6*, and *Sncg*[171,174-176]. Unfortunately, none of these genes are strict markers for either population[160]. These data clarified that single genes weren't sufficient to label any subpopulation of DA neurons, especially ones as anatomically close as the SNc and VTA. In addition, as evidenced by the diversity within the VTA and SNc outlined above, it became clear there was significant heterogeneity within each population. For this reason, bulk studies wouldn't be able to discover all the heterogeneity within the populations.

To address this, many recent studies have used single cell profiling approaches to catalog DA neuron subpopulations[33,34,97,177-180]. The first single-cell analysis done on DA neurons used a 96-well format and qPCR to cluster DAT-Cre-positive neurons based on

a selection of 96 genes that had been previously identified in the bulk sequencing experiments[177]. Larger scale scRNAseq platforms have been used more recently in the DAT-Cre mouse line[97,178]. Interestingly, other studies have used different genetic mouse lines, like *Th*-eGFP[179], *Pitx*-eGFP[180], or wild type[34]. There have been some major consistencies within the data even with the varying methods and mouse lines[33]. Based on the consensus of the different data sets, there appears to be about 2 subgroups of SNc neurons, and 4 subgroups of VTA neurons. The SNc is split roughly through its medial/lateral axis even though it is a very thin structure. The major delineation genetically between the two groups is the expression of *Aldh1a1* in the lateral portion, and not the medial. In addition, there is a small subset of SNc neurons that express *Vglut2*, typically expressed in glutamatergic neurons, in the very dorsal lateral region. The VTA has more clear delineations, broken down roughly by anatomical areas. The ventromedial VTA has shown consistent expression of *Neurod6, Grp, Gpr83,* and *Otx2* across at least four of the six studies above. The most caudal DA neurons in the caudodorsal VTA and dorsal raphe also show very consistent markers in *Vip,* and *Calb1,* with a lack of *Sox6.* The dorsomedial VTA is less definitive. It makes up the majority of the parabrachial pigmented area (PBP), and its strongest marker is *Slc32a1* (*V*gat). Finally, the laterodorsal VTA, which runs in part adjacent to the SNc shows consistent *Lypd1*/*Sox6* labeling with a lack of *Aldh1a1*[33].

Given the heterogeneity and close proximity of DA neurons, none of these anatomic and genetic markers have strict delineations. Even the strongest markers here like *Vip* or *Neurod6* are often found outside of the caudodorsal or ventromedial VTA[97,177]. Even markers like *Neurod6* and *Grp* that consistently mark the same subgroup through cluster analysis don't show close to perfect overlap[97]. So too, these markers just represent what the majority of the neurons within that cluster express, and don't mark 100% of those neurons. Thus, it is important that any of these clusters are further analyzed to determine whether or not they represent functional subgroups. Evidence that genetically-defined dopaminergic subpopulations can define functional populations has come from two studies. The *Neurod6* subpopulation in the ventromedial VTA has been shown to have strong projection targets to the NAc MSh, lateral septum, and olfactory tubercle with few projections outside those areas[97,181] (also see chapter 2 and 3). *Neurod6*+ DA neurons have distinct physiological properties as compared to their neighboring neurons, and represent a population that is largely spared in a 6-OHDA model of PD[97]. In addition to this in depth study of the *Neurod6* subpopulation, the projection targets of other genetically defined subgroups have been explored. Through intersectional targeting of DA neurons expressing *Aldh1a1, Vglut2,* and *Vip,* among others, Poulin *et al.* found genetic subpopulations had restricted projection targets with limited overlap[182]. These data are vital as they indicate the functional relevance of dopaminergic subpopulations and point towards potential ways to uncover the behavioral roles each subpopulation has.

In addition to the scRNAseq-defined genetic clusters there are also groups of neurons within the VTA that express markers typically assigned to excitatory or inhibitory neurons that aren't ascribed to clustered subpopulations. Dorsomedial VTA neurons express *Vglut2*, the gene responsible for the packaging of glutamate into vesicles[6,61,161].

Further, these neurons show functional co-release of glutamate[183-185]. In addition to glutamate, DA neurons also co-release the main inhibitory neurotransmitter GABA[186-188]. These DA neurons don't express common GABAergic markers[187], and use non-canonical methods to synthesize and package GABA[187,189]. Beyond co-release, subsets of DA neurons express different peptidergic receptors like neurotensin receptor 1 (*Nstr1*) and oxytocin receptor (*Oxtr)* making them uniquely able to respond to peptidergic inputs from the hypothalamus and other regions[54,55]. Taken together with the scRNAseq data, it appears there are layers of genetic heterogeneity, with some foundational clusters that may arise through development, and others that are defined based on their expression of single functional genes.

Through many bulk and scRNAseq studies, the genetic heterogeneity of DA neurons is clear. While the exact markers show some variability, there is a foundational description of different subgroups and evidence they represent functional populations. In addition to the scRNAseq defined subpopulations, there are further populations based pre-identified functional genes like markers for glutamatergic or GABAergic neurons that show DA neurons can co-release different transmitters. There are also peptidergic receptors that indicate the ability for some subpopulations to respond to peptidergic signaling. The stage is now set for further work to uncover the behavioral functions of each of the subtypes.

Neuropeptide subpopulations in DA neurons and their unknown role in the brain

Through scRNAseq data, it has become clear that neuropeptides are consistent markers of neuronal subtypes[34,35]. Neuropeptides are a class of small signaling peptides found throughout the central and peripheral nervous system, and represent an ancient, fundamental family of slow signaling neuromodulators. They are thought to be one of the original signaling molecules as they are expressed widely throughout the animal kingdom and are still prevalent in invertebrates where rapid signaling with fast-acting neurotransmitters isn't as crucial[190]. Interneurons serve as a perfect example, as their diversity is heavily reliant on neuropeptides, with the vast majority defined by two different neuropeptides; vasoactive intestinal peptide (VIP) and somatostatin (SST)[15,191].

It is only recently becoming appreciated how ubiquitous neuropeptide expression is in the brain. Smith *et al*. has shown that 97% of sequenced mouse cortical neurons in the visual and motor cortex express *at least* one neuropeptide gene, and 98% express *at least* one neuropeptide receptor gene[192]. In addition, they show that using just expression of neuropeptides and receptors is sufficient to successfully cluster neuronal subgroups[192]. While unlikely, neuropeptide signaling in the central nervous system may represent a vestigial phenomenon that often holds no current functional relevance. This could be evidenced by a lack of coordination between neuropeptides and their receptors in some circuits[193]. However, the peripheral and central nervous system has countless documented circuits involving neuropeptides. Most of the work in neuropeptide signaling has been done in *C. Elegans* and *Aplysia*, but there numerous examples of it happening in the rodent brain[194,195]. The majority of this work has been done in the mouse thalamus and hypothalamus where neuropeptide Y (NPY), oxytocin (OXT), and vasopressin (VP) play important roles in local circuitry[194,195].

Interestingly, there are two major neuropeptides that are consistently found to label distinct subpopulations of DA neurons. Gastrin releasing peptide (GRP) has been found in several studies to mark a ventromedial portion of the VTA and project to the DMS and NAc MSh[97,177,178,196]. In addition, DA neurons expressing VIP are found in dorsal raphe DA neurons and project to the central amygdala (CEA) and BNST[177,178,182]. What has yet to be explored is whether the neuropeptides are co-released from these populations, whether the cognate receptors are found at their projection targets, or whether the peptide has a measurable effect on the target neurons that have the receptor. Co-release allows for a neuron to have multi-dimensional effects on several timescales simultaneously. If neuropeptide signaling truly is as ubiquitous as the data suggest, it represents an additional, underappreciated aspect to brain circuitry. It would have major impacts on neuronal physiology and drastically increase the dimensionality of neuronal signaling.

Conclusions

Neurons are a unique cell type because the vast majority are mitotically inactive and must survive throughout the life of the organism. They have become extremely specialized to allow for multifaceted computations and brain processes. In order to begin understanding the vast complexity of the brain, it is vital to have a cellular 'parts list'. However, even creating guidelines that define neuronal groups is difficult because no one gene or characteristic is sufficient to define discrete subtypes. In addition to this, another major challenge is ensuring there is functional relevance to any group that is defined. Because they are so heterogeneous, there are many ways that a population of neurons can be subdivided. The foundation of each of these traits, however, can be defined by their gene expression. Recent advances in single-cell RNA sequencing have allowed unprecedented access to the genetic signatures of individual neurons throughout the brain. With this, many neuronal genetic subclasses have now been cataloged, but the important next step is to validate these genetically-defined subpopulations.

Mouse dopaminergic neurons are a vital population of neuromodulatory cells that project throughout the brain and play a role in a various behaviors. While their heterogeneity has always been evident, recent work has outlined how truly diverse DA neurons are in their anatomy, circuitry, physiology, and response to disease. Importantly, their gene expression at the single cell level has also recently been uncovered, revealing approximately 6 subpopulations of DA neurons within the midbrain. This information paves a path forward towards reproducible targeting of specific subpopulations and the building of new tools to access these subgroups. What has become clear through scRNAseq is the need for multiple genetic markers to label neurons, necessitating the use of new intersectional mouse models. Intersectional genetic approaches have been used for nearly two decades in *Drosophila* and *C. Elegans*, but it wasn't until recently that they have started to be developed to study mouse neuronal heterogeneity. With new tools we can start to explore the behavioral consequences of DA neuron subpopulation activation, and the impact of neuropeptide expression in specific sub-circuits.

Dissertation research goals

Given their close anatomical proximity and similar genetic makeup, it has been a challenge to parse the functional and behavioral differences between dopaminergic subpopulations consistently and reliably. For this reason, it is important to determine their inherent genetic 'ground-state' to define discrete genetic differences and subclasses of DA neurons and allow new tools to access them. The goal of this dissertation is to first determine the genetically-defined subpopulations of dopamine neurons through scRNAseq. This will provide a foundation upon which DA neurons can be reliably subdivided. Second, using this information, the next task is to uncover whether genetically defined dopaminergic populations are functionally relevant in regards to their anatomy, projections, and response to disease. Finally, we want to build tools to help address and explore dopaminergic heterogeneity. With these tools, we can parse out DA's role in discrete behaviors and explore sub-circuits that are defined by the expression of different genes of interest.

Figures and legends
Figure 1.
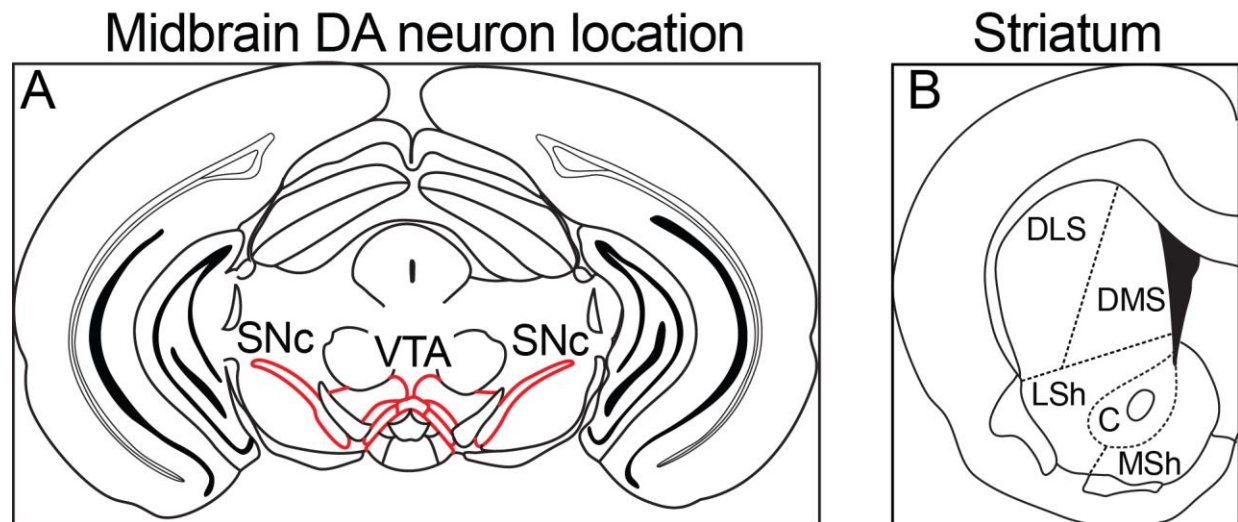
Figure 1. A) Coronal view of the mouse midbrain. Location of midbrain DA neurons shown in red. Substancia nigra pars compacta – SNc, ventral tegmental area – VTA. **B)** Coronal image of the striatum, the major target of midbrain DA neurons. Dorsal lateral striatum – DLS, dorsal medial striatum – DMS, nucleus accumbens lateral shell – LSh, nucleus accumbens core – C, nucleus accumbens medial shell – MSh. Schematics based on the Paxino's Mouse Brain Atlas[197]

Chapter 2: Combinatorial expression of *Grp* and *Neurod6* defines dopamine neuron populations with distinct projection patterns and disease vulnerability

Daniel Joseph Kramer, Davide Risso, Polina Kosillo, John Ngai, & Helen Bateup
Previously published in eNeuro, May 21st, 2018 (DOI: 10.1523/ENEURO.0152-18.2018)

Department of Molecular and Cell Biology
University of California Berkeley

Introduction

Midbrain dopamine (DA) neurons of the substantia nigra pars compacta (SNc) and ventral tegmental area (VTA) make widespread projections throughout the brain and modulate a host of behaviors from motor function to reward learning to cognition[60]. Although they represent only about 0.03% of neurons in the mouse brain, DA neurons are heterogeneous as they vary significantly in their circuitry[59,112,118,119], physiology[100,113], gene expression[177,178], and response to disease[58,76,198,199]. VTA DA neurons are particularly diverse, as they comprise multiple sub-circuits projecting to different brain regions and have distinct electrophysiological properties according to their projection target[61,100,110]. Depending on their connectivity, VTA neurons can also mediate opposing behaviors, such as reward and aversion[145], necessitating tools that can parse this functional heterogeneity to allow selective manipulation of specific VTA subpopulations[200,201]. Building on prior studies that identified genetic differences between SNc and VTA neurons[171,174,175,199], recent single-cell genetic profiling studies have uncovered further genetic heterogeneity in the dopamine system, including several subtypes of VTA neurons[177,178]. However, it is currently unknown how these genetically-defined classes of DA neurons map onto subtypes defined by their circuitry and physiology.

A notable feature of dopaminergic subpopulations is their differential vulnerability to disease. For example, in the neurodegenerative disorder Parkinson's disease (PD), SNc DA neurons degenerate earlier and to a greater degree than VTA DA neurons[76,96]. The reason for this selective vulnerability is not well understood, although current hypotheses point to differences in the expression of ion channels and metabolic proteins between SNc and VTA neurons[58,92,174,175,202,203]. Despite the relative sparing of the VTA compared to the SNc, about 40-77% of VTA DA neurons still degenerate[96] and the molecular features that define susceptible versus spared VTA neurons are unknown.

Here our goal was to define dopaminergic subpopulations based on gene expression and determine how these populations map on to DA subtypes defined by physiology and circuitry. To do this we analyzed DA neuron populations marked by two genes, *Grp* and *Neurod6,* that we identified by unbiased single cell-RNA-sequencing, and which have previously been reported to mark subpopulations of VTA dopamine neurons[174,175,177,178,196,204]. With a combination of anatomy, retrograde tracing, and physiology, we show that these genes define overlapping yet distinct DA neuron populations. We further demonstrate that the combinatorial expression of these two genes influences susceptibility to degeneration in a 6-OHDA mouse model of PD. Together, our findings further our understanding of dopaminergic cell type diversity and validate genetic approaches for defining functional cell types in the brain.

Materials and Methods

Mice

Animal procedures were carried out in accordance with protocols approved by the University of California, Berkeley Institutional Animal Care and Use Committee (IACUC) and Office of Laboratory Animal Care (OLAC).

For single-cell RNA-sequencing experiments, DAT[IRES]Cre mice[205] (Jackson Laboratories strain #006660, RGD_12905031) were crossed and maintained with the Ai9 tdTomato Cre-reporter line[206] (Jackson Laboratories strain #007909). For physiology experiments, NEX-Cre mice were obtained from Dr. Klaus-Armin Nave[207] and crossed with the Ai9 mouse line. C57BL/6J mice were used for retrograde bead injections. The ages, sexes, and numbers of mice used are indicated for each experiment in the results and figure legends.

Single-cell RNA-sequencing

Postnatal day (P) 26-34 male and female DAT[IRES]Cre;Ai9 mice were briefly anesthetized with isoflurane, decapitated, and brains were removed and placed in ice-cold, oxygenated ACSF (NaCl 125 mM, $NaHCO_3$ 25 mM, NaH_2PO_4 1.25mM, KCl 2.5 M, $MgCl_2$ 1 mM, $CaCl_2$ 2 mM, glucose 25 mM). The brain was cut coronally into 275 µm sections on a vibratome (Leica VT1000 S) in oxygenated ice cold choline cutting solution (choline chloride 100 mM, $NaHCO_3$ 25 mM, NaH_2PO_4 1.25 mM, KCl 2.5 mM, $MgCl_2$ 7 mM, $CaCl_2$ 0.5 mM, glucose 25 mM, sodium ascorbate 11.6 mM, sodium pyruvate 3.1 mM). Midbrain sections were incubated for 15 minutes in ACSF at 34°C. Midbrain (including the hypothalamus) was dissected in ACSF using forceps under a dissection microscope. Midbrain sections were incubated in 10 mL oxygenated papain solution (Papain 10 U/mL (Worthington #LK003176) in ACSF with 10 mM HEPES, 10 U/ml DNase, 2.5 mM EDTA, 2.5 mM cysteine, 1 mM kynurenic acid, and 5 mM $CaCl_2$) for 25 minutes at 34°C. Following papain digestion, tissue was placed into 9 mL oxygenated STOP-ovomucoid inhibitor solution (1 mL/mg ovomucoid (Worthington #LK003182) in HEPES-ACSF, 10 U/mL DNase, 1 mM kynurenic acid, and 5 mM $CaCl_2$) and bubbled gently at 34°C. 8 mL of the supernatant solution was removed, and the tissue was triturated serially in the remaining 2 mL of solution with polished 3, 2, and 1 mm glass pipettes to create a single cell suspension. The 2 mL single-cell suspension was spun down in a 20% percoll solution (600 µL percoll (Sigma #P4937) in 2.4 ml STOP-ovomucoid solution) at 430 x g for 6 minutes at room temperature (RT). The supernatant was aspirated leaving ~50 µL of solution and the cell pellet. The pellet was resuspended in 1 mL HEPES-ACSF with 1 mM kynurenic acid and 5% FBS (Life Technologies #16140063).

This single cell suspension was sorted on a BD Influx cell sorter in the Flow Cytometry Facility at UC Berkeley. Cells were gated for PI-/tdTomato+ and sorted into a PCR tube. Based on the number of neurons sorted and cell viability count, neurons were brought to ~200,000 neurons/mL. Neurons were then put into a large Fluidigm C1 chip and each of the 96 wells were visually inspected to verify cell presence, cell health, and tdTomato expression. Wells containing cell doublets were excluded from further processing.

Cells went through single-cell mRNA extraction using the Fluidigm C1 system in the Functional Genomics Laboratory at UC Berkeley. Single cell cDNA was removed and measured via Qubit. Any cell that gave less than 0.3 µg/mL of cDNA was removed due to likely low quality. cDNA from single cells that passed the initial quality check was diluted to 0.3 µg/mL. 379 single neuron cDNA extracts were library prepped using the Nextera DNA library prep protocol (Illumina #FC-121-1012). The cDNA was then sequenced on a HiSeq 2500 in the Vincent J. Coates Genomics Sequencing Laboratory at UC Berkeley.

Single-cell RNA-seq preprocessing

Reads were aligned to the GRCm38.3 (mm10, patch release 3) mouse genome assembly with *Tophat2* (v. 2.1.1)[208] and low quality reads were removed with *Trimmomatic* (v. 0.3.2)[209]. Gene expression was quantified using *featureCounts* (v 1.5.0-p3)[210] and RefSeq transcript annotation. Reads that aligned to more than one gene as well as chimeric fragments were excluded. We used a quality control (QC) pipeline that computes an extensive set of quality metrics, relying in part on *FastQC* (v 0.3.2) and the *Picard tools* (v. 2.5.0 with *samtools* 1.3.1) as done previously[211]. We used the Bioconductor package *scone* (https://bioconductor.org/packages/scone; v. 0.99.6) to perform data-adaptive cell and gene filtering. This yielded the following exclusion criteria: any cell with fewer than 500,000 aligned reads or a percentage of aligned reads below 85%. In addition, we filtered out cells with large drop-out rates, as defined by the "false negative curves" of scone. This procedure resulted in a total of 232 retained cells (out of 379). Finally, we retained only those genes having at least 10 reads in at least 10 cells (10,983 genes).

Single-cell RNA-seq statistical analysis

We performed and assessed several normalization schemes using *scone*[212] and selected full-quantile normalization[213,214]. We then applied principal component analysis on the normalized data and retained the first 50 principal components, which explained 41% of the variance. Cluster analysis was performed on the first 50 principal components using the *RSEC* method[215] implemented in the Bioconductor package *clusterExperiment* (https://bioconductor.org/packages/clusterExperiment; v. 1.0.0), as previously described[211]. We used RSEC with the following specific parameters: alphas = 0.3, minSizes = 5, combineProportions = 0.5; all the other parameters were left at their default values. RSEC found 9 stable clusters. We used *limma* (v. 3.30.13) with *voom* correction weights[216], as implemented in the *clusterExperiment* function *getBestFeature*, to find marker genes for each cluster. To visualize the clustering results, we applied ZINB-WaVE[215] (with K=10) for dimensionality reduction, followed by t-Distributed Stochastic Neighbor Embedding (t-SNE; perplexity parameter set to 20) .

Code Accessibility

The computer code for the single-cell RNA-seq analysis is available at https://github.com/drisso/striatum. This code was run on an Apple Mac computer with macOS Sierra 10.12.4 operating system.

Fluorescent *in situ* hybridization

To visualize mRNA we used the RNAScope fluorescent *in situ* hybridization (FISH) method (ACDBio). Fresh-frozen tissue was processed as per RNAScope instructions. Briefly, mouse brain tissue from male and female mice aged P21-120 was fresh-frozen in OCT on dry ice and stored at least overnight at -80°C. Tissue was then cut on a cryostat (Leica Microm HM550) into 12 µm sections and mounted onto slides. Slides were fixed in 4% PFA in 1x PBS for 15 minutes. Slides were dehydrated using 5 minute incubations in 50%, 70%, and twice with 100% ethanol. Slides were incubated with RNAScope Protease IV (ACDBio #322340) at RT for 30 minutes, and washed with 1x PBS. FISH was then performed using the RNAScope Multiplex Fluorescent assay (ACDBio #320850) per the manufacturer's instructions and protocols. Following FISH, slides were briefly dried and coverslipped using ProLong Gold Antifade mounting media (Invitrogen #P36934).

RNAScope probes used: mM-Neurod6 (#444851), mM-Grp (#317861), mM-Th (#317621), mM-Slc6a3 (#315441), mM-Lydp1 (#447081).

Microscopy and image analysis

Two confocal microscopes were used to take Z-stack images of FISH-labeled or immunostained sections: an Olympus FV1000 with a 20x Nikon Eclipse objective and a Zeiss LSM 710 AxioObserver with Zeiss 10x, 20x, and 63x oil objectives housed in the Molecular Imaging Center at UC Berkeley. Images were analyzed using the FIJI image analysis toolbox. Cells were considered positive for *Neurod6*, *Grp,* or *Lypd1* if they contained three fluorescent puncta within the boundary created by a cell marker: *DAT*, *TH,* or DAPI.

Retrobead and virus intracranial injections

P14-P18 wild-type male and female mice were used for retrograde labeling experiments. Green Retrobeads IX (Lumaflour #G180) were diluted 1:7 in sterile 1x PBS unless otherwise noted. Beads were bilaterally injected using a pulled glass pipette. The following coordinates from bregma and bead volumes were used to target each projection site: dorsomedial striatum (DMS) (M/L +/-1.35 mm, A/P +.75 mm, D/V -2.60 mm, 400 nL beads), dorsolateral striatum (DLS) (M/L +/-2.15 mm, A/P +.70 mm, D/V -2.50 mm, 400 nL beads), nucleus accumbens (NAc) medial shell (M/L +/-0.75 mm, A/P +1.20 mm, D/V -4.15 mm, 300 nL beads), NAc core (M/L +/-1.2 mm, A/P +1.10 mm, D/V -4.05 mm, 300 nL beads), NAc lateral shell (M/L +/-1.75 mm, A/P +1.05 mm, D/V -3.95 mm, 300 nL beads), basolateral amygdala (M/L +/-2.65 mm, A/P -1.05 mm, D/V -4.40 mm, 120 nL beads at 1:3 dilution), medial prefrontal cortex (four injections per hemisphere at two different depths per injection: M/L +/-0.35 mm, A/P +1.50 mm, +1.65 mm, +1.80 mm, and +1.95 mm, D/V -2.00 mm and -1.40 mm, 400 nL total per hemisphere), lateral septum (M/L +/-0.45 mm, A/P +0.40 mm, D/V -2.70 mm, 300 nL beads).

To allow for sufficient DA neuron labeling, mice were sacrificed at various time points following injection: 7 days for the DMS and DLS, 21 days for the prefrontal cortex, and 14 days for the NAc (MSh, core, and LSh), lateral septum and amygdala. Brains were harvested and cut to separate the injection site and midbrain. The midbrain was frozen

26

for cryostat sectioning as described above for FISH. The brain region containing the injection site was incubated in 4% PFA overnight at 4˚C, then cryoprotected in 30% sucrose in 1x PB until the tissue sank. Injection site tissue was sectioned on a freezing microtome, mounted with Vectashield hardset mounting media with DAPI (Vector laboratories #H-1500), and analyzed for bead expression at the injection site. Brains with correctly targeted injection sites and minimal off-target bead expression were chosen for analysis.

To selectively label NEX-Cre expressing neurons in the VTA, we unilaterally injected 800 nL of a Cre-dependent tdTomato virus (AAV1.CAG.Flex.tdTomato.WPRE.bGH, Penn Vector Core #AV-1-ALL864) into heterozygous NEX-Cre mice at P16. To target the VTA we used the following coordinates from bregma: M/L +/-0.25 mm, A/P -2.9 mm, D/V -4.45 mm.

Immunohistochemistry
Immunohistochemistry was performed as described previously[217]. The following antibodies were used: tyrosine hydroxylase (TH, ImmunoStar #22941, RRID:AB_572268), Alexa-488 goat anti-mouse secondary (ThermoFisher Scientific #A-11001, RRID:AB_2534069), Alexa-633 goat anti-mouse secondary (ThermoFisher Scientific #A-21050, RRID:AB_2535718), streptavidin Alexa-488 conjugate (ThermoFisher Scientific #S32354, RRID:AB_2315383), streptavidin Alexa-633 conjugate (ThermoFisher Scientific #S21375, RRID:AB_2313500).

Electrophysiology
275 µm thick coronal midbrain slices were prepared from P56-105 NEX-Cre;Ai9 or DAT^{IRES}Cre;Ai9 mice of both sexes on a vibratome (Leica VT1000 S) in ice cold high Mg^{2+} ACSF containing in mM: 85 NaCl, 25 NaHCO$_3$, 2.5 KCl, 1.25 NaH$_2$PO$_4$, 0.5 CaCl$_2$, 7 MgCl$_2$, 10 glucose, and 65 sucrose. Slices were recovered for 15 minutes at 34°C followed by 50 minutes at RT in ACSF containing in mM: 130 NaCl, 25 NaHCO$_3$, 2.5 KCl, 1.25 NaH$_2$PO$_4$, 2 CaCl$_2$, 2 MgCl$_2$, and 10 glucose. NEX-Cre+ VTA neurons were identified by tdTomato fluorescence in NEX-Cre;Ai9 mice. SNc neurons were defined either by the presence of green retrobeads injected into the dorsolateral striatum in NEX-Cre;Ai9 mice or by tdTomato fluorescence and anatomical location in DAT^{IRES}Cre;Ai9 mice. For whole cell recordings, 2.5-6 mΩ glass pipettes were filled with a potassium-based internal solution containing in mM: 135 KMeSO$_3$, 5 KCl, 5 HEPES, 4 Mg-ATP, 0.3 Na-GTP, 10 phospho-creatine, 1 EGTA, and 4mg/ml neurobiotin (Vector laboratories #SP-1120). Recordings were obtained using a MultiClamp 700B amplifier (Molecular Devices) and ScanImage software. Passive membrane properties were recorded in voltage clamp with the membrane held at -70 mV. Spontaneous action potentials were recorded in current clamp. In current clamp, 500 ms steps of negative current were delivered (-25 to -150 pA) to hyperpolarize the membrane to approximately -100 mV. During the steps, current was injected to maintain the baseline membrane potential at -70 mV. All recordings were performed at RT in the presence of synaptic blockers (NBQX 10 µM, CPP 10 µM, picrotoxin 50 µM, final concentration). Data were analyzed in Igor (Wavemetrics) using custom scripts.

6-OHDA injection

6-hydroxydopamine (6-OHDA) (6-hydroxydopamine hydrobromide with ascorbic acid: Sigma-Aldrich #H116-5MG) injections were made into the medial forebrain bundle of P120 female mice as previously described[218]. Thirty minutes prior to 6-OHDA injection, a solution containing 0.5 mg/mL pargyline (Sigma Aldrich #P8013 500mg) and 2.5 mg/mL desipramine hydrochloride (Tocris #3067) was injected intraperitoneal at a dose of 5mg/kg pargyline and 25 mg/kg desipramine. 200 nL injections of freshly prepared 15 mg/mL 6-OHDA in sterile saline + 0.02% ascorbic acid were injected into the medial forebrain bundle (MFB, coordinates from bregma: M/L +/- 1.2mm, A/P 1.2mm, D/V - 4.90). Adult female wild-type mice were used as younger mice and male mice showed poor recovery following injection. 250-350 µL of meloxicam (5-10 mg/kg dose) was injected subcutaneously as an analgesic.

Mice were monitored daily following the injection to ensure recovery. Kitten Milk Replacement (Santa Cruz #sc-362120) was fed to mice daily for up to two weeks following the injection to aid recovery and meloxicam was injected subcutaneously to alleviate pain if necessary. Motor function was assessed using the cylinder test each week following the injection (see below). Four weeks following 6-OHDA injection, mice were quickly anesthetized using isoflurane, decapitated, and their brains were fresh-frozen as described above for FISH.

Cylinder test

To test the severity of Parkinsonian-like symptoms following unilateral 6-OHDA injection, we used the cylinder test to score limb use asymmetry. Mice were habituated to the behavior room for a minimum of 30 minutes during their dark cycle under red light illumination. Mice were placed into a clear plastic cylinder 12 cm in diameter and 20 cm in height. The cylinder was placed next to two mirrors to visualize paw use. The mouse was both video recorded and observed by the experimenter while it was allowed to move around freely in the cylinder for 10 minutes. Full 360˚ ipsiversive and contraversive rotations (relative to the 6-OHDA injection side) were counted. Forelimb asymmetry was measured by counting the number of times the ipsilateral paw, contralateral paw, or both paws were used for support when the mouse reared against the wall of the cylinder. The percentage of ipsilateral or contralateral paw use was calculated based on total rears (e.g. ipsilateral paw touches/ipsilateral + contralateral + both paw touches). A greater number of ipsiversive turns and ipsilateral paw use indicates a successful 6-OHDA injection and unilateral Parkinsonian-like symptoms.

Experimental Design and Statistical Analysis

A one-way ANOVA was used to compare the means of three or more groups. Post-hoc pairwise comparisons were made using either Bonferroni or Tukey's multiple comparisons tests. Unpaired, two-tailed t-tests were used to compare the means of two groups. A paired, one-way ANOVA with Dunnett's multiple comparisons post-hoc test was used to compare DA neuron subpopulations to the entire VTA DA population for the 6-OHDA experiments. Data are reported as the mean +/- S.E.M.

Results

Single-cell RNA-sequencing of midbrain dopamine neurons

To define subclasses of DA neurons in an unbiased way, we performed single-cell RNA-sequencing of DA neurons from P26-P34 male and female mice in which dopamine transporter (DAT)-expressing neurons were labeled with a tdTomato reporter (DAT[IRES]Cre;Ai9, Fig. 1-1A). A bioinformatic and statistical workflow revealed nine clusters of DA neurons based on differential gene expression (Fig. 1-1B-E). We identified markers for each cluster and validated eight of the nine clusters. Two of the clusters corresponded to DA subpopulations in the hypothalamus, four defined subclasses of VTA neurons, and two corresponded to the SNc (Fig. 1-1F). These populations are consistent with recent single-cell DA neuron profiling studies[177,178,219].

Grp and *Neurod6* define anatomically overlapping but distinct midbrain subpopulations

Consistent with prior studies[177,178] , we identified a cell cluster that showed relatively high and selective expression of *Grp*, *Neurod6,* and *Gpr83* (cluster #8, Fig. 1-1C). Given recent interest in *Neurod6* and *Grp* as markers that label ventromedial VTA dopamine neurons[178,196,204] we chose to quantitatively analyze their expression patterns in the midbrain and examine the extent of their co-expression. Using multiplex fluorescent *in situ* hybridization (FISH) we found that in adult mice, *Grp*-expressing neurons represented 29.9% +/- 0.5% of the total midbrain DA neuron population (1804/6407 neurons from 8 mice) and 35.9% +/- 0.4% of DA neurons in the VTA (1570/4377 neurons from 8 mice) (Fig. 1A-D). 97.4% +/- 0.7% of *Grp+* cells in the midbrain were dopaminergic, defined by co-expression of tyrosine hydroxylase (*TH*) mRNA (1780/1822 cells from 4 mice). *Grp+* DA neurons were found in all subregions of the VTA but were enriched in the ventromedial portions of the VTA, the interfascicular nucleus (IF) and paranigral/para-interfascicular nuclei (PN/PIF) (p<0.0001[a], one-way ANOVA with Tukey's post-hoc test, Fig. 1E). Notably, while *Grp* was previously identified as a VTA marker[174,175,196], we also found *Grp*-expressing DA cells in the ventromedial portion of the SNc (22.7% +/- 1.8% of DA neurons in this region, Fig. 1A-F).

Neurod6 expression defined a more restricted DA population, accounting for 26.8% +/- 0.5% of VTA DA neurons (1172/4377 neurons from 8 mice), with the highest density of *Neurod6+* DA neurons in the ventromedial IF and PN/PIF regions (p<0.0001[b], one-way ANOVA with Tukey's post-hoc test, Fig. 1E). In contrast to *Grp*, *Neurod6* mRNA was not expressed in the SNc (Fig. 1A-F). 93.1% +/- 0.6% of *Neurod6+* VTA neurons were dopaminergic (948/1016 cells from 4 mice). Consistent with our RNA-seq data, we found that while the majority (77.5% +/- 0.8%, 909/1172 cells from 8 mice) of *Neurod6+* DA neurons co-expressed *Grp*, only about half (57.9% +/- 1.0%, 909/1570 cells from 8 mice) of *Grp+* VTA DA neurons co-expressed *Neurod6*. Broken down by sub-region, the majority of *Neurod6+* DA neurons in the IF and PN/PIF co-expressed *Grp*, however, a third of *Neurod6+* DA neurons in the PBP did not have detectable *Grp* expression of *Grp* (Fig. 1F-H). *Grp*-expressing but *Neurod6*-lacking DA neurons were found throughout the VTA and nearly all of the *Grp+* DA neurons in the SNc were lacking *Neurod6* (Fig. 1F-I). Together, these data show that *Grp* is expressed in a subpopulation of midbrain DA neurons spanning the VTA and ventromedial portion of

the SNc. *Neurod6* is expressed in a more restricted midbrain population, defining a subgroup of the *Grp+* DA population located exclusively in the VTA. In addition, we find a small subset of neurons that express *Neurod6* but not *Grp*.

To determine whether these cell populations were present throughout development, we assessed *Grp* and *Neurod6* expression at multiple ages. We found that while there were subtle increases in the percentages of *Grp+* VTA DA neurons from 8 to 16 weeks (p=0.036[c], one-way ANOVA with Tukey's post-hoc test, Fig. 1G) and *Neurod6+* VTA DA neurons from 2 to 16 weeks (p=0.024[d], one-way ANOVA with Tukey's post-hoc test, Fig. 1H), the proportions of DA neurons expressing these markers were largely stable from two weeks postnatal through adulthood (P14 to P112). We also investigated whether these cell populations were similar between sexes. We found that the *Grp* and *Neurod6*-expressing DA subpopulations were present in male and female mice in similar proportions throughout VTA and SNc subregions (see statistics worksheet for unpaired t-test p values[g-o], Fig. 1I,J). Furthermore, in the RNA-sequencing data, we found no significant differences in expression levels of *Grp* or *Neurod6* between males and females (log2-fold-change of 1.70 for *Neurod6*, p=0.51[e] and 0.94 for *Grp*, p=0.68[f] in males versus females). These data demonstrate that the *Grp+* and *Neurod6+* DA neuron populations are present in both sexes and stable over time.

Grp and *Neurod6*-expressing neurons strongly project to the nucleus accumbens medial shell

VTA DA neurons comprise multiple sub-circuits, which send projections to different brain regions with distinct functional consequences[220]. To determine whether the *Grp* and *Neurod6* VTA DA populations have specific projection targets, we combined retrograde labeling from eight primary DA neuron projection sites with *Grp* and *Neurod6* FISH (Fig. 2A and Fig. 2-1A). We found that of the DA neurons projecting to the medial shell of the nucleus accumbens (NAc), 75.0% +/- 1.1% were *Grp* positive and 70.4% +/- 2.5% were *Neurod6* positive indicating that these markers were expressed in the majority of medial shell-projecting DA neurons (Fig. 2B,C,F,H). *Grp+* and *Neurod6+* DA neurons also projected to the NAc core and lateral shell but represented a smaller fraction of the neurons projecting to these regions compared to the medial shell (Fig. 2F,H). When quantified as a percentage of the total marker-positive bead-labeled DA neurons across all injection sites, the NAc medial shell was the primary target region for both *Grp+* and *Neurod6+* DA neurons (Fig. 2G,I). Together these findings indicate a strong mesoaccumbens projection from *Neurod6+/Grp+* VTA DA neurons.

We found that *Neurod6* mRNA was largely absent from DA neurons projecting to regions outside of the NAc, indicating a selective output of the *Neurod6+* DA neuron population (Fig. 2H,I). By contrast, *Grp+* DA neurons represented a substantial percentage (47.3% +/- 2.4%) of DA neurons projecting to the dorsomedial (DMS), but not dorsolateral (DLS), striatum (Fig 2D-G). 87.7% +/- 2.5% of the DMS projecting *Grp*-positive neurons were located in the ventromedial portion of the SNc (Fig. 2-1B), consistent with prior reports mapping dopaminergic projections to the DMS[113]. These neurons lacked expression of *Neurod6* as essentially no DMS-projecting neurons were *Neurod6*-positive (Fig. 2H,I). Taken together, these results indicate that there are at

least two populations of DA neurons that express *Grp*: those located in the VTA that project primarily to the medial NAc and those in the ventromedial SNc, which project selectively to the DMS (Fig. 2-1B,C).

A recent study showed that *Neurod6*-expressing DA neurons, labeled by a Cre reporter in NEX-Cre mice (*Neurod6* was previously referred to as *NEX*[207]), project to the lateral septum[204]. We found relatively few lateral septum-projecting neurons in the midbrain, of which 37.4% +/- 3.1% were non-dopaminergic (92/252 cells from 4 mice). Of the DA neurons projecting to the lateral septum, 17.0% +/- 2.3% were *Grp*+ and 24.0% +/- 3.0% were *Neurod6*+ (Fig. 2F,H). Quantified as a percentage of total bead-labeled neurons, less than 2% of *Grp*+ or *Neurod6*+ DA neurons projected to the lateral septum (Fig. 2G,I). These results indicate that compared to other brain regions, the lateral septum is not a major target for *Grp* or *Neurod6*-expressing VTA DA neurons.

<u>*Neurod6*+ DA neurons have unique physiological properties</u>
DA neurons projecting to different target areas possess distinct electrophysiological profiles[100,110,113]. To investigate whether *Neurod6*-expression defines a physiologically distinct subclass of DA neurons, we used NEX-Cre knock-in mice[207]. We injected virus expressing a Cre-dependent tdTomato reporter into the midbrain (AAV-Flex-tdTomato) and found NEX-Cre+ DA neurons along the ventromedial portion of the VTA (Fig. 3A), consistent with the expression pattern of *Neurod6* mRNA. In agreement with our tracing data, we found that tdTomato-labeled NEX-Cre+ neurons projected strongly to the NAc medial shell and core (Fig. 3B). To visualize NEX-Cre+ neurons for physiology, we crossed NEX-Cre mice to the Ai9 tdTomato Cre-reporter mouse line[206]. We performed FISH for *Neurod6* mRNA in NEX-Cre;Ai9 mice (Fig. 3C) and found that 93.6% +/- 1.2% of tdTomato–positive DA neurons in the VTA co-expressed *Neurod6* (331/353 cells from 4 mice), making this a suitable model to use for targeted electrophysiology recordings. Consistent with the 77.5% of *Neurod6*+ neurons that co-expressed *Grp*, 73.7% +/- 2.9% of the NEX-Cre;tdTomato positive VTA DA neurons expressed *Grp* (175/232 cells from 4 mice). We did observe that not all *Neurod6*+ VTA DA neurons expressed tdTomato in the NEX-Cre;Ai9 mice (30.4% +/- 1.7% of *Neurod6*+ DA neurons were tdTomato positive, 361/1092 cells from 4 mice). In addition, a third of the tdTomato-positive midbrain neurons were non-dopaminergic (36.9% +/- 3.4% TH negative, 193/546 cells from 4 mice). This discrepancy may be due to transient Cre expression in non-DA neurons during development. These data suggest that NEX-Cre mice may not be appropriate for studies requiring selective access the entire *Neurod6*+ VTA DA subpopulation, but can be used to target *Neurod6*+ cells for whole cell recordings in which dopaminergic identity can be confirmed post-hoc.

To determine whether *Neurod6*-expressing neurons represent a functionally distinct cell class, we recorded from tdTomato-labeled NEX-Cre+ neurons in the VTA and analyzed their intrinsic membrane properties, action potential waveform, and response to hyperpolarizing current injection (see Table 3-1 for a complete summary of the physiology data including sample sizes). We confirmed that the NEX-Cre+ neurons analyzed were dopaminergic by filling patched neurons with neurobiotin and co-staining for TH (Fig. 3D,E). We found that NEX-Cre+ DA neurons had a distinct electrophysiological signature compared to "classical" SNc DA neurons. Specifically,

NEX-Cre+ DA neurons exhibited a more depolarized membrane potential (Vm, p=0.0075^p, unpaired t-test), had higher membrane resistance (Rm, p<0.0001^q, unpaired t-test), and reduced membrane capacitance (Cm, p<0.0001^r, unpaired t-test) compared to SNc DA neurons (Fig. 3F-H). NEX-Cre+ DA neurons also had significantly shorter action potentials (p<0.0001^s, unpaired t-test) with a less pronounced afterhyperpolarization (AHP, p=0.0002^t, unpaired t-test) (Fig. 3I-K). Due to their high membrane resistance, NEX-Cre+ DA neurons required less negative current to hyperpolarize to -100 mV compared to SNc DA neurons (-25 to -50 pA for NEX-Cre+ neurons versus -150 pA for SNc neurons). However, they had a significantly smaller sag component, which is indicative of smaller I$_h$ (p<0.0001, unpaired t-test, Fig. 3L-N) and less rebound depolarization (p<0.0001, unpaired t-test, Fig. 3L,M & O). The non-canonical electrophysiological characteristics of NEX-Cre+ neurons are consistent with those reported for NAc medial shell-projecting DA neurons[100], suggesting that *Neurod6* is a useful marker for this VTA subpopulation.

Neurod6-lacking VTA DA neurons show increased susceptibility to degeneration in a 6-OHDA mouse model

In addition to their anatomical location, projection target, and physiology, vulnerability to degeneration is a key feature of DA neurons that differs by subtype. Previous *in vitro* studies have implicated both *Neurod6* and *Grp* as being potentially neuroprotective[98,99,174,221]. In mice, expression of *Neurod6* and the related transcription factor *Neurod1* are important for survival of dopamine neurons during development[204]. *Grp*-expressing cells have been observed in post-mortem tissue from Parkinson's disease patients, suggesting that *Grp*-expression may be related to cell survival[196]. We therefore investigated the sensitivity of *Neurod6* and/or *Grp*-expressing VTA dopamine neurons to degeneration in a mouse model of PD. To do this, we injected the dopaminergic toxin 6-hydroxydopamine (6-OHDA) unilaterally into the medial forebrain bundle of adult (P120) female mice[218]. 6-OHDA resulted in a progressive, unilateral loss of DA neurons with a 96.0% +/- 0.6% reduction in SNc DA neurons and a 69.3 +/- 1.1% loss of VTA DA neurons after four weeks (Fig. 4A). We confirmed DA axon denervation throughout the striatum in the 6-OHDA injected hemisphere, with notable sparing of DA projections to the NAc medial shell and core (Fig. 4B). DA neuron loss led to unilateral motor impairment as measured by the cylinder test (p=0.0002^w, one-way ANOVA with Tukey's post-hoc test: saline paw vs. 6-OHDA paw p=0.0163, saline paw vs. both paws p=0.0157, 6-OHDA paw vs. both paws p=0.0002, n=4 mice).

To determine how *Grp* and *Neurod6*-expressing DA neurons in the VTA responded to neurotoxic stress (Fig. 4C-F), we compared the reduction of *Grp*+ and/or *Neurod6*+ VTA DA neurons between the saline and 6-OHDA hemisphere to all VTA DA neurons defined by *Th* expression (p<0.0001^x, paired one-way ANOVA with Tukey's post-hoc test, Fig. 4G). For this analysis, we only included VTA DA neurons as essentially all SNc neurons (including *Grp*+ SNc neurons) degenerated in the 6-OHDA-injected hemisphere (Fig. 4A,C & D). We found that four weeks following 6-OHDA injection, 26.1% +/- 2.7% of *Grp+/Neurod6*+ DA neurons survived, which was similar to the percentage of total *Th*+ VTA neurons surviving (30.7% +/- 1.1%) (Fig. 4G). Notably, VTA DA neurons that expressed only *Neurod6* and not *Grp* (*Grp-/Neurod6*+) were

significantly spared compared to the rest of VTA DA neurons, with 82.7% +/- 4.2% of neurons surviving (Fig. 4G). By contrast, VTA DA neurons that expressed *Grp* but not *Neurod6* (*Grp+/ Neurod6-*) showed slightly increased vulnerability compared to all VTA DA neurons with 21.7% +/- 2.0% surviving (Fig. 4G). Therefore, the DA neuron subpopulations marked by expression of *Grp* and/or *Neurod6* have different responses to 6-OHDA and VTA neurons lacking *Neurod6* are more susceptible to degeneration.

An increase in the proportion of *Neurod6+* DA neurons in the VTA following 6-OHDA could be due to selective sparing of the *Neurod6* cell population or from *Neurod6* expression turning on in surviving neurons of other VTA subpopulations. To attempt to distinguish these possibilities, we performed FISH for another VTA DA neuron subtype marker *Lypd1*[178]. Under normal conditions, *Lypd1* was expressed almost exclusively in the PBP subregion of the VTA as well as throughout the SNc (Fig. 4D,F). *Neurod6* was generally not co-expressed in *Lypd1+* DA neurons (7.0% +/- 1.6% of *Lypd1+* DA neurons co-expressed *Neurod6*, Fig. 4D,F & H), indicating that these markers define distinct cell populations. In response to 6-OHDA, we found that 20.4% +/- 1.3% of *Lypd1+*/Neurod6- VTA DA neurons survived, which was significantly lower than the total VTA DA population (Fig. 4G). The surviving *Lypd1+* VTA DA neurons did not turn on expression of *Neurod6*, as the proportion of *Neurod6+/Lypd1+* double positive VTA DA neurons remained low and was the same between the saline injected and 6-OHDA injected hemispheres (p=0.8091^y, paired t-test, Fig. 4H). These results suggest that the VTA DA subpopulation defined by *Neurod6* expression, which lacks *Grp* or *Lypd1*, is preferentially spared in response to a neurotoxic challenge.

Discussion

Midbrain DA neurons are small in number but vast in their behavioral influence[60,220]. As such, dopaminergic dysfunction is associated with numerous psychiatric and neurologic disorders ranging from drug addiction to Parkinson's disease[76,96,222]. Recent studies have revealed that the dopaminergic system is heterogeneous at multiple levels from gene expression to circuitry to physiology to behavior[61,220] . To tackle this heterogeneity, it is necessary to identify genetic markers that define functional DA neuron subtypes. This would enable the generation of tools that allow selective manipulation of dopaminergic subpopulations. Here we investigated two markers that we and others have identified as labeling dopaminergic subpopulations, *Grp* and *Neurod6*. We show that the combinatorial expression of these genes defines the anatomical location, projection target, physiology, and disease susceptibility of DA neurons.

We found that *Grp*, which encodes the neuropeptide gastrin-releasing peptide[223], was expressed in a third of midbrain DA neurons, of which more than half co-expressed *Neurod6.* These *Grp+*/*Neurod6+* neurons resided in the VTA and projected to the medial portions of the NAc. This is consistent with prior reports showing that *Grp* is expressed in a subpopulation of VTA DA neurons that shows overlap with *Neurod6-*expressing neurons[174,175,177,178,196]. The fact that these neurons project to the NAc corroborates a projection-specific translational profiling study reporting that ribosome-bound *Grp* mRNA was enriched in the population of VTA DA neurons projecting to the NAc compared to the rest of the VTA[224]. Notably, we also identified a previously undiscovered population of *Grp+* DA neurons that lack *Neurod6*, which were located in the ventromedial portion of the SNc. These neurons sent projections to the dorsomedial striatum with very little innervation of the dorsolateral striatum. The anatomical location of these cells in the ventral SNc is consistent with dopamine neurons that project to the DMS, which have unique physiological and behavioral properties compared to DLS-projecting DA neurons located in the dorsal SNc[113].

Neurod6-expression defined a smaller population of DA neurons that were located in the ventromedial VTA, projected selectively to the medial NAc, and exhibited non-canonical physiological properties. While *Neurod6* has previously been identified as a VTA marker[174,178,196,204], our study is the first to systematically map the projection sites of these cells, revealing a specific medial NAc projection with very little output to other DA target regions. This medial NAc projection is consistent with the physiology of *Neurod6+* DA neurons, which showed unique characteristics similar to those previously reported for medial NAc-projecting DA neurons defined by retrograde labeling[100]. Mesoaccumbens projections are important for mediating reward-seeking behaviors[112,147,225,226] . Therefore, our identification of *Neurod6* as a marker for this cell population enables future mechanistic investigations into how this DA sub-circuit controls motivated behaviors, the dysfunction of which may be important for the pathophysiology of psychiatric disorders such as drug addiction.

It was previously reported that *Neurod6+* neurons project to the lateral septum based on the axon projections of NEX-Cre mice and fluorogold retrograde labeling[204]. However, projections from the VTA to the lateral septum are relatively sparse compared to the

striatum and NAc[118,227,228]. To investigate this further, we performed retrobead injections into the dorsal and intermediate regions of the lateral septum and found that relatively few VTA DA neurons projected to this area. The lateral septum therefore represented only 2% of total bead-labeled *Neurod6*+ DA cells across all injection sites. This indicates that under our conditions, the lateral septum was not a primary projection site of *Neurod6*+ DA neurons. One possible reason for the discrepancy is that the Khan *et al* study relied exclusively on the NEX-Cre mouse line, as opposed to endogenous *Neurod6*-expression as done here. We found that a substantial proportion (37%) of the VTA neurons labeled in NEX-Cre mice are non-dopaminergic and that many of the VTA neurons projecting to the lateral septum are also non-dopaminergic (37%), which may have contributed to the differing results.

A defining feature of dopaminergic neurons is their susceptibility or resilience to degeneration in the context of Parkinson's disease (PD)[76,96]. As such, significant effort has been made to identify the molecules that determine vulnerability as this has clear clinical importance[58]. Interestingly, in addition to being genes that define specific DA neuron subtypes, both *Neurod6* and *Grp* have been shown to confer neuroprotection in cell culture models[98,99,174,221]. To determine whether the neuronal populations defined by *Neurod6* and/or *Grp* are preferentially spared in the context of PD, we performed unilateral 6-OHDA injections and compared the relative abundance of these markers in the 6-OHDA versus control hemisphere. We found that expression of either of these genes alone was not sufficient to confer neuroprotection as *Grp*+ neurons in the SNc degenerated completely and *Grp*+ neurons in the VTA showed either similar (*Grp+/Neurod6+*) or greater (*Grp+/Neurod6-*) susceptibility relative to all VTA DA neurons. Notably, we did find that the small population of *Neurod6*+ VTA DA neurons that lack *Grp* was significantly spared compared to neighboring DA neurons. This finding is consistent with a potential neuroprotective effect of *Neurod6* but indicates that other factors are likely involved since *Neurod6*+ VTA DA neurons that co-expressed *Grp* were not preferentially spared. Together, these results refine our understanding of the genetic factors contributing to vulnerable and spared DA cell types and suggest that the combinatorial expression of genes in a given cell population is important for defining vulnerability.

In summary, our work provides in-depth characterization of *Neurod6* and *Grp* expression in the midbrain and reveals previously unappreciated complexity in how these markers define specific DA subpopulations. Our results provide new insights into the genetic and functional heterogeneity of the DA system, which is just beginning to be unraveled. Future studies can utilize this information to design intersectional genetic tools based on the expression of two or more genes that will allow access to specific dopaminergic subpopulations. These types of tools represent powerful approaches to dissecting the complex ways in which the DA system contributes to behavior and disease.

Figures and Legends
Figure 1
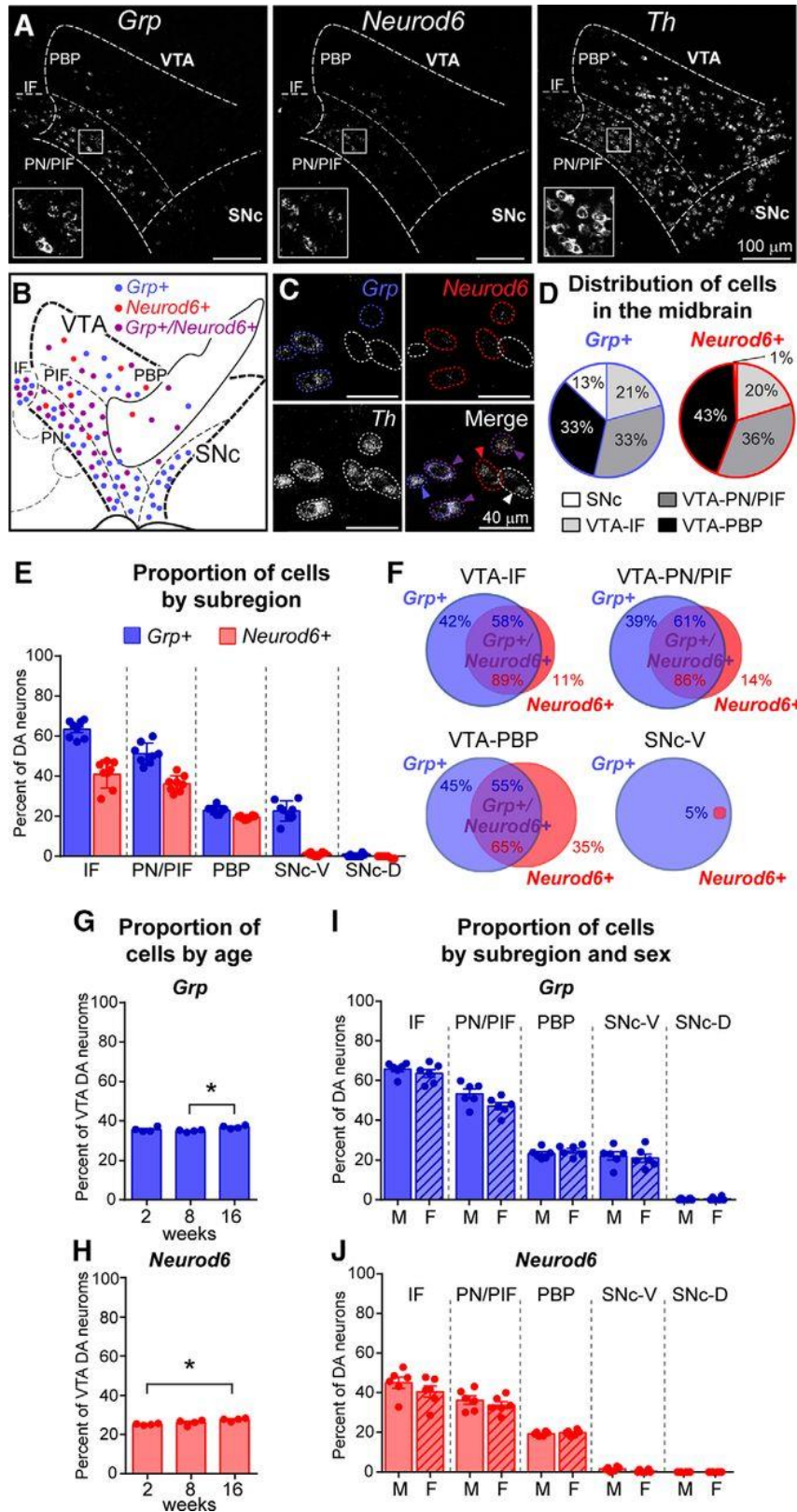
Figure 1: Anatomic analysis of Grp and Neurod6-expressing DA neurons in the midbrain. A) Confocal images of multiplex fluorescent in situ hybridization using probes against Grp (left), Neurod6 (middle), and tyrosine hydroxylase (Th, right) mRNA. Inset boxes show higher-magnification images of the boxed regions. **B)** Schematic showing the location of Grp + (blue), Neurod6+ (red), and Grp+/Neurod6+ (purple) DA neurons in the midbrain. **C)** High-magnification confocal images showing Th-positive VTA neurons expressing Grp (blue circles), Neurod6 (red circles), Grp and Neurod6 (purple circles), or neither marker (white circles). **D)** Charts show the distribution of Grp+ or Neurod6 + neurons across different midbrain regions, expressed as a percentage of the total Grp+ or Neurod6 + population. Only DA neurons, defined by expression of Th mRNA, were included in the analysis, n = 4377 cells quantified from 8 mice (4 male and 4 female). **E)** Quantification of the number of Th + DA neurons that coexpress Grp or Neurod6 in subregions of the VTA and SNc. Bars represent mean ± SEM, dots represent the values from individual mice, n = 4377 Th + cells quantified from 4 male and 4 female mice. Grp one-way ANOVA, p < 0.0001; Tukey's post hoc tests revealed significant (p < 0.0001) differences for each subpopulation compared to all others except the PBP versus SNc-V (p = 0.9998). Neurod6 one-way ANOVA, p < 0.0001; Tukey's post hoc tests revealed significant (p < 0.0001) differences for each subpopulation compared to all others except the IF versus PN/PIF (p = 0.0842) and SNc-V versus SNc-D (p = 0.9699). **F)** Venn diagrams display the extent of overlap between the Grp and Neurod6-expressing DA neuron populations across four midbrain subregions. 1833 cells were quantified from 8 mice (4 male and 4 female). **G-H)** Graphs display the mean ± SEM percentage of Grp+ (G) or Neurod6 + (H) DA neurons in the VTA at 2, 8, and 16 wk. Statistical comparisons were made with a one-way ANOVA with Tukey's post hoc test; Grp 8 wk (34.9%) vs. 16 wk (36.9%), *, p = 0.0316, Neurod6 2 wk (25.2%) vs. 16 wk (27.6%), *, p = 0.0201. Dots represent values from individual mice, n = 2053–2324 cells from 2 male and 2 female mice per time point. **I-J)** Graphs display the mean ± SEM percentage of Grp+ (I) or Neurod6 + (J) DA neurons across subregions of the VTA and SNc in male (M) and female (F) mice. Unpaired t tests between males and females for each region revealed no significant sex differences. Dots represents values from individual mice, n = 3586 cells from 6 male mice and 3424 cells from 6 female mice. IF, interfascicular nucleus; PN/PIF, paranigral/ parainterfascicular nuclei; PBP, parabrachial pigmented nucleus; SNc-V, substantia nigra pars compacta-ventral portion; SNc-D, substantia nigra pars compacta-dorsal portion.

Figure 2

A — Prefrontal Cortex; Striatum and Nucleus Accumbens; Basolateral Amygdala

B — NAc Medial Shell; Retrobeads; 0.5 mm

C — VTA; PBP; IF; PN/PIF; *Slc6a3*; *Neurod6*; Retrobeads; 100 µm

D — Dorsomedial Striatum; Retrobeads; 0.5 mm

E — VTA; PBP; PN/PIF; SNc; *Th*; *Grp*; Retrobeads; 200 µm

F — *Grp* projection targets

G — Percent of *Grp*+/bead+ cells projecting to each region

H — *Neurod6* projection targets

I — Percent of *Neurod6*+/bead+ cells projecting to each region

Figure 2. Projection targets of Grp + or Neurod6+ DA neurons. **A)** Schematic of retrobead injection sites in sagittal view. Numbers correspond to the coronal section schematics below showing the eight projection target sites. mPFC, medial prefrontal cortex; DLS, dorsolateral striatum; DMS, dorsomedial striatum; LSh, lateral shell; C, core; MSh, medial shell; LS, lateral septum; BLA, basolateral amygdala. **B)** Image showing a green fluorescent retrobead injection into the nucleus accumbens (NAc) medial shell with DAPI staining in blue. **C)** Image of the VTA showing fluorescent in situ hybridization (FISH) for Slc6a3 (DAT) mRNA (white), Neurod6 mRNA (red), and green retrobeads from a NAc medial shell injection. **D)** Image showing a green retrobead injection into the dorsomedial striatum (DMS) with DAPI staining in blue. **E)** FISH image of the midbrain showing Th mRNA (white), Grp mRNA (red), and green retrobeads from a DMS injection. Insets boxes in C and E show higher-magnification images of the boxed regions. Red circles identify Neurod6+ (C) or Grp + (E) neurons, green circles define bead-positive neurons, and yellow circles show bead-positive neurons expressing Neurod6 (C) or Grp (E). White circles identify neurons expressing Th only. **F)** Quantification of the percentage of Th +/bead+ midbrain neurons that coexpressed Grp mRNA for each of the projection sites. Bars represent mean ± SEM, each dot represents one mouse. **G)** Summary of the projection targets of Grp + DA neurons expressed as a percentage of total bead+/Grp +/Th + neurons. **H)** Quantification of the percentage of DAT +/bead+ midbrain neurons that coexpressed Neurod6 mRNA for each of the projection sites. Bars represent mean ± SEM, each dot represents one mouse. **I)** Summary of the projection targets of Neurod6 + DA neurons expressed as a percentage of total bead+/Neurod6 +/DAT + neurons. For panels F–I: NAc MSh n = 850 cells from 2 male and 2 female mice, NAc Core n = 858 cells from 2 males and 2 females, NAc LSh n = 1215 cells from 3 males and 1–2 females, DMS n = 637 cells from 3 males and 2 females, DLS n = 1038 cells from 2–4 males and 2–3 females, mPFC n = 211 cells from 3–4 males and 1 female, BLA n = 297 cells from 3 males, and LS n = 345 cells from 2 males and 4 females

Figure 3
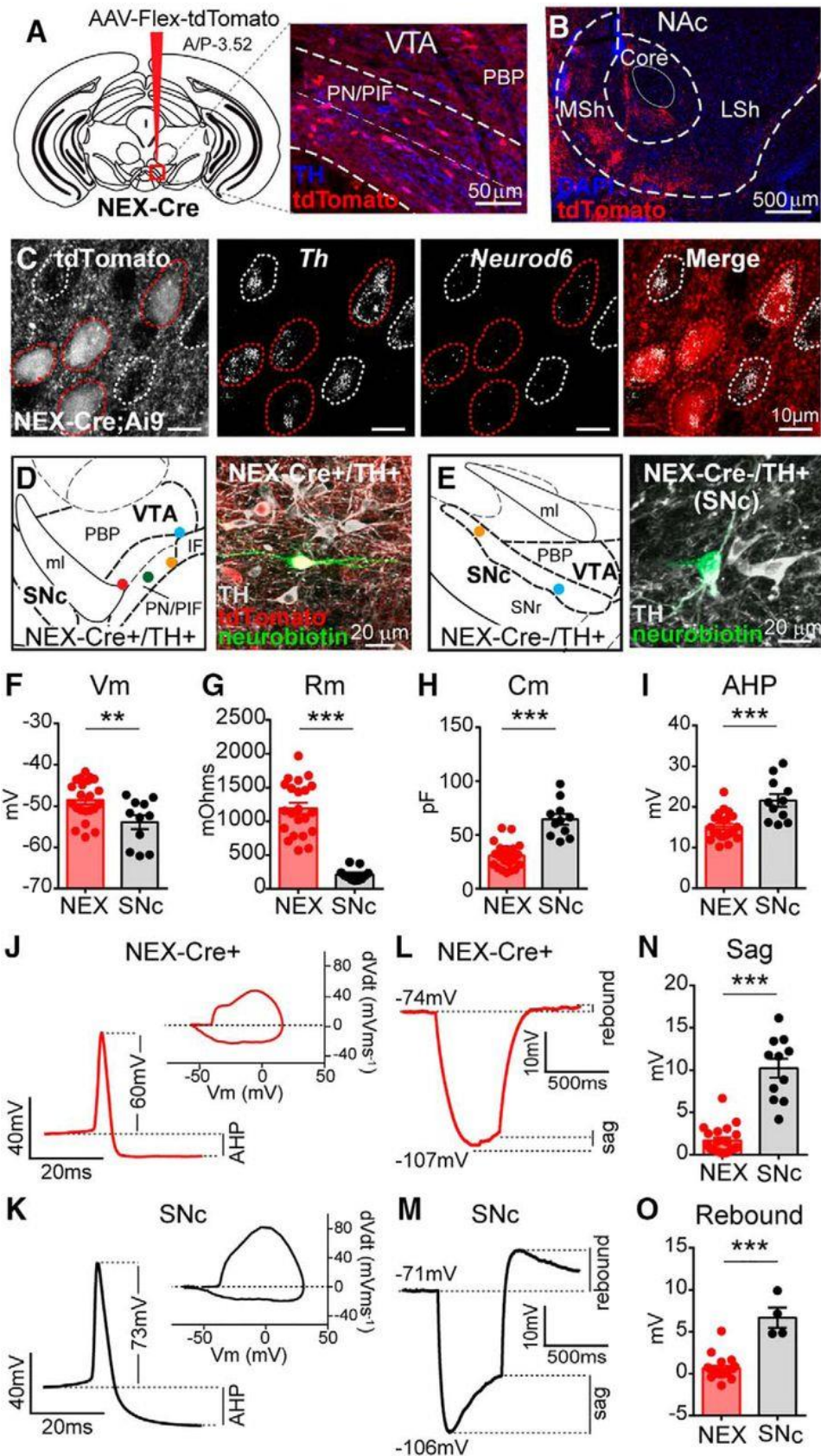
Figure 3. Neurod6-expressing DA neurons have non-canonical physiological properties. **A)** Cre-dependent tdTomato-expressing virus (AAV-Flex-tdTomato) was injected unilaterally into the VTA of a NEX-Cre mouse. Right panel shows tdTomato-labeled NEX-Cre+ neurons in the ventromedial VTA. Tyrosine hydroxylase (TH) staining is in blue. **B)** Confocal image of the nucleus accumbens (NAc) showing tdTomato-labeled projections from midbrain NEX-Cre+ neurons. MSh, medial shell; LSh, lateral shell. **C)** Confocal images of VTA neurons from NEX-Cre;Ai9 mice with fluorescent in situ hybridization (FISH) for tyrosine hydroxylase (Th) and Neurod6 mRNA. The tdTomato Cre-reporter is expressed in NEX-Cre+ neurons. NEX-Cre+/Neurod6 + DA neurons are circled in red, NEX-Cre-/Neurod6+ DA neurons are circled in white. **D-E)** Left panels show representative recording sites of NEX-Cre+ VTA (D) and NEX-Cre-SNc neurons (E). Circles show the locations of recorded DA neurons. Right panels show examples of recorded, neurobiotin-filled neurons positive for TH. **F-I)** Graphs display the mean ± SEM membrane potential (F, V_m, **, $p = 0.0075$), membrane resistance (G, R_m, ***, $p < 0.0001$), capacitance (H, C_m, ***, $p < 0.0001$), and afterhyperpolarization (I, AHP, ***, $p = 0.0002$) for NEX-Cre+ and SNc neurons. **J-K)** Representative action potential traces and phase plots ($mVms^{-1}/mV$) from a NEX-Cre+ (J) and SNc (K) neuron. **L-M)** Representative responses to a 500 ms negative current step from a NEX-Cre+ (–25 pA, L) and SNc (–150 pA, M) neuron. **N)** Quantification of the mean ± SEM sag component in NEX-Cre+ and SNc neurons (***, $p < 0.0001$). **O)** Quantification of the mean ± SEM rebound depolarization from neurons hyperpolarized to –100 ± 7 mV (***, $p < 0.0001$). An unpaired t test was used for all comparisons. For all panels, dots represent values from individual cells, NEX-Cre+ n = 7 male and 7 female mice, NEX-Cre-/SNc n = 4 male mice and 1 female mouse. See Fig. 3-1 for a complete summary of the electrophysiology results.

Figure 4
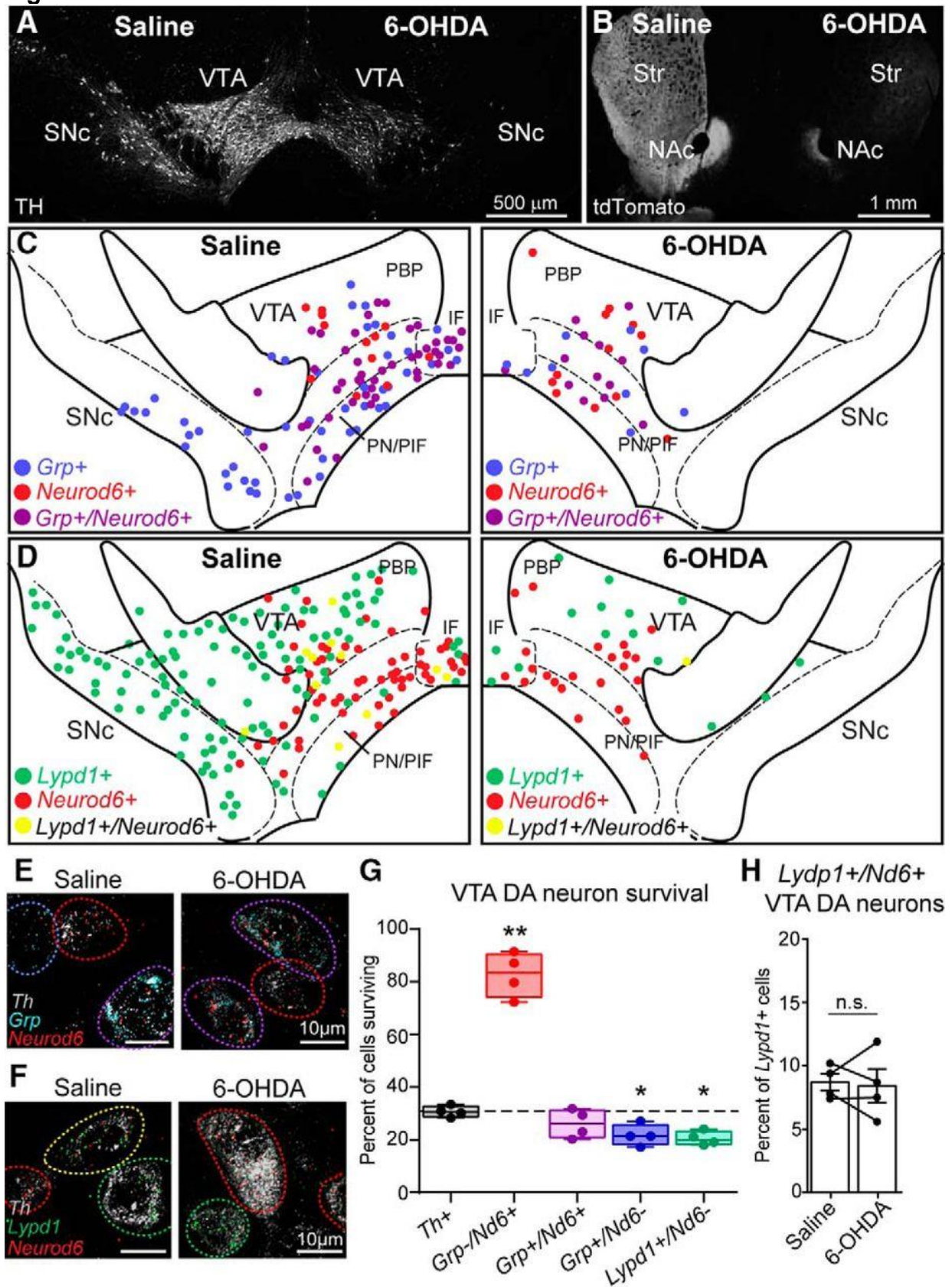
Figure 4. Neurod6-expression affects susceptibility to 6-OHDA–induced degeneration. **A)** Confocal image of a midbrain section stained with a tyrosine hydroxylase (TH) antibody 4 wk after unilateral saline (left) or 6-OHDA (right) injection into the medial forebrain bundle. **B)** Image of a striatal (Str) section showing loss of tdTomato+ axon terminals 4 wk following unilateral 6-OHDA injection in a DATIRESCre;Ai9 mouse. NAc, nucleus accumbens. **C)** Schematic showing the location of DA neurons in the saline and 6-OHDA injected hemispheres labeled with different markers by fluorescent in situ hybridization (FISH): blue circles are Grp+, red circles are Neurod6+, and purple circles are Grp+/Neurod6+. **D)** Schematic showing the location of Lypd1+ (green), Neurod6+ (red), and Lypd1+/Neurod6+ (yellow) DA neurons in the midbrain following saline and 6-OHDA injection. E, F, Confocal images of FISH for the indicated markers. **E)** Images show Grp+ (blue circle), Neurod6+ (red circles), and Grp+/Neurod6+ (purple circles) DA neurons in the VTA following saline and 6-OHDA injection. **F)** Images show Lypd1+ (green circles), Neurod6+ (red circles), and Lypd1+/Neurod6+ (yellow circle) DA neurons in the VTA following saline and 6-OHDA injection. **G)** Box-and-whisker plots (min to max) show the percentage of VTA DAT neurons expressing each set of markers in the 6-OHDA–injected hemisphere compared to the saline-injected hemisphere. Dotted line represents the percentage of all VTA DA neurons (Th+) surviving in the 6-OHDA hemisphere. Dots represent data from individual mice, n = 4 female mice. A paired one-way ANOVA with Dunnett's multiple comparisons test was used to compare each subpopulation to all Th+ VTA DA neurons (n = 4376 saline and 1352 6-OHDA cells): Grp–/Neurod6+ (n = 184 saline and 151 6-OHDA cells), ** p = 0.0022; Grp+/Neurod6+ (n = 763 saline and 207 6-OHDA cells), p = 0.3169; Grp+/Neurod6– (n = 749 saline and 165 6-OHDA cells), * p = 0.0246; Lypd1+/Neurod6– (n = 1056 saline and 171 6-OHDA cells), * p = 0.0313; Nd6 = Neurod6. **H)** Bar graphs display the percentage of Lypd1 + VTA DA neurons that co-express Neurod6 mRNA in the saline-injected (n = 102/3750 cells) and 6-OHDA–injected (n = 16/904 cells) hemispheres. Bars represent mean ± SEM, dots represent the values from individual mice, n = 4 female mice; paired t test, n.s., not significant, p = 0.8091.

Supplemental Figure 1.
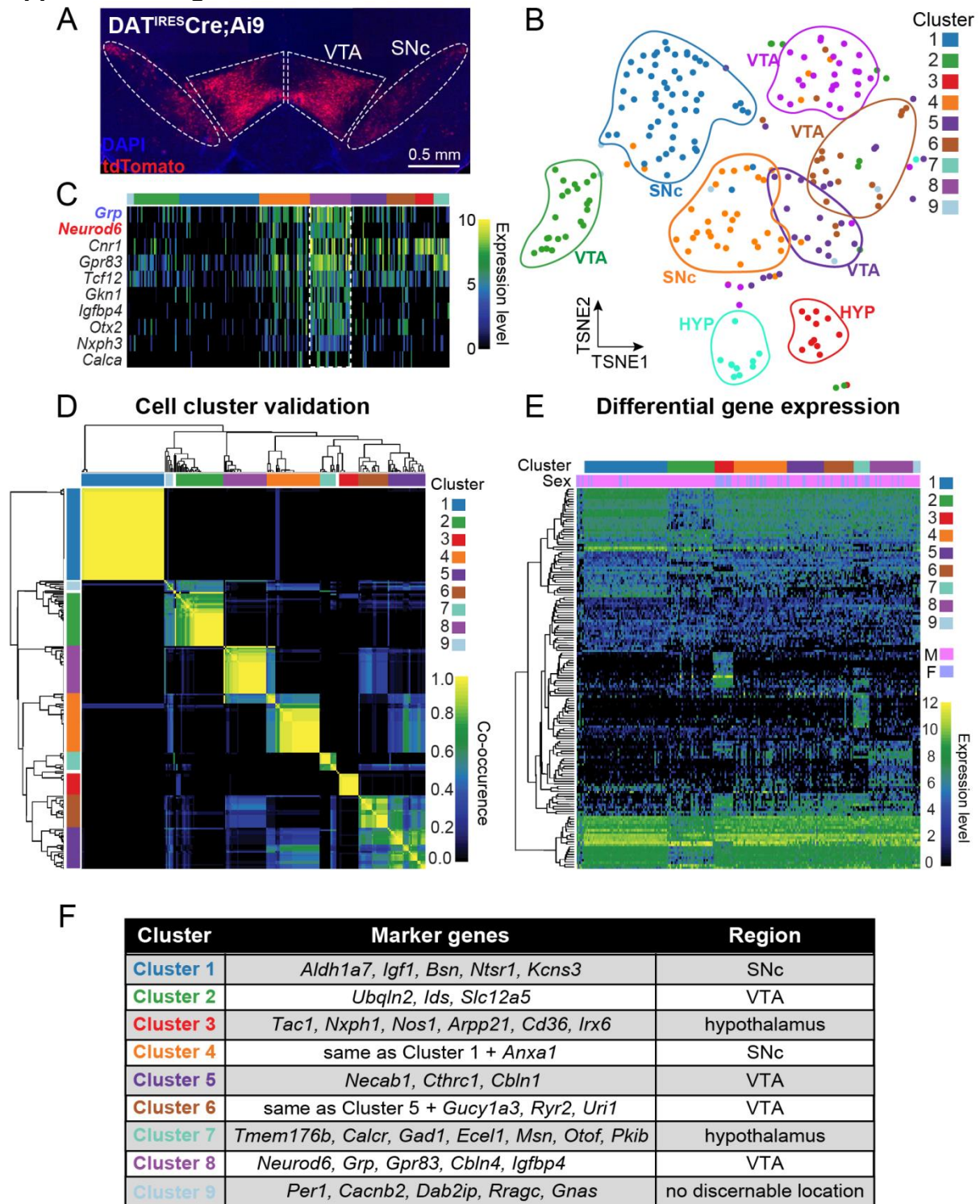
Supplemental Figure 1. Single-cell RNA-sequencing defines genetic subpopulations of mouse midbrain dopamine neurons. A), Confocal image of a midbrain section from a DAT[IRES]Cre;Ai9 mouse showing tdTomato Cre-reporter expression in midbrain dopamine (DA) neurons. **B)** *t*-distributed stochastic neighborhood embedding (tSNE) plot shows genetically defined clusters of DA neurons. 232 cells were analyzed from 8 mice. **C)** Heatmap displays a selection of differentially expressed genes in cluster 8 (highlighted by the dashed box). Individual genes are along the *Y*-axis and individual cells are along the *X*-axis. Colored bars at the top indicate the assigned cell cluster. **D)** Heatmap of cell co-clustering. The RSEC clustering method is based on consensus clustering over many parameters. To assess the robustness of the final clustering, we generated a co-clustering matrix where, for each pair of cells, we recorded the proportion of times in which two cells clustered together. The cells that failed to cluster at least 50% of the time were dropped from the analysis. The plot can be used to assess the robustness of the clustering procedure. Clusters 1, 2, 3, 7, and 8 are very robust, as almost all of the cells cluster together 100% of the time. Clusters 4, 5, and 6 are less robust, meaning that their boundaries are not well defined. Both the *X*- and Y-axis correspond to cells, ordered according to hierarchical clustering; colored bars at the top indicate the final nine cluster labels. **E)** Heatmap of the top 151 differentially expressed genes. Individual genes are along the *Y*-axis and individual cells are along the *X*-axis (n = 232 cells). Colored bars at the top indicate cell cluster and sex of the animal. Differentially expressed genes were obtained by performing all pairwise comparisons among the nine defined clusters with the R package *limma*. Genes were sorted by *p*-value, and the top 10 genes per comparison were selected for visualization (with nine clusters there are a total of 36 pairwise comparisons). If a gene was identified as differentially expressed in more than one comparison, it was reported in the heatmap only once. This procedure resulted in 151 distinct differentially expressed genes. **F)** Table summarizing selected markers and the anatomical location of each genetically defined cluster. Anatomical location was determined by *in situ* hybridization of marker genes and expression data from the Allen Brain Atlas. Marker genes were included in the table if there was significant differential expression from at least three other clusters

Supplemental Figure 2

A **Nucleus Accumbens**

Medial Shell   Core   Lateral Shell

Medial Prefrontal Cortex

A/P +1.10mm

D
L — M
V

A/P +0.50mm

Dorsal Striatum

Dorsolateral   Dorsomedial

Basolateral Amygdala

Lateral Septum

A/P +0.74mm

A/P -2.06mm

A/P +0.50mm
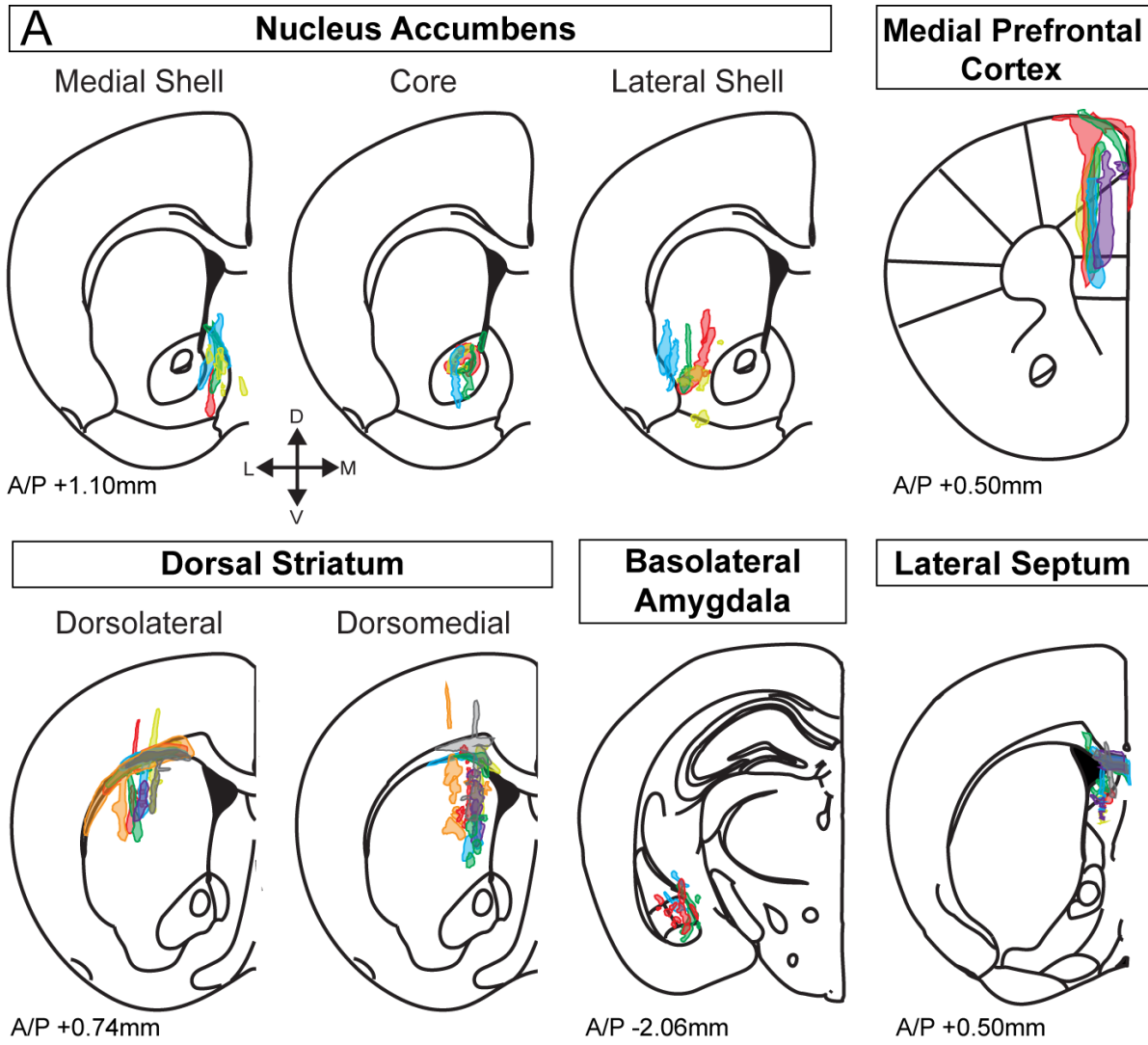
B **Dorsomedial striatum-projecting *Grp*+ DA neurons**

Grp+/*Th*+/bead+
PBP
VTA
PN/PIF
SNc
Bregma: -3.40
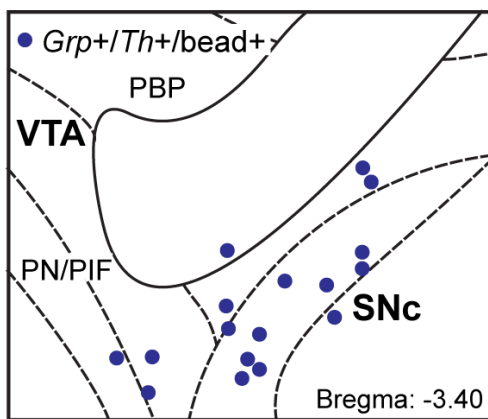
C **NAc medial shell-projecting *Grp*+ DA neurons**

Grp+/*Th*+/bead+
IF
PBP
PN/PIF
VTA
SNc
Bregma: -3.40

46
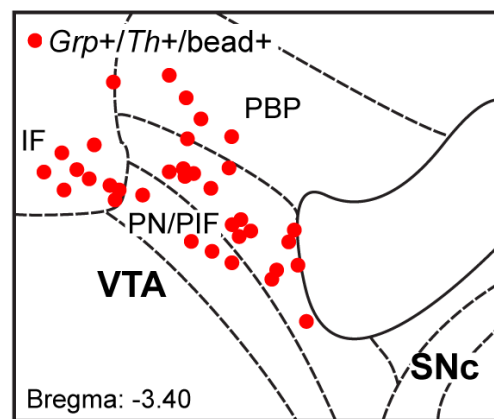
Supplemental Figure 2. Retrobead injection sites and location of *Grp*$^+$ DA neurons projecting to the dorsomedial striatum or NAc medial shell. A) Schematics of coronal brain sections from the indicated anterior/posterior (A/P) positions from bregma. Colored regions represent retrobead injection sites from individual mice, NAc MSh n = 2 male and 2 female mice, NAc Core n = 2 male and 2 female mice, NAc LSh n = 3 male and 2 female mice, DMS n = 3 male and 2 female mice, DLS n = 4 male and 3 female mice, mPFC n = 4 male and 1 female mouse, BLA n = 3 male mice, and LS n = 2 male and 3 female mice. **B-C)** Schematics showing the locations of *Grp*$^+$/*TH*$^+$/bead$^+$ cells in the midbrain that project to the dorsomedial striatum (***B***) or nucleus accumbens (NAc) medial shell (***C***). Schematics were generated from representative single FISH images.

Chapter 3: Generation of a DAT-Flp mouse line for intersectional genetic targeting of dopamine neuron subpopulations

Daniel Joseph Kramer, Polina Kosillo, Drew Friedmann, David Stafford, Liqun Luo,
Angus Yiu-Fai lee, Dirk Hockemeyer, John Ngai, Helen S. Bateup

Department of Molecular and Cell Biology
University of California Berkeley

Introduction

Despite their modest numbers, dopamine (DA) neurons project widely throughout the brain and influence a diverse set of behaviors and neural processes including movement, motivation, reward learning, and cognition[56,60]. Historically, DA neurons have been categorized into 17 main sub-types, the cell groups A1-A17[60,69]. A9 and A10 are the most numerous and reside within the midbrain in the substantia nigra pars compacta (SNc) and ventral tegmental area (VTA), respectively. It has been long been recognized that SNc and VTA DA neurons differ significantly in their projection targets, electrophysiological properties, behavioral influence, and vulnerability to degeneration[60,61,63,100,146,147,201,229]. However, recent single cell profiling studies have revealed that each sub-region is, in fact, made up of smaller, somewhat overlapping populations based on their specific gene expression patterns[33,34,97,177-179]. How these dopaminergic subpopulations differ in terms of their anatomical location, inputs and outputs, neurotransmitter identity and functional properties is just beginning to be defined.

To better understand the connections and behavioral functions of newly identified dopamine neuron populations, additional tools are needed that allow genetic access to these subtypes. This is essential as even neighboring populations of DA neurons can project to very different places in the brain and exert opposing behavioral effects, i.e. signaling reward versus aversion[146,147]. From gene expression profiling studies, it is clear that combinatorial approaches utilizing the intersectional expression of two or more genes will be needed as there are rarely single marker genes that are exclusively expressed by a given subtype[34,97,178]. In addition, even when the expression of a single gene can distinguish discrete DA populations, these genes may also be expressed outside of the midbrain and are thus not useful for exclusive targeting of DA neuron subtypes[97,181,182].

To address this challenge, intersectional mouse genetics approaches have been developed whereby the combinatorial expression of different recombinases can be used to define a neuronal subpopulation[44,182,230,231]. This approach was recently applied to the DA system through the generation of mice that express Flp recombinase from the endogenous tyrosine hydroxylase (*Th*) locus[182]. Using these Th-2A-Flpo mice, Poulin and colleagues successfully generated detailed maps of the projection targets of various genetically-defined dopaminergic subpopulations. However, TH is the rate limiting enzyme in the synthesis of all catecholamines, including DA, norepinephrine and epinephrine. Thus, available transgenic mouse lines that use *Th* to drive expression of recombinases and reporter genes in dopamine neurons (e.g. Th-IRES-Cre, Th-2A-Flpo, and TH-EGFP) also have expression in other catecholamine-expressing neurons[162,182,232-234]. As a result, the use of *Th*-driven reporters to investigate the behavioral functions of specific dopaminergic circuits may be confounded by contributions from these other cell types[162].

To address this challenge and provide an additional tool for studying dopaminergic subpopulations, we generated a mouse that expresses Flp recombinase from the endogenous *Slc6a3* (dopamine active transporter, DAT) locus. DAT is responsible for

the re-uptake of DA back into the presynaptic terminal following neurotransmitter release and is expressed almost exclusively in dopaminergic neurons[69,162,205,232]. As a result, DAT-reporter mouse lines have been shown to be more selective and label canonical DA neurons more specifically than *Th*-driven lines[162,205,235]. Here we show that midbrain DA neurons are robustly and selectively labeled in DAT-Flp mice using Flp-dependent viral or transgenic reporters.

To provide proof-of-concept for intersectional labeling of a DA neuron subpopulation, we crossed DAT-Flp mice with NEX-Cre mice and verified selective targeting of *Neurod6*+ DA neurons in the ventromedial VTA[207]. We further performed Adipo-clear brain clearing[236] and fast scan cyclic voltammetry to demonstrate the highly selective anatomical and functional output of this discrete DA subpopulation. DAT-Flp mice therefore represent a novel tool, which adds to our growing arsenal of mouse genetic approaches that allow precise targeting of specific DA neuron subpopulations. Collectively, these new mouse models provide a valuable means to dissect the contributions of dopaminergic sub-circuits to behavior.

Materials and Methods

Mice

Animal procedures were conducted in accordance with protocols approved by the University of California, Berkeley Institutional Animal Care and Use Committee (IACUC) and Office of Laboratory Animal Care (OLAC).

The DAT-Flp mice were generated at UC Berkeley as described below. DAT[IRES]Cre mice (Jackson Laboratory, strain #006660[205]) were crossed and maintained with C57BL/6J wild-type mice (Jackson Laboratory, strain #000664). RCE:FRT mice[237] were used to endogenously label Flp-expressing neurons with EGFP (Gt(ROSA)26Sortm1.2(CAG-EGFP)Fsh/Mmjax, MMRRC stock #32038-JAX). To label neurons co-expressing Flp and Cre recombinase, the Ai65 mouse line[238] was used (Ai65(RCFL-tdT)-D, Jackson Laboratory strain #021875). To target *Neurod6* expressing neurons, we used the NEX-Cre mouse line (NEX was the previous name of *Neurod6*) obtained from Dr. Klaus-Armin Nave[207,239]. Mice were housed on a 12 h light/dark cycle and given ad libitum access to standard rodent chow and water. The ages, sexes, and numbers of mice used are indicated for each experiment in figure legends.

Generation of DAT-Flp mice

CRISPR/Cas9-editing in mESCs

DAT-Flp mice were generated from Ai65 mouse embryonic stem cells (mESCs) from the Allen Institute for Brain Science (a gift from Tanya Daigle, Ph.D.). These mESCs were derived from the Ai65 mouse line[238] harboring a Flp- and Cre-dependent tdTomato fluorescent reporter in the ROSAβgeo26 locus. Ai65 mESCs were karyotyped (Cell Line Genetics, Inc. Madison, WI) to ensure chromosomal health both before and after gene editing. Clonal cell lines that showed normal chromosome numbers and no deletions/insertions in at least 19 of 20 cells analyzed were considered to be chromosomally normal. mESC cultures were maintained in 6-well plates on a layer of inactivated mouse embryonic fibroblasts (MEFs, CD-1 strain, Charles River) in mESC culture media composed of DMEM/F12 (no pyruvate, Life Technologies – MT15090CV) containing 15% HyClone FBS (GE Healthcare, SH30070.03E), 5% KnockOut Serum Replacement (KSR, Thermo Fisher Scientific – 10828028), 2 mM L-glutamine (Thermo Fisher Scientific – 25030081), 1,000 U/ml[-1] penicillin-streptomycin (Thermo Fisher Scientific – 15140122), 1% nonessential amino acids (Thermo Fisher Scientific – 11140050), 0.1 mM 2-mercaptoethanol (Thermo Fisher Scientific – 21985023), and 1,000 U/ml mouse leukemia inhibitory factor (mLIF, Millipore – ESG1107). Media was changed daily, and cultures were passaged every 7 days.

We inserted a 2A-Flpo recombinase sequence before the stop codon in the last exon (exon 15) of the *Slc6a3* gene. To do this, we designed two plasmids: a donor plasmid and a Cas9 plasmid. For the donor construct, we generated a 2499 bp gBlock gene fragment (Integrated DNA technologies, IDT) that contained a 15 bp overhang for integration into a plasmid, a 552 bp homology arm on the 5' end, a P2A sequence starting with a GSG[240], a nuclear localization sequence, the optimized Flp-recombinase (Flpo) sequence[238,241], a 552 bp homology arm on the 3' end, and a 15 bp overhang for integration into a plasmid. This sequence was inserted into a donor plasmid (pCRII-

TOPO) using In-Fusion HD cloning (Takara – 639649). For the Cas9 plasmid, a single-guide RNA (sgRNA) targeting the NGG sequence immediately downstream of the exon 15 stop codon (sgRNA forward: 5' *CACCG*CATTGGCTGTTGGTGTAAG 3', sgRNA reverse: 5' *AAAC*CTTTACACCAACAGCCAATG*C* 3', *italic* portions represent sequences present for px330 plasmid insertion) was inserted into the CRISPR-Cas9-encoding px330 plasmid[242].

To target and edit Ai65 mESCs with the donor construct and Cas9 plasmid, we trypsinized 3 wells of mESCs with trypsin-EDTA media (Thermo Fisher Scientific – 25200056), spun them down (5 minutes at 1000 rpm) and resuspended them in fresh media. Cells were then counted and $5x10^6$ Ai65 mESCs were nucleofected with 6 µg donor plasmid, 3 µg px330 plasmid, and 1 µg of an EGFP-encoding plasmid (Addgene – 6081-1). For nucleofection, we used the Lonza mouse ES cell nucleofector kit (Lonza – VPH-1001) per the manufacturer's instructions. Cells were then nucleofected in a Lonza 4D nucleofector (Lonza – Hayward, CA). Following nucleofection, cells were placed back into culture as before, split evenly onto a 6-well, MEF-coated plate.

Bulk genotyping for successful Flp construct insertion
24 hours following nucleofection, cells underwent FACS to sort 60 EGFP⁺ cells into each well of a 96-well flat-bottom plate containing a monolayer of MEFs. Five days following FACS, each well of the 96-well plate was trypsinized and resuspended in a 1:1 mix of media and FBS. This mixture was split 4:1 into one well of two duplicate 96-well plates containing either freezing media (45% mESC culture media, 45% FBS, and 10% DMSO (Thermo Fisher – BP231)) or a MEF layer with mESC culture media. The 96-well plate containing freezing media was frozen immediately at -80˚C to be thawed following confirmation of successful gene editing. The second 96-well culture plate was placed back in the incubator for 3-4 days until substantial colony growth was achieved. DNA was isolated from each well for genotyping. To do this, media was aspirated and each well was washed once with 1x PBS. Cells were lysed by adding 100 □l lysis buffer (5 mM EDTA, 10 mM Tris HCl, 0.2% SDS, 200 mM NaCl, and 0.08 mg/ml Proteinase K added day of) into each well and incubating the plate overnight at 37˚C. The next day, the lysate of each well was transferred to an individual eppendorf tube, 100 □l of isopropanol was added, and shaken vigorously to precipitate DNA. Pellets were spun down (3 minutes at 13,000 x g) and washed twice with 70% EtOH. DNA pellets were then resuspended in 50 □l of TE. Following DNA isolation, each sample was genotyped to determine the status of the gene editing for each well.

We designed a genotyping strategy with a forward primer immediately upstream of the first homology arm in exon 15 of *Slc6a3* (DAT-Flp geno forward: 5' CATGCAGAAGGACAGACACT 3'), a reverse primer in the Flp sequence 650 bp away from the forward primer (Flp insert reverse: 5' AGGATGTCGAACTGGCTCAT 3'), and a reverse primer in the 3' UTR of the *Slc6a3* gene, 1,100 bp away from the forward primer when there is no insert (DAT-Flp geno reverse: 5' ACCCTGCGTGTGTGTAATAT 3'). Flp insertion was confirmed the presence of a 650 bp PCR product. With this strategy, the forward primer falls outside of the homology arm; therefore we could confirm on-target insertion.

Isolation of clones with Flp insertion
By genotyping the bulk sample, we identified individual wells that showed successful gene editing. We then expanded the corresponding wells of the frozen duplicate 96-well plate and expanded it into 3 wells of a 6-well plate. Cultures were grown for 3-4 days until sparse colonies were visible by eye, and individual colonies were picked. 96 individual colonies were picked and then dissociated into single cells in a round bottom 96 well plate filled with 100 □l of mESC culture media. Cells were then split 4:1 into two duplicate 96-well plates. One plate contained freezing media; the other was coated with MEFs and contained mESC culture media. The plate containing freezing media was quickly frozen at -80˚C. The culture dish was grown for 3-4 days until there were visible colonies. Each well was then genotyped as described above to identify colonies with successful gene editing. Positive colonies were expanded onto 6-well plates for freezing, further genotyping, karyotyping, and aggregation.

Following confirmation of correctly targeted Ai65 mESC clones with normal karyotypes, mESCs were trypsinized from the 6-well plate, spun down, and suspended in 12 ml culture media plus 3 µM CHIR99021 & 1 µM PD03259010 (2i media; Stemcell technologies – 72054 & 72184). This suspension was put onto a gelatinized 10 cm dish for 1 hour at 37˚C to remove MEFs, which adhered to the plate within an hour. The supernatant was then put onto a gelatinized 6 cm dish overnight at 37˚C to form stem cell aggregates. These plates were given to the Berkeley Cancer Research Laboratory Gene Targeting Facility for the generation of chimeras using aggregation of mESCs and morula embryos as described previously[243]. Pups born from these females were checked for chimerism by coat color and tail DNA genotyping. F1 pups and subsequent generations were genotyped using tail DNA. Tail DNA was isolated used small (1 mm) tail clips at P10 and overnight tissue lysis at 55˚C using Viagen Biotech Direct PCR lysis reagent and Promega proteinase K (Fisher Scientific – NC9724951 & PRMC5005) per the manufacturer's instructions.

Stereotaxic intracranial injections
Intracranial injections were performed on male and female 40-60 day old mice. Mice were briefly anesthetized with 3% isoflurane (Piramal Healthcare – PIR001710) and oxygen. Their heads were shaved and mice were mounted on a stereotaxic frame (Kopf instruments – Model 940) with stabilizing ear cups and a nose cone delivering constant 1.5% isoflurane in medical oxygen. Viruses were injected using a pulled glass capillary at a rate of 100 nl/minute. Following injection, the capillary remained in place for 1 minute per every minute spent injecting to allow the tissue to recover and prevent virus backflow up the injection tract upon retraction. The following coordinates from Bregma were used to target each site: SNc (M/L ±1.5 mm, A/P -2.8 mm, D/V -4.0 mm), VTA (M/L ±0.6 mm, A/P -3.1 to -3.7 mm for multiple injections, D/V -4.2 mm).

For ChR2 experiments, 400 nl of AAV8 Flp- and Cre-dependent ChR2 (pAAV-hSyn Con/Fon hChR2(H134R)-EYFP: Addgene – 55645-AAV8: titer 2.1 x 10^{13}) diluted 1:7 in sterile saline was injected bilaterally into the anterior and posterior VTA of DAT-FLP;Nex-Cre mice. For DAT-Flp EYFP labeling experiments, 400 nl of undiluted AAV5

Flp-dependent EYFP (rAAV5.hSyn-Coff/Fon-eYFP-WPRE: UNC vector core: titer 3.5 x 10^{12}) was injected bilaterally into the SNc and VTA of DAT-Flp heterozygous mice. For Intersectional labeling of *Neurod6*-negative DA neurons, 400 nl of AAV5 Coff/Fon-EYFP (rAAV5.hSyn-Coff/Fon-eYFP-WPRE: UNC vector core: titer 1.7 x 10^{12}) diluted 1:1 in sterile saline was injected bilaterally into the SNc and the VTA of DAT-Flp;Nex-Cre mice.

Brian sectioning and immunohistochemistry

Immunohistochemistry was performed as described[97]. Briefly, adult mice were anesthetized with isoflurane and transcardial perfusion was performed with 7.5 ml of 1x PBS following by 7.5 ml of ice cold 4% PFA in 1x PBS (EMS – 15710-S). Brains were then dissected out and post-fixed in 4% PFA in 1x PBS for 2 hours at 4°C. Brains were transferred to cryoprotectant solution (30% sucrose in 0.1M PB) at 4°C until they sank. 30 µm coronal sections were made using a freezing microtome (American Optical, AO 860). Sections were collected in serial wells of a 24 well plate in 1x PBS with 0.02% sodium azide (NaN_3; Sigma-Aldrich – 26628-22-8) and stored at 4°C. For immunohistochemistry, individual wells of sections were washed with gentle shaking for 3 x 5 minutes with 1x PBS, then blocked for 1 hour at RT with BlockAid blocking solution (Life Tech: B10710). Primary antibodies diluted in PBS-Tx (1x PBS with 0.25% triton-X-100 (Sigma – T8787)) were then added and the tissue was incubated for 48 h with gentle shaking at 4°C. Sections were then washed with gentle shaking 3 x 10 minutes with PBS-Tx. Secondary antibodies diluted in PBS-Tx were added and incubated with shaking for 1 h at room temperature. Sections were then washed 3 x 10 minutes gently shaking with 1x PBS. Sections were mounted onto SuperFrost slides (VWR: 48311-703) and coverslipped with hard-set Vectashield mounting media (Vector Labs: H-1500). The following antibodies were used: anti-tyrosine hydroxylase (TH, 1:1000, mouse, Immunostar #22941), anti-RFP (1:1000, rabbit, Rockland #600-401-379), Alexa Fluor 488 goat anti-mouse secondary (1:500, Thermo Fisher Scientific #A-11001), Alexa Fluor 633 goat anti-mouse secondary (1:500, Thermo Fisher Scientific #A-21050), and Alexa Fluor 546 goat anti-rabbit secondary (1:500, Thermo Fisher Scientific #A-11035).

Confocal microscopy and image analysis

Images of 30 µm sections processed for immunohistochemistry were acquired using an Olympus FV3000 confocal microscope equipped with 405, 488, 561, and 633 nm lasers and a motorized stage for tile imaging. Z-stack images captured the entire thickness of the section at 2-2.5 µm steps for images taken with a 20x air objective (Olympus #UCPLFLN20X) and 10 µm steps for images taken with a 4x air objective (Olympus #UPLXAPO4X).

Quantification of EGFP overlap with TH immunolabeling in DAT-Flp:RCE:FRT mice was done on max projected Z-stack images from 2 hemispheres per mouse and averaged together. Every clearly identifiable EGFP⁺ neuron in the SNc and VTA was manually counted using the Cell Counter Image J (NIH) plug-in. A neuron was considered TH⁺ if there was a clear TH signal in the entirety of the EGFP⁺ cell body. Boundaries of each

sub-region of the VTA and SNc were made according to the Paxinos mouse brain atlas[197].

Western Blotting

Bilateral punches (3 mm diameter) were taken from 275 μm thick striatal sections prepared from male and female (P50-90) DAT-Flp and DAT-IRES-Cre mice. Sections were cut on a vibratome in cold ACSF-Sucrose cutting solution (In mM: 85 NaCl, 25 NaHCO$_3$, 2.5 KCl, 1.25 NaH$_2$PO$_4$, 0.5 CaCl$_2$, 7 MgCl$_2$, 10 glucose, and 65 sucrose). Punches contained dorsal striatum and small neighboring portions of the lateral septum and nucleus accumbens. Tissue punches were put into a 1.5 mL tube and frozen on dry ice. Samples were resuspended in 300 μl lysis buffer (1x PBS, 1% SDS, 1% Triton-X-100, 2 mM EDTA, and 2 mM EGTA) with Halt phosphatase buffer inhibitor (Fisher: PI78420) and Complete mini EDTA-free protease inhibitor (Roche: 4693159001). Samples were sonicated at low power (Qsonica Q55) until homogenized. Homogenized samples were then boiled for 5 minutes, spun down, and put on ice. Total protein concentration was determined using a BCA assay (Fisher: PI23227).

4x Laemmli sample buffer (Bio-Rad: 161-0747) with 5% 2-mercaptoethanol (Thermo Fisher Scientific) was added 3:1 to an aliquot of each sample. 15 μg of total protein were loaded onto a 4-15% Criterion TGX gel (Bio-Rad: 5671084). Proteins were transferred to an activated PVDF membrane (BioRad: 1620177) at 4°C overnight using the Bio-Rad Criterion Blotter. Membranes were then removed, cut, washed, and blocked in 5% milk in 1x TBS + 1% Tween-20 (TBS-T) for 1 h at RT. Blots were incubated with primary antibodies diluted in TBS-T + 5% milk overnight at 4°C. The next day, the blots were washed 3 x 10 minutes with TBS-T followed by 1 hour of incubation at RT with HRP-conjugated secondary antibodies (1:5000). Membranes were washed 6 x 10 minutes with TBS-T and incubated for one minute with a chemiluminesence substrate (Perkin-Elmer: NEL105001EA) and exposed to GE Amersham Hyperfilm ECL (VWR: 95017-661). Membranes were then stripped 2 x 6 minutes with 6 mM Guanidinium Chloride + 5% 2-mercaptoethanol, washed with TBS-T, and incubated with primary antibody overnight at 4°C as before.

The following primary antibodies were used for western blotting: mouse anti-tyrosine hydroxylase (TH, 1:3000, Immunostar - 22941); mouse anti-Histone-3 (1:1500, Cell Signaling - 96C10); rabbit anti-Vmat2 (1:1400, Alomone Labs - AMT-006), mouse anti-Dopamine Transporter [6V-23-23] (DAT, 1:1,400, Abcam – 128848). The following secondary antibodies were used: goat anti-rabbit HRP (1:5000, Bio-Rad: 170-5046) and goat anti-mouse HRP (1:5000, Bio-Rad: 170-5047)

Fast-Scan Cyclic Voltammetry

DA release was monitored using fast-scan cyclic voltammetry (FCV) in acute coronal slices. Paired site-sampling recordings were performed in one WT reference animal and one heterozygous experimental animal from a sex- and age-matched mouse pair recorded on the same day. The genotype order of the tissue prep and recording chamber position were counterbalanced between experiments. Male and female mice (P50-90) were deeply anesthetized by isoflurane and decapitated. 275 μm thick coronal

striatal slices were cut on a vibratome (Leica VT1000 S) in ice cold ACSF-Sucrose cutting solution (in mM: 85 NaCl, 25 NaHCO$_3$, 2.5 KCl, 1.25 NaH$_2$PO$_4$, 0.5 CaCl$_2$, 7 MgCl$_2$, 10 glucose, and 65 sucrose). Slices recovered for 1 h at RT and were recorded from in ACSF (in mM: 130 NaCl, 25 NaHCO3, 2.5 KCl, 1.25 NaH2PO4, 2 CaCl2, 2 MgCl2, and 10 glucose). All solutions were continuously saturated with 95% O$_2$ and 5% CO$_2$. Slices between +1.2 mm and +0.5 mm (A/P) from Bregma that had both dorsal striatum and the entire nucleus accumbens were used for experimentation.

Prior to recording electrically- or light-evoked transients, ex vivo slices were equilibrated to the bath temperature of 32˚C for 30 min with an ACSF flow rate of 1.2-1.4 ml/min. Extracellular DA concentration ([DA]$_o$) was monitored with FCV at carbon-fiber microelectrodes (CFMs) using a Millar voltammeter (Julian Millar, Barts and the London School of Medicine and Dentistry). CFMs were fabricated in-house from epoxy-free carbon fiber ~7 μm in diameter (Goodfellow Cambridge Ltd) encased in a glass capillary (Harvard Apparatus: GC200F-10) pulled to form a seal with the fiber and cut to a final tip length of 70-120 μm. The CFM was positioned 100-130 μm below the tissue surface at a 45˚ angle. A triangular waveform was applied to the carbon fiber scanning from -0.7 V to +1.3 V and back, against a Ag/AgCl reference electrode at a rate of 800 V/s. Evoked DA transients were sampled at 8 Hz, and data were acquired at 50 kHz using AxoScope 10.5/10.7 (Molecular Devices). Evoked oxidation currents were converted to [DA]$_o$ from post-experimental calibrations of the CFMs. Recorded FCV signals were identified as DA by comparing oxidation (+0.6 V) and reduction (-0.2 V) potential peaks from experimental voltammograms with currents recorded during calibration with 2 μM DA dissolved in ACSF.

DA release was evoked every 2.5 minutes with electrical or optical stimulation delivered out of phase with voltammetric scans. For electrical stimulation, a concentric bipolar stimulating electrode (FHC: CBAEC75) was positioned on the slice surface within 100 μm of the CFM. DA release was evoked using square wave pulses (0.6 mA amplitude, 2 ms duration) controlled by an Isoflex stimulus isolator (A.M.P.I., Jerusalem, Israel). For site sampling experiments with electrical stimulation, three stimulations were delivered at a given site before progressing to a corresponding site in the other slice. For optical stimulation of ChR2-expressing DA terminals, release was evoked using 5 ms pulses of 473 nm light delivered through a 10x water-immersion objective coupled to a CoolLED system (CoolLED pE-300; 26.6mW light power output) controlled by a Master-8 pulse stimulator (A.M.P.I., Jerusalem, Israel). Optically evoked DA events were evoked with 10 light pulses delivered at 25 Hz.

Open Field Behavior
Behavioral testing was carried out during the dark phase of the light cycle under white lights. Male and female mice (P50-90) were habituated to the behavior room under a blackout curtain for 1 hour prior to testing. General locomotor activity and avoidance behavior was assessed using a 60 minute session in an open field chamber (40 cm length x 40 cm width x 34 cm height) made of transparent plexiglass (ANY-maze, Stoelting). Horizontal photobeams were used to measure rearing and were positioned at

9 cm above the chamber floor. The chamber was cleaned between each mouse with 70% ethanol followed by water and let dry for 5 minutes. The apparatus was cleaned with water and mild soap detergent at the end of each testing day. The experimenter was blind to genotype throughout the testing and scoring procedures.

For open field testing, the mouse was placed in the front, right hand corner of the chamber, facing away from the center and activity was recorded using both an overhead camera and side-facing camera. A smaller center field of 20 cm length x 20 cm width was defined digitally to measure the time spent in the center of the open field. The observer manually scored grooming bouts and time spent grooming during the first 20 min of the test. A grooming bout was considered any licking, nibbling, or scratching that lasted more than one second. If there was a break of more than 2 seconds between actions, this was considered a separate grooming bout. The following parameters were measured using ANY-maze tracking software: total distance traveled, time spent in center, and number of rears.

AdipoClear brain clearing

Brains from male and female (P40-60) DAT-Flp;Nex-Cre;Ai65 mice were cleared using AdipoClear[236] and imaged as described previously[44]. Mice were perfused with 20 ml of 1x PBS, followed by ice-cold 4% PFA (16% PFA diluted in 1x PBS, EMS – 15710-S), followed by 10 ml of 1x PBS. Brains were post-fixed in 4% PFA in 1x PBS with shaking overnight at 4°C. Brains were then washed for 3 x 1 h in 1x PBS with 0.02% NaN_3 (Sigma Aldrich – 58032) at RT. The brains were then delipidated. The samples were initially dehydrated with a MeOH gradient (20%, 40%, 60%, and 80%, 1 h each, Fisher – A412SK-4) with B1n buffer (in H_2O – Glycine: 0.3 M, Triton X-100: 0.1% (v/v), NaN_3: 0.01% (w/v) with pH adjusted to 7.0) shaking gently at RT. Samples were then washed 2 x 1 h in 100% MeOH followed by overnight incubation at RT in DiChloroMethane:MeOH (DCM, Sigma – 270997) 2:1. The next day, samples were washed for 1 h in 100% DCM followed by 3 washes in MeOH for 30, 45, and 60 minutes. Samples were then bleached in H_2O_2 buffer (5% H_2O_2 in MeOH; hydrogen peroxide 30%, Sigma – 216763) for 4 hours at RT. Samples were rehydrated in a reverse MeOH/B1n gradient (from 80%, down to 20%) at RT for 30 minutes each followed by a 1 h incubation with B1n buffer. Samples were then washed in 5% DMSO/0.3% glycine/PTxwH buffer (DMSO, Fisher – D128-4;Glycine, Sigma – G7126; PTxwH buffer: in PBS - Triton X-100: 0.1% (v/v), Tween 20: 0.05% (v/v), Heparin: 2 ug/ml, NaN_3: 0.01% (w/v)). Samples were washed in PTxwH buffer 4x for 30 minutes, overnight, 1 h, and 2 h.

Brains were immunolabeled with anti-RFP primary antibody (final concentration 1:1000, rabbit, Rockland #600-401-379). The antibody was first diluted in PTxwH buffer (1:500 in ~5 ml) then spun down (13,000 x g) and the supernatant was transferred to an additional 5 ml of PTxwH buffer in order to remove any debris. The final 1:1000 anti-RFP in PTxwH buffer was added to the brains and put on a shaker at 37°C for 11 days. Samples were then washed 2 x 1 h, 2 x 2 h, and 2 x 1 day in PTxwH buffer at 37°C. Secondary antibody was diluted in 500 μl of PTxwH and spun down at max speed for 30 minutes to remove any aggregates or debris. The supernatant (~480 μl) was then

added to 4.5 ml of PTxwH (final secondary concentration of 1:500) (secondary antibody: donkey anti-rabbit 647, Thermo Fisher Scientific – A-31573) and brains were incubated at 37˚C with shaking for 8 days. The secondary antibody was then washed as described following the primary antibody.

Following immunolabeling, brains were dehydrated in an MeOH gradient with H_2O (20%-80%, as before) shaking at RT for 30 minutes for each step. Samples were then washed 3x in 100% MeOH at RT for 30, 60, and 90 minutes followed by a wash with 2:1 DCM:MeOH overnight rocking at RT. The following morning, brains were washed in 100% DCM at RT 3x 1 h. The clearing step started with a wash in DiBenzylEther (DBE, Sigma – 108014) for 4 h, gently rocking at RT. Following this, the DBE was replaced with fresh DBE and brains were stored in the dark at RT prior to imaging.

Light sheet imaging and whole brain projection analysis
Whole brains were imaged on a LaVision Ultramicroscope II lightsheet using a 2x objective and 3 µm z-step size. Whole brain fluorescence was collected using 640 nm laser excitation and autofluorescence was collected using 480 nm laser excitation.

Image alignments between channels and sample auto-fluorescence to the Allen Brain Atlas (ABA) serial two-photon tomography reference brain, were performed using elastix (https://elastix.lumc.nl/). Computational identification, extraction, and skeletonization of axon collaterals was performed using the U-Net-based 3D convolutional neural network TrailMap[44,244]. Regional statistics were generated by transforming the arborizations into the ABA Common Coordinate Framework using the same parameters and vectors from the registration step. Axon content in each region was normalized to the size of the region and the total axon content in each brain and was expressed as a density metric.

Results

Generation of DAT-Flp mice

To allow for intersectional targeting of dopaminergic sub-populations, we developed a DAT-Flp mouse that expresses Flp recombinase from the endogenous *Slc6a3* (DAT) locus. We used CRISPR/Cas9-based gene editing to knock-in a P2A-Flpo-recombinase sequence 3' to the final coding exon of DAT, replacing the stop codon in the 15th exon and the 3' UTR (Fig. 1A). The self-cleaving P2A sequence allows for bicistronic expression of both endogenous DAT and Flp recombinase following translation of a single mRNA. For gene editing, we used mouse embryonic stem cells derived from the Ai65(RCFL-tdT)-D mouse line (herein referred to as Ai65)[238]. These cells harbor a Flp- and Cre-dependent tdTomato fluorescent reporter in the Rosa26 locus. F0 chimeric mice were PCR genotyped to confirm successful targeting (Fig. 1B). Targeted F0 male mice had successful germline transmission and produced pups that expressed the Flp recombinase insert (Fig. 1B).

Characterization of DAT-Flp mice

To determine whether Flp recombinase was efficiently expressed in DA neurons, adult heterozygous DAT-Flp mice were injected with an AAV expressing a Flp-dependent EYFP reporter in the midbrain (Fig. 1C). We observed the expected labeling of midbrain dopamine neurons in the injected area and greater than 97% of EYFP positive neurons were TH positive (Fig. 1D). Following this confirmation, we crossed the DAT-Flp mice to a mouse line expressing Flp-dependent EGFP (RCE:FRT)[237] (Fig. 1E). This cross resulted in Flp-dependent EGFP expression in canonical DA neuron-containing areas including the VTA, SNc, caudate linear nuclear raphe (CLi), dorsal raphe (DR), and arcuate nucleus (Fig. 1F-J). As expected, the vast majority (97%) of neurons in the SNc and VTA were TH+ (Fig. 1M), which matches expression patterns in the widely used DAT-IRES-Cre mouse line[162,205]. There was no expression, however, in regions that contain TH-positive, DAT-negative neurons[160] such as the interpeduncular nucleus (Fig. 1F, white arrow, IPN), the locus coeruleus (LC, Fig. 1K), and the zona incerta/A13 (Fig. 1L). Therefore, DAT-Flp mice do not label non-dopaminergic neurons that express TH and will thus allow for the specific intersectional labeling of dopaminergic neurons. Together, these data demonstrate successful generation of a novel transgenic mouse line with robust Flp-dependent recombination in DA neurons with no detected off-target expression.

The effects of Flp recombinase insertion into the DAT 3' UTR.

It has been reported in DAT-IRES-Cre mice that knock-in of Cre recombinase affects endogenous DAT expression[205]. In adult heterozygous animals there is a reported 17% reduction in DAT protein expression[205], a 21%-24% reduction in DA uptake, and a 25%-42% increase in peak-evoked DA concentration determined by fast-scan cyclic voltammetry (FCV)[245]. To test whether endogenous DAT expression is altered in DAT-Flp mice, which use a P2A sequence instead of an IRES sequence to achieve bicistronic expression and don't disrupt exon 15, we compared DAT protein expression, DAT re-uptake kinetics, and gross motor behaviors between DAT-Flp heterozygotes and their wild-type (WT) littermates.

Consistent with the previously observed reduction in DAT protein expression in DAT-IRES-Cre mice, which was replicated here (Sup. Fig. 1A,B), we found a significant decrease in DAT protein in tissue punches from the dorsal striatum of heterozygous DAT-Flp mice compared to WT controls (Fig. 2A,B). This change was selective for DAT as there were no significant differences in TH expression, or VMAT2, which is the vesicular monoamine transporter responsible for loading DA into vesicles (Fig. 2A,B). To measure DAT function, we used FCV to compare electrically evoked peak DA concentration and re-uptake kinetics between WT and heterozygous DAT-Flp mice in ex vivo striatal slices. We measured single pulse evoked DA release and re-uptake at seven locations throughout the striatum and nucleus accumbens (Fig. 2C). We found an average 32% increase in peak-evoked DA concentration across all dorsal striatum sites (dStr, sites 1-5, Fig. 2D) and a 30% increase in the nucleus accumbens core (NAc, sites 6+7, Fig. 2E) in DAT-Flp heterozygous mice. Using peak concentration-matched transients, we observed slower DA re-uptake in DAT-Flp heterozygous mice (Fig. 2F) consistent with their reduced DAT protein expression. An increase in peak-evoked DA concentration and decrease in DA re-uptake rate were also observed in DAT-IRES-Cre mice[245] (Sup. Fig. 1C-F). Notably, the overall peak evoked DA levels between the two mouse lines were three-fold different which likely reflects the differences in genetic background. The DAT-IRES-Cre mice were on a pure C57BL/6J background, while the DAT-Flp mice were on a CD-1/C57BL/6J mixed background. Previous work has shown clear differences in the dopaminergic system depending on the background of the mice, from cell number[246] to DA concentration throughout different brain regions[247,248]. Therefore, these results show that DA release and uptake dynamics are highly sensitive to both DAT expression levels and mouse background strain.

To test whether changes in DAT expression and function resulted in any gross behavioral alterations, we tested DAT-Flp mice of both sexes in the open field and measured locomotor activity, avoidance behavior, and repetitive behaviors (i.e. grooming). We found no significant difference in total distance traveled or number of rears between DAT-Flp heterozygous mice and WT littermate controls (Fig. 2G,H). We also found no changes in the time spent in center, a proxy for avoidance behavior, and no changes in time spent grooming for DAT-Flp mice (Fig. 2I,J). We tested DAT-IRES-Cre mice for comparison (Sup. Fig. 1G-J) and did find a small but significant increase in locomotor activity and decrease in grooming time in DAT-IRES-Cre heterozygous mice as compared to littermate controls. Together, these analyses show that even with use of a smaller self-cleaving P2A sequence instead of an IRES sequence, there can be changes in expression of the endogenous gene with a knock-in strategy. While this needs to be taken into consideration when designing experiments with DAT-IRES-Cre or DAT-Flp mice, our behavioral data show that changes in DAT do not strongly affect baseline motor activity or avoidance behavior. Therefore, DAT-Flp mice should be a useful tool for the selective analysis of DA neuron subpopulations.

Intersectional labeling of *Neurod6*-expressing midbrain DA neurons
Previous studies have revealed that DA neurons comprise genetically distinct subclasses[97,177-179,196]. One of these subpopulations, marked by the expression of the

transcription factor *Neurod6,* is found in the ventromedial VTA and projects to the nucleus accumbens medial shell (NAc MSh)[97,181,196,204]. This subpopulation is of interest because it is selectively spared in a 6-OHDA model of Parkinson's disease[97]. Moreover, recent studies have identified distinct behavioral roles for VTA DA neurons that project to the medial shell versus the lateral shell (LSh) of the NAc[146]. In particular, LSh-projecting DA neurons show canonical dopaminergic responses to rewards and reward predictive cues, whereas MSh-projecting DA neurons respond more to aversive stimuli and aversive cues[146]. Since both the cell bodies and projection sites of these two functionally distinct subpopulations are in close spatial proximity, it has been a challenge to selectively target them for further study. The restricted projections of *Neurod6*-expressing DA neurons, as previously defined by retrograde labeling and fluorescent in situ hybridization (FISH), make *Neurod6* a compelling marker gene to label MSh-projecting DA neurons[97,181]. However, *Neurod6* is also highly expressed outside the midbrain including in excitatory neurons of the cortex and in nuclei adjacent to the VTA (Fig. 3A-F)[207,239]. Therefore, intersectional tools are needed to selectively and reliably target Neurod6+ DA neurons.

To access *Neurod6*-positive DA neurons, we crossed DAT-Flp;Ai65 mice to NEX-Cre mice[207], which label the majority of *Neurod6*+ neurons (NEX is the former name for *Neurod6*) (Sup. Fig. 2A). In the resulting triple transgenic offspring, we found remarkably specific tdTomato labeling of a small population of neurons in the ventromedial VTA (Fig. 3G,H). The anatomical location of these *Neurod6/*DAT+ neurons matched closely to what was previously observed by FISH[97]. As predicted by prior retrograde tracing studies[97], we found that *Neurod6*/DAT+ neurons projected strongly to the NAc MSh, with some additional projections going to the olfactory tubercle and lateral septum (Fig. 3I,K, Sup. Fig. 2B). We confirmed that the Neurod6/DAT+ neurons and projections from these mice expressed TH (95% co-expression) (Fig. 3J,K).

To test whether dopaminergic projections to the NAc MSh arise exclusively from the *Neurod6*+ population, we injected an AAV expressing a Flp-on/Cre-off-EYFP construct[230] into the midbrain of DAT-Flp;NEX-Cre;Ai65 mice (Sup. Fig. 2C). In this experiment, only DA neurons that do not express NEX-Cre will be labeled with tdTomato (Fig. 3L). We observed the expected tdTomato+ axonal arborizations throughout the dorsal striatum, with a notable lack of projections in the NAc MSh and olfactory tubercle (Fig. 3M). This analysis demonstrates that *Neurod6*+ DA neurons make up the majority of NAc MSh-projecting DA neurons. Together, these data highlight the utility of viral and transgenic intersectional strategies to label subpopulations of DA neurons based on their expression of Flp and Cre recombinase.

Whole-brain imaging of *Neurod6*+ DA neurons

To measure the projection patterns of *Neurod6*+ DA neurons in an unbiased, brain-wide manner, we optically cleared whole brains from DAT-Flp;NEX-Cre;Ai65 mice using the iDISCO[249]-based brain clearing method AdipoClear[236] and imaged the intact brain using a light sheet microscope (Fig. 4). We confirmed the remarkable specificity of the intersectional strategy, with tdTomato+ cell bodies located almost exclusively in the VTA and clearly defined projections going towards the NAc MSh (Fig. 4A-E). We analyzed

the tdTomato+ projections of these neurons to determine the innervation pattern of *Neurod6+* DA neurons using TrailMap[250]. NAc mSh projections were too dense and complex to computationally recognize as individual fibers and were excluded from quantification. The most numerous projections outside of the NAc were found in the olfactory tubercle (OT), with additional sparse projections in the hypothalamic lateral zone (lateral preoptic area, LPO; preparasubthalamic nucleus, PST; parasubthalamic nucleus, PSTN; perifornical nucleus, PeF; Sup. Fig. 3A). TdTomato+ processes were detected in the midbrain (paranigral nucleus, PN; retrorubral area, RR) and the raphe nuclei (interpeduncular nucleus, IPN; rostral linear nucleus raphe, RL; central linear nucleus raphe, CLi), which likely represent the dendritic arbors of *Neurod6+* DA neurons (Sup. Fig. 3A). Together, these data show that the vast majority of projections from *Neurod6+* DA neurons go to the NAc mSh with minor projections to the olfactory tubercle and hypothalamus. These projection patterns are reproducible and consistent across multiple mice.

We did observe a small number of tdTomato⁺ neurons outside of traditional dopaminergic regions. We found a few tdTomato⁺ neurons in the cortex and hippocampus (Fig. 4A). To test whether these neurons were bona fide *Neurod6+* DA neurons or off-target recombination events, we performed antibody staining against TH. None of the neurons were TH⁺ (Sup. Fig.2D). Given the robust expression of *Neurod6* throughout the cortex (see Fig. 3A) and lack of tdTomato+ cortical neurons in DAT-Flp;RCE-FRT mice (see Fig. 3D), these neurons likely represent NEX-Cre positive neurons with leaky recombination events leading to tdTomato expression. In addition to the cortex, we also found small numbers of tdTomato+ cells in the anterior olfactory area and cerebellum (Sup. Fig. 2E,F).

Functional specificity of DA release from *Neurod6+* DA neurons

The anatomical data described above indicate a robust and selective projection from *Neurod6+* DA neurons to the NAc MSh. To confirm the functionality of this projection, we bilaterally injected an AAV expressing Flp- and Cre-dependent ChR2[230] into the midbrain of DAT-Flp;NEX-Cre mice (Fig. 5A-C). To assess whether activation of *Neurod6+* neurons leads to DA release, we measured DA levels with FCV in response to optical stimulation of ChR2+ terminals in different subregions of the striatum. We observed robust optically-evoked DA release in the NAc MSh (Fig. 5D). This DA release was reliable as we observed stable peak-evoked DA levels over the course of 20 minutes (Fig. 5D). Optical stimulation outside the MSh did not result in measurable DA transients, consistent with the lack of ChR2 expression in those regions (Fig. 5C,D). These results confirm the utility of DAT-Flp mice for future functional assays using optogenetics and demonstrate the specificity of intersectional approaches to label discrete dopaminergic subpopulations.

Discussion

Here we describe a novel transgenic mouse line expressing Flp recombinase from the endogenous DAT locus, which provides a new tool for the visualization and manipulation of DA neurons. We provide anatomical validation of this new mouse line by demonstrating robust and specific Flp-mediated recombination of genetic and viral reporters in TH+ midbrain DA neurons. We further show functional validation that Flp-dependent ChR2 can be used to evoke NAc DA release. We demonstrate proof-of-concept that DAT-Flp mice can be crossed to mice expressing Cre under specific gene promoters to allow for the intersectional targeting of dopaminergic subpopulations defined by their co-expression of DAT and any other gene of interest.

Single-cell sequencing studies of neuronal populations throughout the brain have provided unprecedented access to the gene expression profiles of different cell types[33-35]. These studies have highlighted the need for genetically targeted approaches to enable the study of neuronal subpopulations in an accurate and reproducible way[200]. This is especially important for heterogeneous cell types in which spatially adjacent or intermingled neurons can have different functional roles, thus constituting distinct subtypes, such as in the striatum or midbrain dopaminergic system[113,117,146,147,251-254]. In recent years, there have been major efforts to generate mouse lines that express Cre recombinase from different cell type-specific promoters (for example, see Huang and Zeng, 2013[14]). These mouse lines have become essential tools for neuroscience and other areas of biology. However, with the limited repertoire of genes that are expressed in neurons, there is often substantial expression of 'marker' genes in more than one cell type. Therefore, single genes often aren't sufficient to label specific neuronal subtypes within functionally diverse neuronal populations.

Mouse genetic intersectional strategies, based on the expression of different recombinases under the control of two or more genes, represent emerging approaches that greatly increase our ability to target newly defined neuronal subpopulations[231]. This strategy has been successfully applied to neuromodulatory populations, including serotonergic and dopaminergic neurons[44,182,230]. The DAT-Flp mouse line described here contributes to this growing toolkit of intersectional mouse genetic resources. For labeling DA neurons specifically, DAT-Flp mice have some important advantages over currently available intersectional mouse models, such as the Th-2A-Flpo mouse. Namely, DAT drives Flp expression selectively DA neurons, whereas Th-2A-Flpo is expressed in catecholaminergic neurons throughout the brain. This an important consideration when attempting to target midbrain DA neurons with viral or genetic approaches as TH is expressed in non-dopaminergic neurons in the interpeduncular nucleus (IPN) and the linear raphe (LR), which reside just adjacent to the VTA[160,162]. In addition, TH+ neurons are found in the locus coeruleus, dorsal raphe, hypothalamus, and zona Incerta, among others[160]. Therefore Th-2A-Flpo mice label a larger population of neurons. Together DAT-Flp and Th-2A-Flpo mice represent complementary tools that will have different utility depending on which neuronal population is to be targeted.
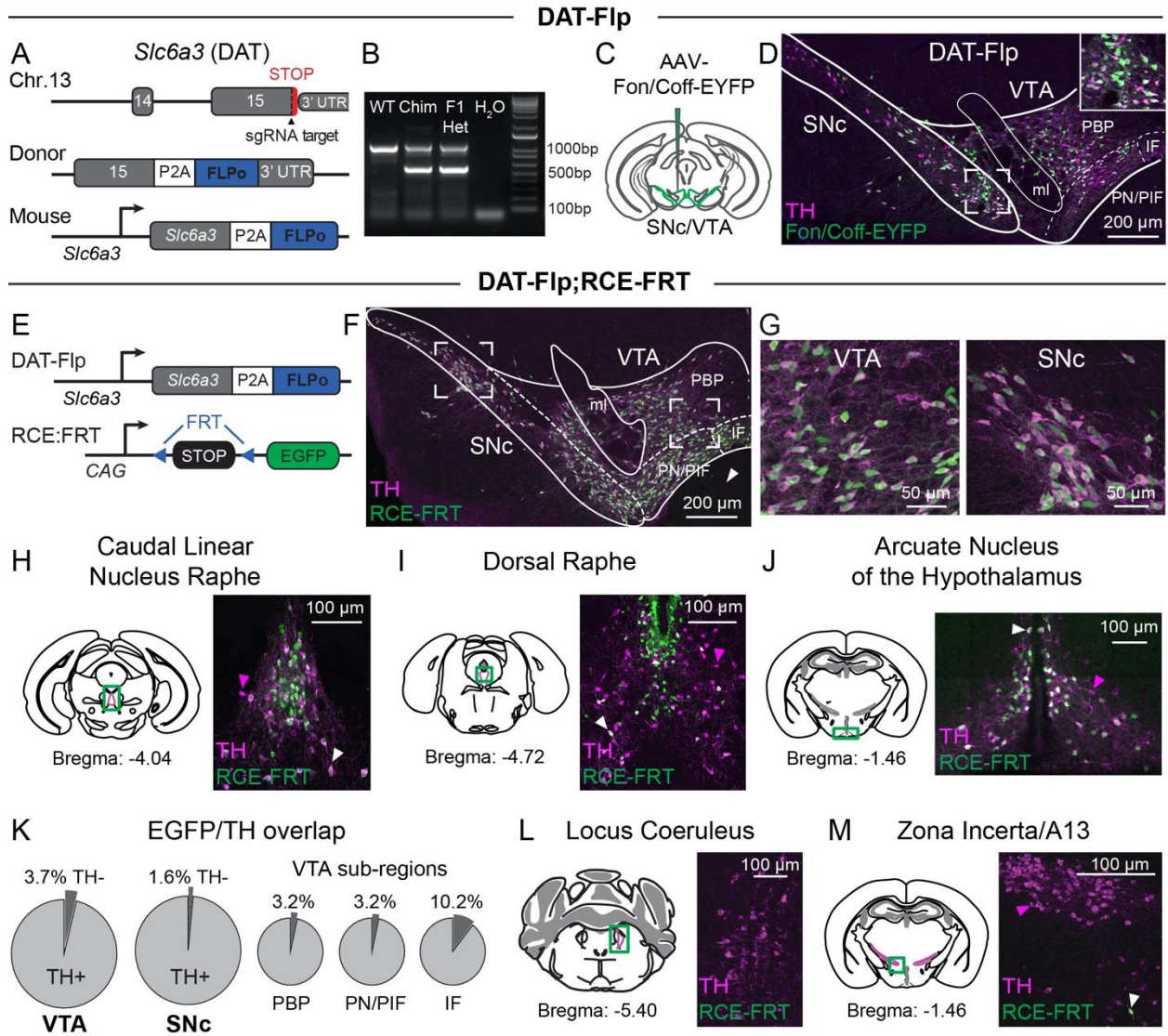
Here we find that similar to the commonly used DAT-IRES-Cre mouse line[205], bicistronic expression of Flp from the endogenous *Slc6a3* locus alters DAT protein expression. We

found a reduction in DAT levels in the dorsal striatum in mice that were heterozygous for DAT-Flp, which resulted in detectable changes in peak-evoked DA concentration and re-uptake kinetics in the striatum. While the mechanism for this is unknown, it may result from loss of the 3' UTR or the instability of the long mRNA transcript that is produced from the targeted locus, which contains the coding sequence for both DAT and Flp. This change in DAT expression will need to be considered when designing experiments with DAT-Flp mice, especially if measures related to DAT function are being explored. That said, we did not find changes in gross locomotor activity in DAT-Flp heterozygous mice, suggesting that they should be useful for many types of experiments. We suggest designing experiments so that all mice are DAT-Flp positive, and thus have similar DAT expression, and avoid comparing DAT-Flp heterozygotes directly with WT mice.

In addition to characterizing the DAT-Flp mice, we highlight an example of how an intersectional genetic approach can be used to visualize and manipulate a specific subpopulation of DA neurons. This population is marked by the expression of a transcription factor *Neurod6,* which is expressed in about 25% of DA neurons in the ventromedial VTA and was previously shown to comprise the majority of projections to the NAc MSh by retrograde labeling[97]. This population is of considerable interest given recent studies showing that *Neurod6* marks a DA population that is spared in a 6-OHDA model of Parkinson's disease[97], and could be neuroprotective by maintaining mitochondrial health[98,99]. In addition, *Neurod6* and its related family member *Neurod1* have been shown to be important for the developmental survival of this VTA subpopulation[204].

At the behavioral level, there is evidence that MSh-projecting DA neurons in the VTA are activated by unexpected aversive events[146]. Somewhat contrary to these findings, it has also been shown that while increased DA release in the NAc core may signal reward, this is not correlated with cell body firing in the VTA[255]. While axonal DA release can be gated by local mechanisms independent of cell body firing[256], without stable and consistent labeling of the same DA population it is difficult to confirm the relationship between the activity of VTA neurons and axonal DA release at the projection targets. These variable and somewhat conflicting results highlight the need for consistent and trackable marking of dopaminergic subpopulations without the labeling of off-target cell types. The DAT-Flp;NEX-Cre mice described here represent a new tool that will allow selective access to this behaviorally and disease-relevant subpopulation of DA neurons.

DAT-Flp

A — Chr.13 — *Slc6a3* (DAT), STOP, Donor, Mouse

B — WT, Chim, F1 Het, H₂O — 1000bp, 500bp, 100bp

C — AAV-Fon/Coff-EYFP — SNc/VTA

D — DAT-Flp, VTA, SNc, PBP, IF, ml, PN/PIF, TH, Fon/Coff-EYFP, 200 μm

DAT-Flp;RCE-FRT

E — DAT-Flp, *Slc6a3*, P2A, FLPo; RCE:FRT, FRT, STOP, EGFP, CAG

F — VTA, PBP, ml, SNc, IF, PN/PIF, TH, RCE-FRT, 200 μm

G — VTA, SNc, 50 μm, 50 μm

H — Caudal Linear Nucleus Raphe — Bregma: -4.04 — TH, RCE-FRT, 100 μm

I — Dorsal Raphe — Bregma: -4.72 — TH, RCE-FRT, 100 μm

J — Arcuate Nucleus of the Hypothalamus — Bregma: -1.46 — TH, RCE-FRT, 100 μm

K — EGFP/TH overlap — 3.7% TH-, 1.6% TH-, VTA sub-regions, 3.2%, 3.2%, 10.2%, TH+, TH+, VTA, SNc, PBP, PN/PIF, IF

L — Locus Coeruleus — Bregma: -5.40 — TH, RCE-FRT, 100 μm

M — Zona Incerta/A13 — Bregma: -1.46 — TH, RCE-FRT, 100 μm

Figure 1. Generation of DAT-Flp mice. **A)** Targeting scheme to generate DAT-Flp knock-in mice. Mouse embryonic stem cells (mESCs) were nucleofected with Cas9 and an sgRNA targeting the stop codon of the *Slc6a3* gene, which encodes the dopamine active transporter (DAT). A donor plasmid containing two homology arms flanking a P2A sequence followed by Flpo recombinase was inserted 3' to exon 15 of *Slc6a3*. **B)** PCR genotyping strategy for DAT-Flp mice. The 1000 bp band denotes the WT allele. The 600 bp band indicates the presence of the P2A-Flpo insert. Expression in the F1 generation indicates successful germline transmission. Chim = chimeric founders **C)** Schematic of the unilateral injection of AAV-Fon/Coff-EYFP into the medial SNc/VTA. **D)** Coronal midbrain section stained with an antibody against tyrosine hydroxylase (TH, magenta) showing expression of Fon/Coff-EYFP in the midbrain (green). Inset shows a zoomed-in image of SNc neurons. [PBP = parabrachial pigmented nuclei; PN/PIF = paranigral nucleus/parainterfascicular nucleus; IF = interfascicular nucleus; ml = medial lemniscus] **E)** Schematic of the genetic cross used to generate DAT-Flp;RCE:FRT mice. **F-G)** Coronal midbrain section showing DAT-Flp-dependent recombination of a Flp-dependent EGFP reporter (green) in DAT-Flp;RCE:FRT mice, demonstrating nearly complete overlap with endogenous TH immunostaining (magenta). White arrowhead indicates lack of EGFP expression in the interpeduncular nucleus. Panel G shows zoomed-in images of the VTA and SNc from the boxed regions in F. **H-J)** Confocal images of DAT-Flp-dependent recombination outside of the midbrain in a DAT-Flp;RCE-FRT mouse. The caudal linear nucleus raphe and arcuate nucleus show the expected partial overlap between the EGFP Flp reporter (green) and TH immunostaining (magenta) (white arrowheads). The dorsal raphe shows distinct EGFP labeling immediately ventral to the ventricle. These regions also contain TH+/EGFP- neurons that are likely non-dopaminergic (magenta arrowheads). **K)** Charts showing the percentage of EGFP overlap with TH in different midbrain regions in DAT-Flp;RCE-FRT mice. >96% of EGFP+ neurons express TH in the SNc and VTA. Averaged from two P56 mice, 1 male and 1 female. **L-M)** Confocal images of sections of the locus coeruleus and zona incerta from a DAT-Flp;RCE-FRT mouse showing nearly no EGFP expression in TH+ neurons in these regions.

Figure 2

A **DAT-Flp**

B DAT   TH   Vmat2

DAT-Flp dopamine release

C —WT —Het

D dStr (sites 1-5)

F dStr (peak matched)

E NAc (sites 6+7)

DAT-Flp open field behavior

G Total distance traveled

H Rearing

I Time in center

J Grooming

67
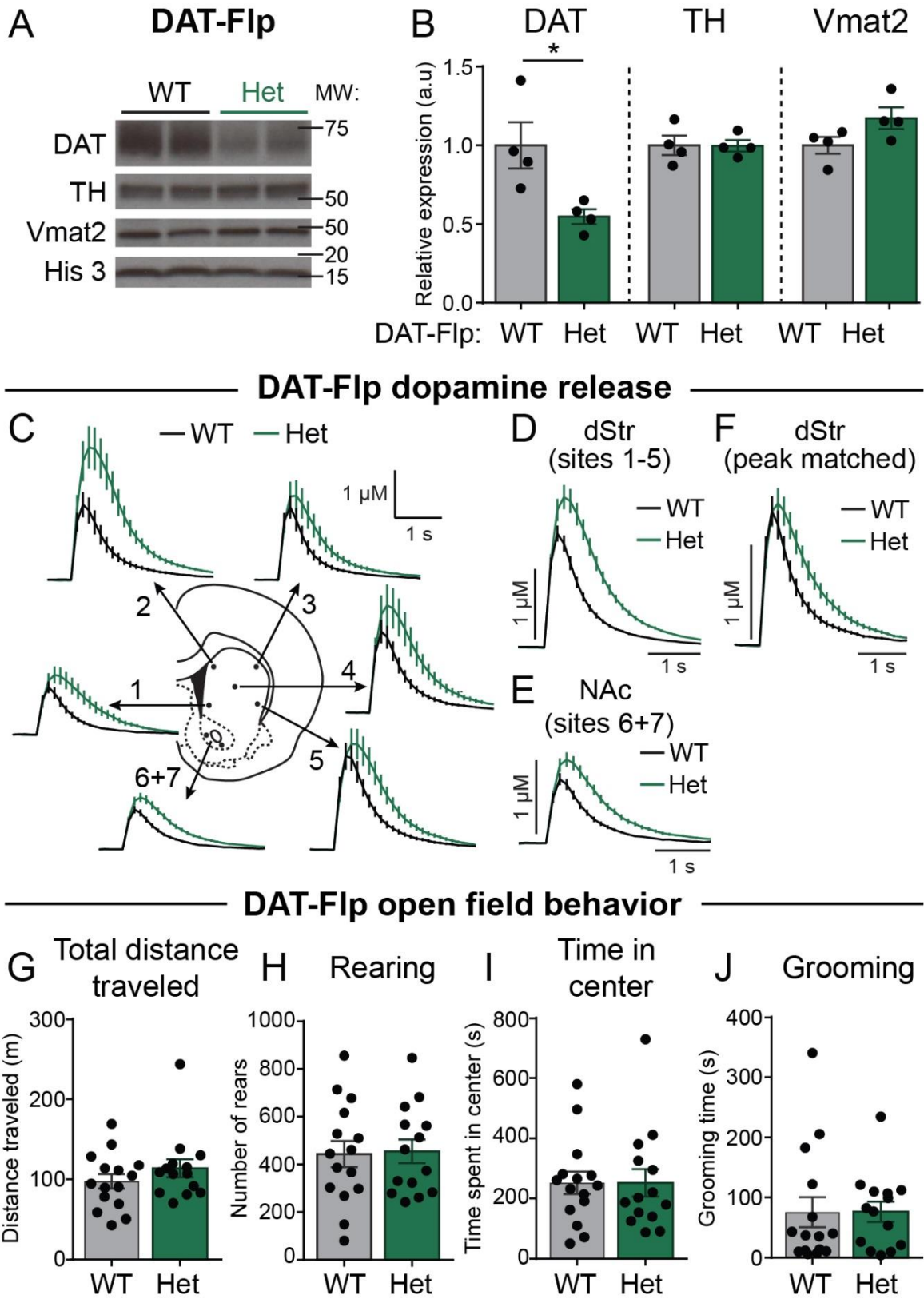
Figure 2. DAT expression and function in DAT-Flp mice. A) Representative western blot images of dopamine active transporter (DAT), tyrosine hydroxylase (TH), vesicular monoamine transporter 2 (Vmat2), and histone H3 (His 3) loading control from striatal lysates from DAT-Flp wild-type (WT) and heterozygous (Het) mice. Two independent samples per genotype are shown. Images were cropped to show the relevant bands. Molecular weight (MW) in KD is indicated on the right. **B)** Quantification of protein levels relative to histone H3, normalized to WT. Bars represent mean +/- SEM. Each dot represents the average of two striatal samples from one mouse (n=4 mice per genotype). DAT: p=0.0259, TH: p=0.9639, Vmat2: p=0.0930; unpaired t-tests. **C)** Extracellular DA ($[DA]_o$) transients evoked by single electrical pulses and recorded with fast-scan cyclic voltammetry (FCV) in different striatal sub-regions. Traces are mean +/- SEM $[DA]_o$ versus time (average of 32 transients per recording site from 4 pairs of DAT-Flp WT and Het mice, 2 male pairs and 2 female pairs). 1: dorsomedial striatum, 2: dorsolateral striatum, 3: ventromedial striatum, 4: central striatum, 5: ventrolateral striatum, 6-7: nucleus accumbens. **D)** Mean +/- SEM $[DA]_o$ versus time (average of 80 transients per genotype) from the dorsal striatum sites #1-5. **E)** Mean +/- SEM $[DA]_o$ versus time (average of 32 transients per genotype) from the nucleus accumbens sites #6-7. **F)** Region- and peak-matched mean +/- SEM $[DA]_o$ versus time from the dorsal striatum of DAT-Flp WT and Het mice (average of 22 transients per genotype). DAT-Flp heterozygous mice have significantly slower $[DA]_o$ re-uptake than WT mice (p<0.0001, single-phase exponential decay curve fit; WT tau=0.409, Het tau=0.648). **G-J)** Behavioral performance of DAT-Flp mice in a 60-minute open-field test. For all graphs, bars represent mean +/- SEM and dots represent values for individual mice. n= 15 WT mice, 6 males and 9 females; n=14 Heterozygous mice, 5 males and 9 females, P50-90. **G)** Total distance traveled in 60 minutes; p=0.2680, unpaired t-test. **H)** Total number of rears in 60 minutes; p=0.8847, unpaired t-test, **I)** Total time spent in the center of open field in 60 minutes; p=0.9981, unpaired t-test. **J)** Total number of grooming bouts in the first 20 minutes; p=0.8061, unpaired t-test.
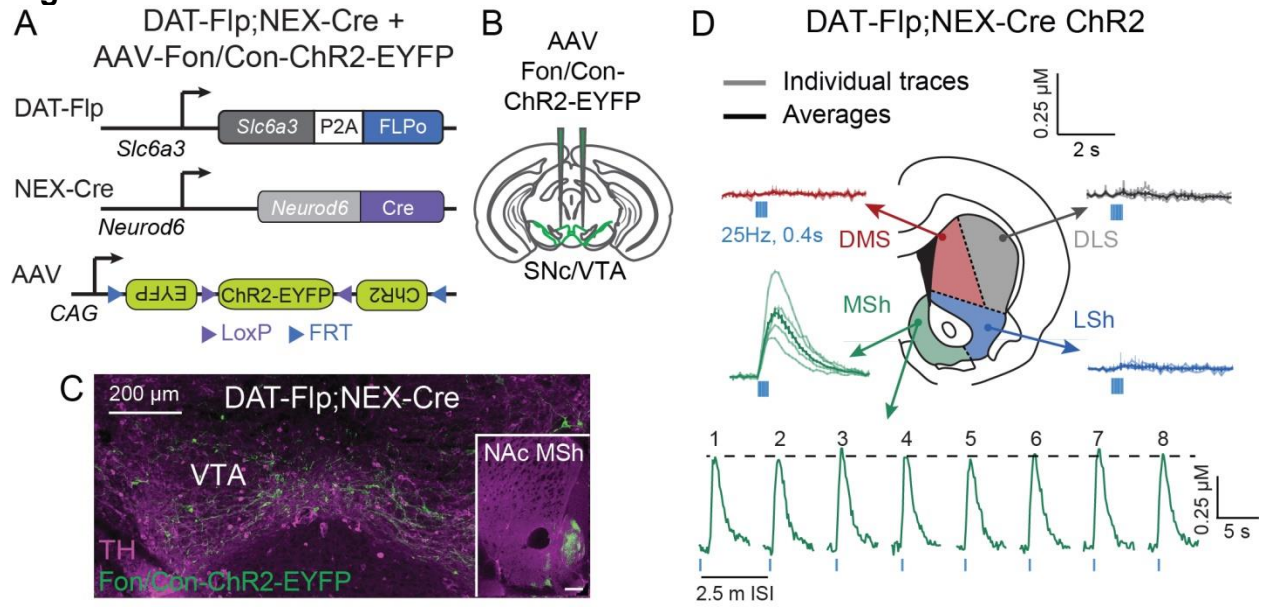
Figure 3

69
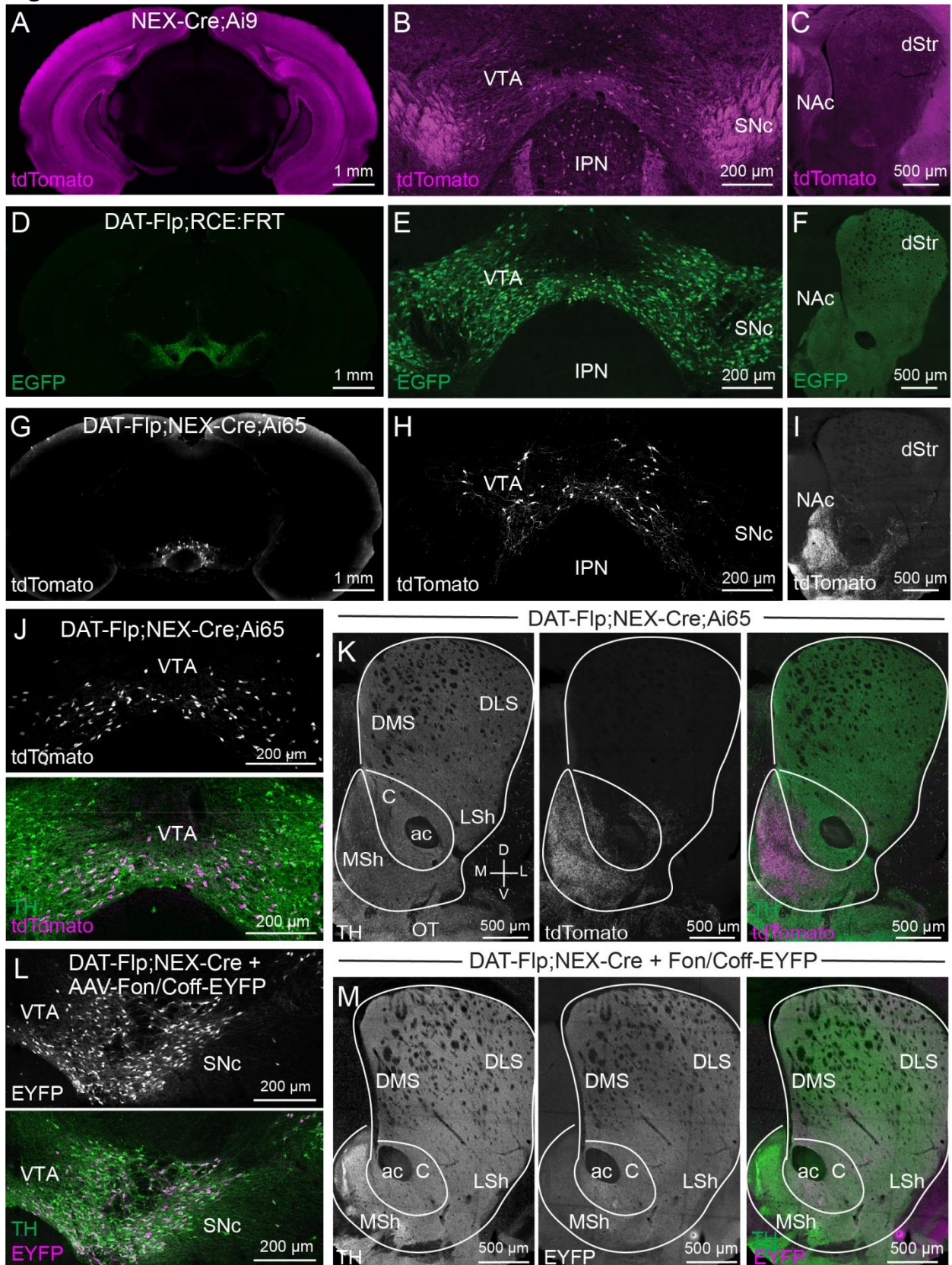
Figure 3. Intersectional genetic targeting of *Neurod6*+ DA neurons. A-C) Confocal images from a P28 male NEX-Cre;Ai9 mouse showing tdTomato expression**. A)** Whole coronal section from a NEX-Cre;Ai9 mouse at A/P -3.4 from Bregma, showing high expression throughout the cortex and hippocampus. **B)** tdTomato expression in the midbrain. Note the fiber tracts in the medial lemniscus and cell bodies in the VTA and adjacent interpeduncular nucleus (IPN). **C)** tdTomato expression in the dorsal striatum (dStr) and nucleus accumbens (NAc) at A/P +1.34 from Bregma. **D-F)** Confocal images from a P50 male DAT-Flp;RCE:FRT mouse showing EGFP expression. **D)** Whole coronal section from a DAT-Flp;RCE:FRT mouse at A/P -3.4 from Bregma, with restricted expression in the midbrain. **E)** tdTomato expression in the midbrain. **F)** tdTomato expression in the striatum and NAc at A/P +1.34 from Bregma. **G-I)** Confocal images from P50 female DAT-Flp;NEX-Cre;Ai65 mouse showing tdTomato expression. **G)** Whole coronal section from a DAT-Flp;NEX-Cre;Ai65 mouse at A/P -3.4 from Bregma, showing restricted expression in the VTA. **H)** tdTomato expression in the midbrain. **I)** tdTomato expression in the striatum and NAc at A/P +1.34 from Bregma. **J)** Confocal images of a section of the VTA from a P50 DAT-Flp;NEX-Cre;Ai65 mouse showing tdTomato (upper panel) co-localization with TH immunostaining (lower panel, merged view). **K)** Confocal images of the projection targets of DAT-Flp;NEX-Cre;Ai65 neurons in the striatum and NAc. Left panel shows TH immunostaining. Middle panel shows tdTomato+ projections from DAT-Flp;NEX-Cre;Ai65 neurons. Right panel shows merged image with TH in green and DAT-Flp;NEX-Cre;Ai65 projections in magenta. [DMS = dorsomedial striatum, DLS = dorsolateral striatum, C = nucleus accumbens core, ac = anterior commissure, LSh = nucleus accumbens lateral shell, MSh = nucleus accumbens medial shell, OT = olfactory tubercle] **L)** Confocal images of the SNc/VTA of a P90 female DAT-Flp;NEX-Cre mouse injected with AAV-Fon/Coff-EYFP (top panel), with TH immunostaining (bottom panel, merged view). **M)** Confocal images of the projection targets of DAT-Flp;NEX-Cre neurons expressing Fon/Coff-EYFP in the striatum and NAc. Left panel shows TH immunostaining. Middle panel shows EYFP+ projections from DAT-Flp-positive/NEX-Cre negative neurons. Right panel shows merged image with TH in green and DAT-Flp-positive/NEX-Cre negative projections in magenta.

Figure 4
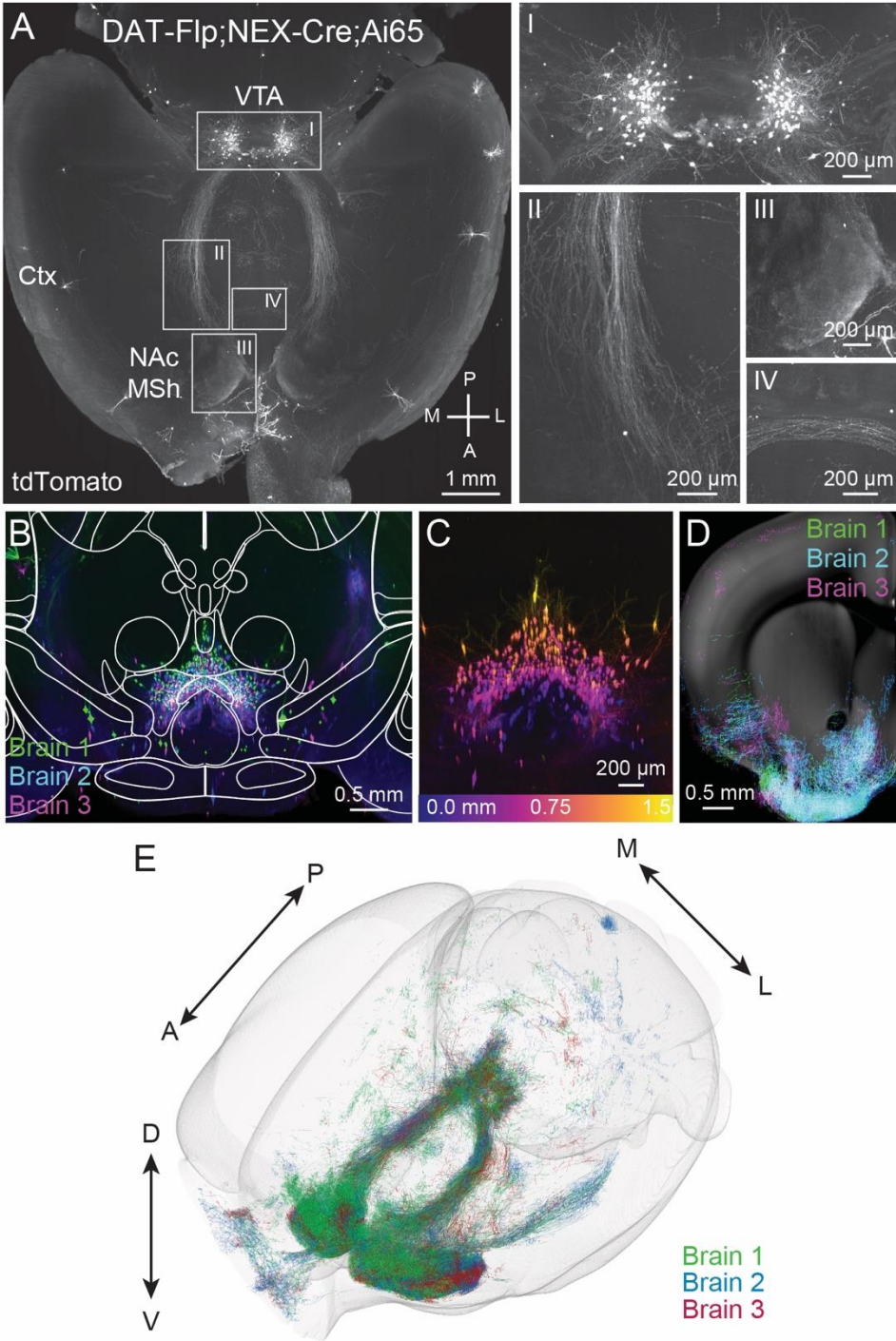
Figure 4. Whole brain expression and projection analysis of DAT-Flp;NEX-Cre;Ai65 mice. A) Whole brains from 2 male and 1 female P120 DAT-Flp;NEX-Cre;Ai65 mice were optically cleared and processed using the Adipo-Clear pipeline. tdTomato fluorescence was amplified with an anti-RFP antibody and whole brains were imaged without sectioning using a light-sheet microscope. Shown is a max projection of 600 µm from a horizontal plane Z-stack. Insets show zoomed-in images of *Neurod6*+ DA neurons in the midbrain (I), axonal tracts from the midbrain to the nucleus accumbens medial shell (NAc MSh) through the medial forebrain bundle (II), *Neurod6*+ DA neuron axon terminals in the MSh (III), and contralateral fibers crossing the midline (IV). Ctx=cortex.**B)** Coronal view (XZ projection) comprising a 1.5 mm A/P cross section of the VTA in optically cleared DAT-Flp;NEX-Cre;Ai65 mice. 3 separate brains were aligned and merged. Image is overlaid with brain region outlines from the middle position of the 1.5 mm cross-section from the Allen Brain Institute reference atlas **C)** Coronal z-stack image of a 1.5 mm cross section of the VTA from a single sample color coded by depth. Depth scale shown in lower panel. **D)** Coronal z-stack image of trailmap-extracted axons from a 500 µm section of the striatum. 3 separate brains were aligned and merged. Extracted axons are overlaid onto a reference slice from the middle position of the 500 µm section from the Allen Brain Institute. **E)** Axonal innervation in a 3D view of trailmap-extracted axons from three aligned DAT-Flp;NEX-Cre;Ai65 brains.

Figure 5

A DAT-Flp;NEX-Cre +
   AAV-Fon/Con-ChR2-EYFP

DAT-Flp — *Slc6a3* | P2A | FLPo
Slc6a3

NEX-Cre — *Neurod6* | Cre
Neurod6

AAV — EYFP | ChR2-EYFP | ChR2
CAG
▶ LoxP ▶ FRT

B AAV Fon/Con-ChR2-EYFP

SNc/VTA

C 200 μm DAT-Flp;NEX-Cre
VTA
NAc MSh
TH
Fon/Con-ChR2-EYFP

D DAT-Flp;NEX-Cre ChR2

Individual traces
Averages

0.25 μM
2 s

25Hz, 0.4s DMS DLS
MSh LSh

1 2 3 4 5 6 7 8

0.25 μM
5 s

2.5 m ISI

Figure 5. Optogenetic activation of DA release in DAT-Flp and DAT-Flp;NEX-Cre mice. A) Schematic of the intersectional genetic strategy to target *Neurod6*+ DA neurons in DAT-Flp;NEX-Cre mice with an AAV expressing Flp- and Cre-dependent channelrhodopsin (ChR2). **B)** Schematic showing bilateral injection of AAV-Fon/Con-ChR2-EYFP into the midbrain of DAT-Flp;NEX-Cre mice. **C)** Confocal image showing midbrain expression of Fon/Con-ChR2-EYFP (green) and co-expression with immunostained TH (magenta) in a DAT-Flp;NEX-Cre mice. Inset shows ChR2-EYFP+ projections in the nucleus accumbens medial shell (NAc MSh) in an injected mouse. Scale bar represents 200μm. **D)** Fast-scan cyclic voltammetry traces of optically-evoked extracellular DA ($[DA]_o$) in striatal slices from DAT-Flp;Nex-Cre mice injected with Fon/Con-ChR2-EYFP. Mean +/- SEM $[DA]_o$ versus time evoked from different striatal subregions by 10 light pulses delivered at 25 Hz. Light colored lines show individual sample traces of n=3-9 transients per recording site, dark colored lines are the average of all samples, recorded from 4 hemispheres of 2 male mice . DMS = dorsomedial striatum, DLS = dorsolateral striatum, LSh = nucleus accumbens lateral shell, MSh = nucleus accumbens medial shell. Bottom panel shows transients recorded in the MSh from 8 consecutive stimulations delivered 2.5 minutes apart.

Supplemental Figure 1
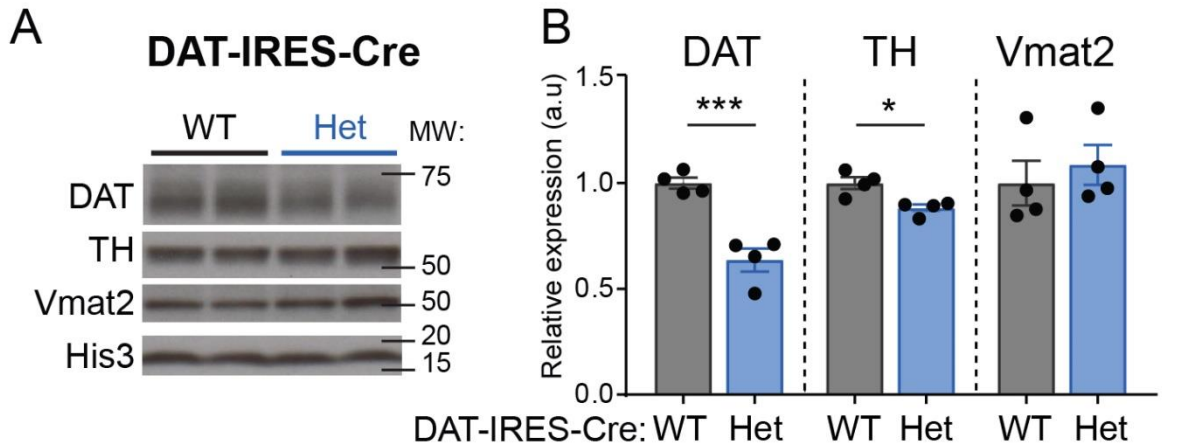
Supplemental Figure 1. DAT expression and function in DAT-IRES-Cre mice. A) Representative western blot images of dopamine active transporter (DAT), tyrosine hydroxylase (TH), vesicular monoamine transporter 2 (Vmat2), and histone H3 loading control from striatal lysates from DAT-IRES-Cre wild-type (WT) and heterozygous (Het) mice. Two samples per genotype are shown. Images were cropped to show the relevant bands. Molecular weight (MW) in KD is indicated on the right. **B)** Quantification of protein levels relative to histone H3, normalized to WT. Bars represent mean +/- SEM. Each dot represents the average of two striatal samples from one mouse (n=4 mice per genotype). DAT: p=0.0009, TH: p=0.0121, Vmat2: p=0.5655; unpaired t-tests. **C)** Fast-scan cyclic voltammetry (FCV) traces of extracellular DA ($[DA]_o$) evoked by single electrical pulses in different striatal sub-regions in DAT-IRES-Cre mice. Traces are mean +/- SEM $[DA]_o$ versus time (average of 27-28 transients per site from 4 pairs of DAT-IRES-Cre WT and Het mice, 1 male pair and 3 female pairs). 1: dorsomedial striatum, 2: dorsolateral striatum, 3: ventromedial striatum, 4: central striatum, 5: ventrolateral striatum, 6-7: nucleus accumbens. **D)** Mean +/- SEM $[DA]_o$ versus time (average of 80 transients per genotype) from the dorsal striatum sites #1-5. **E)** Mean +/- SEM $[DA]_o$ versus time (average of 27-28 transients per genotype) from the nucleus accumbens sites #6-7. **F)** Region- and peak-matched mean +/- SEM $[DA]_o$ versus time from the dorsal striatum of DAT-IRES-Cre WT and Het mice (average of 34-36 transients per genotype). p=0.072, single-phase exponential decay curve fit; WT tau=0.346, Het tau=0.355. **G-J)** Behavioral performance of DAT-IRES-Cre mice in a 60-minute open-field test. For all graphs, bars represent mean +/- SEM and dots represent values for individual mice. n= 15 WT mice, all females; n=12 Heterozygous mice, 12 females and 3 males; age P50-90. **G)** Total distance traveled in 60 minutes; p=0.0099, unpaired t-test. **H)** Total number of rears in 60 minutes; p=0.0668, unpaired t-test, **I)** Total time spent in the center of open field in 60 minutes; p=0.6976, unpaired t-test. **J)** Total number of grooming bouts in the first 20 minutes of open field test; p=0.0258, unpaired t-test.

Supplemental Figure 2

A DAT-Flp;NEX-Cre;Ai65
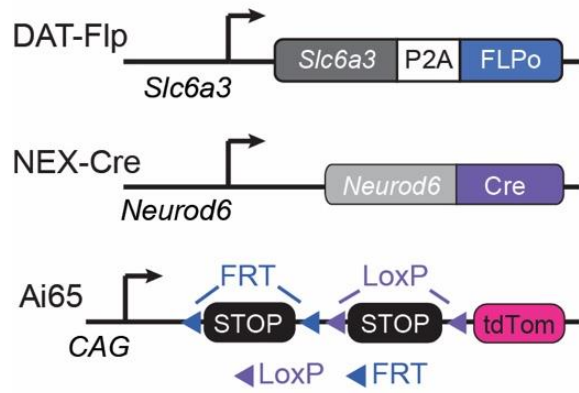
C DAT-Flp;NEX-Cre + AAV-Fon/Coff-EYFP
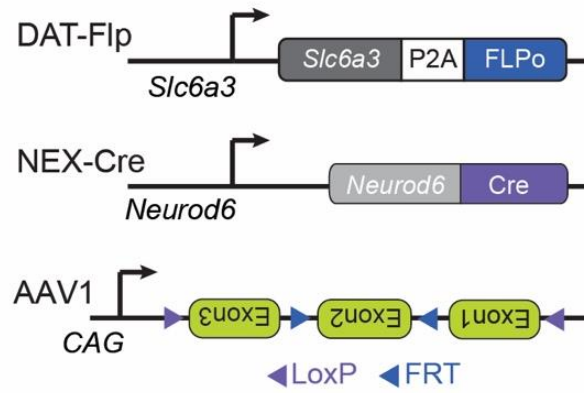
B DAT-Flp;NEX-Cre;Ai65
Lateral septum
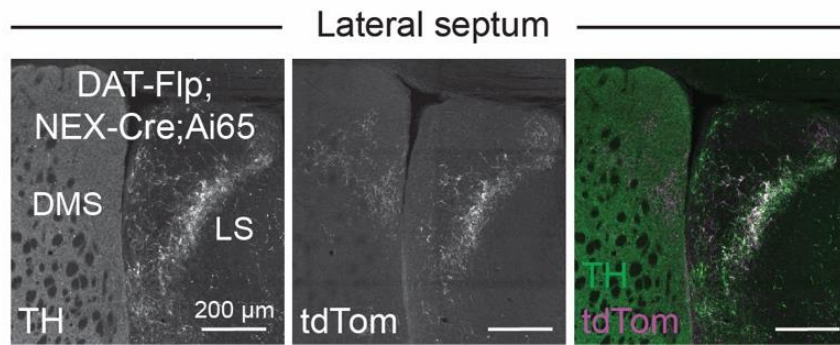
Supplemental Figure 2. Intersectional labeling of neurons and projections in DAT-Flp;NEX-Cre;Ai65 mice. A) Schematic of the generation of DAT-Flp;NEX-Cre;Ai65 mice. In Ai65 mice, tdTomato is expressed in cells that express both Flp- and Cre-recombinase. **B)** Confocal images of projections from DAT-Flp;NEX-Cre;Ai65 neurons to the lateral septum (LS). Left panel shows TH immunostaining. Middle panel shows tdTomato+ projections in the LS. Right panel shows a merged image of TdTomato (magenta) and TH (green) overlap in the LS. DMS = dorsomedial striatum **C)** Schematic of the strategy to label DA neurons that do not express *Neurod6* (see experiment in Fig. 3L,M).

Figure 3

A
DAT-Flp;NEX-Cre;Ai65
Relative projection/process density

Mouse 1 / 2 / 3

Normalized content (a.u.)
.14
.00

Region: AON OT SI LPO PST PSTN PeF PN RR IPN CLi DR

B
DAT-Flp;NEX-Cre;Ai65
Cortical neurons

TH
tdTom
DAPI
50 µm

Anterior Olfactory Area
C
1 mm
300 µm

Cerebellum
D
1 mm
300 µm
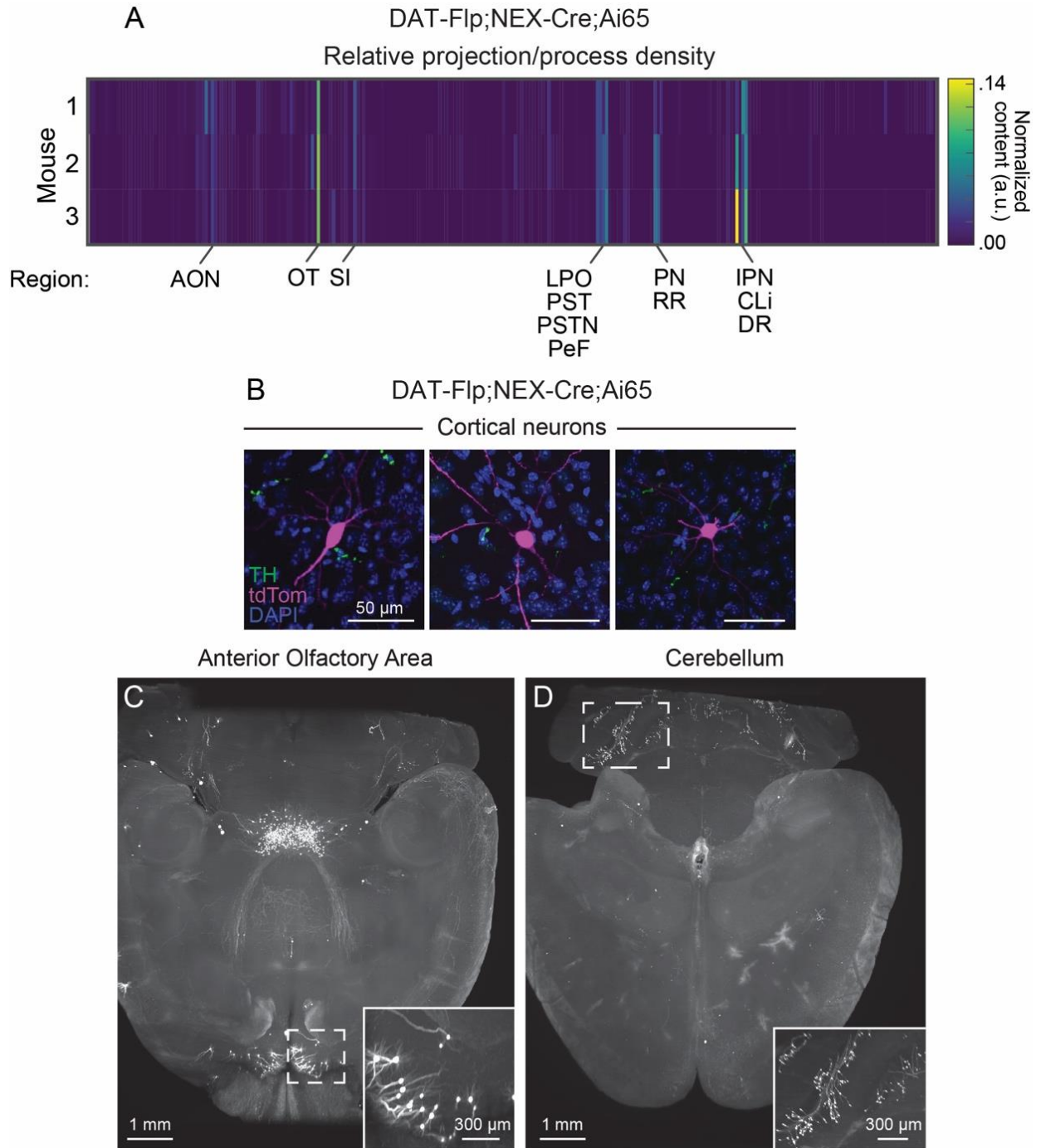
Supplemental Figure 3. Whole brain imaging of DAT-Flp;NEX-Cre;Ai65 mice and projection analysis. A) Brains from DAT-Flp;NEX-Cre;Ai65 mice were processed with AdipoClear and imaged on a light sheet microscope. Projections and processes were quantified using TrailMap. Heatmap shows the total axonal projection/dendrite content of 282 brain regions in using boundaries from the Allen Institute Common Coordinate Framework (CCF). Values are normalized to both the region volume and total projection content per brain. The rows represent 3 independent brains (AON = Anterior optic nucleus; OT = Olfactory tubercle; LPO = Lateral preoptic area; PST = Preparasubthalamic nucleus; PSTN = Parasubthalamic nucleus; PeF = Perifornical nucleus; PN = Paranigral nucleus; RR = Retrorubral area; IPN = Interpeduncular nucleus; CLi = Central linear nucleus raphe; DR = Dorsal nucleus Raphe). **B)** DAT-Flp;Nex-Cre;Ai65 mice exhibit tdTomato expression (magenta) in a small number of cortical neurons that do not co-express TH by immunostaining (green). **C-D)** Horizontal 450 μm z-stack projections of light-sheet microscope whole brain images. DAT-Flp;Nex-Cre;Ai65 mice show consistent tdTomato expression in subpopulations of neurons in the anterior olfactory area (C) and cerebellum (D).

Chapter 4: Final considerations on dopaminergic sub-circuits

Daniel Joseph Kramer

Department of Molecular and Cell Biology
University of California Berkeley

The current and future state of the field

"Unfortunately, nature seems unaware of our intellectual need for convenience and unity, and very often takes delight in complication and diversity."
Santiago Ramon y Cajal[2]

As it stands now, there have been numerous scRNAseq studies on individual neuronal populations, brain regions and the whole brain. We have unprecedented access to the genetic fingerprint of the majority of neuron types throughout the brain[34-36]. While there are some caveats to defining subgroups of neurons based on their gene expression, it is still the most efficient and accurate way to rapidly define neuronal subclasses. However, because it is currently more challenging and time consuming, the efforts to push forward and understand what these subpopulations *represent* has taken a back-seat to accumulating more data. The work presented here has helped advance our understanding as we show that, using scRNAseq, genetically defined DA neuron subpopulations are functionally relevant. They have distinct projection targets, physiology, and respond differently to degenerative disease models[97]. These types of studies are necessary to ensure that neuronal subpopulations defined by their gene expression are *de-facto* populations and not simply statistically significant but biologically meaningless.

Now that we have the information necessary to define different neuronal populations, the field must push forward in building the necessary tools to explore subpopulations. With this, we can take the next step in creating a new brain atlas describing the many distinct circuits based on discrete cells types. Fortunately, some tools are already being used to help parse different neuronal subpopulations. We now have transgenic Flp reporters for DAT (see chapter 3), *Th[182]*, SERT[44], VIATT[257], *Vglut2[257]*, and a host of others[238,257]. In conjunction with the myriad of transgenic Cre lines that exist from the mutant mouse research and resource center (MMRRC) and others[258], the various Flp lines can be combined to intersectionally label countless neuronal subpopulations. These tools open the door to studies that accurately and consistently label many newly discovered subgroups.

While this project defined and characterized subpopulations of DA neurons, and developed a new transgenic tool to promote the further study of dopaminergic subpopulations, there are several lines of questioning that could follow. While genetically defined subgroups of neurons show functional relevance[44,97], defining projection-based subpopulations would help parse different dopaminergic roles as projection target is most associated with behavioral effects. To address this, one could inject retrobeads into the various areas DA neurons project to. After confirming accurate labeling of the projection target, retrobead-positive neurons in the midbrain could be removed and pooled using laser microdissection. The gene expression between

neurons projecting to different regions could be analyzed to find genetic signatures that define projection target. Methods similar to these have been done previously[224]. This study used retrograde based translating ribosomal affinity purification (TRAP) to genetically profile NAc-projecting DA neurons in the VTA. However, this study did not distinguish sub-regions of the NAc or compare the gene profile of NAc-projecting DA neurons to DA neurons with different projections. In addition, given the few numbers of cells generated from retrograde tracing, laser capture may allow for more efficient RNA retrieval than traditional TRAP assays.

Using this information, one can define the marker genes that define projections. With this, mice could be developed if the cre line does not exist yet, and the circuit can then be manipulated to determine the behavioral role of that dopaminergic projection. In addition, it would provide a way to access one of the least studied subpopulations of neurons in the retrorubral field (RRF). While there are no major hypotheses about the effects of RRF activation, one goal moving forward would be to uncover the role these DA neurons play in the brain. There has been little done to study this population, aside from small anatomical analyses and it's response to 6-OHDA[259]. This work has shown RRF DA neurons project in part to the dorsal striatum and contribute to motor behaviors[259]. These experiments would provide an interesting and uncrowded area of research.

Historically, neuronal resistance to degeneration in PD has compared the SNc to the VTA[58,174,176]. While the SNc exhibits substantial degeneration, the VTA also shows a significant, marked reduction of 40%-70% of neurons[76,79,96]. The VTA represents a great model to study what confers resistance to degeneration for some neurons and not others. Our previous work has shown that *Neurod6+* neurons in the VTA are selectively spared in a 6-OHDA model of Parkinson's disease[97]. More specifically, neurons that express *Neurod6* but do *not* express *Grp*, which represent about 25% of Neurod6-DA neurons in the VTA, exhibit a less than 20% reduction following 6-OHDA injection as compared to 70% for the rest of the VTA[97]. What makes these neurons less vulnerable to neurodegeneration is unclear. While Neurod6 expression does help maintain mitochondrial health and reduce degeneration in cell culture models[98,99], *Neurod6+/Grp+* neurons degenerate at a similar rate as the rest of the VTA[97]. To explore this further, our scRNAseq data set or others[34,35,178] could be used to determine what genes are present in *Neurod6+/Grp-* neurons and not in *Neurod6+/Grp+* neurons that could confer a resistance to Parkinson's disease. While very few studies have compared neurons within the VTA[96,97], using the knowledge that *Neurod6+/Grp-* neurons are spared, these experiments could reveal new, unique neuroprotective targets.

Finally, one of the major advancements that tools like the DAT-Flp mouse line allows is the study of various genes that could confer functional relevance. One could choose

specific Cre mouse lines based on different receptors that would confer a different response to neuromodulators from their neighbors[54,55]. Also, one could explore genes that would allow the co-release of neurotransmitters, like glutamate[61,183-185], or GABA[186-188]. This would allow researchers to study what the functional consequences of co-release are. Finally, one of the most exciting possibilities comes from studying neuropeptidergic neurons and co-release in the central nervous system. Preliminary work reveals that there are dopaminergic circuits that have the necessary machinery to sustain peptidergic signaling.

Neuropeptide signaling in the central nervous system

I was once told that being a scientist is like constantly running in front of a slow-moving freight train. There will *always* be other researchers doing competing experiments and the next scoop is right around the corner. Studying dopaminergic heterogeneity and circuitry can be exhausting due to how crowded the space is. It is in *this* scientist's opinion, however, that peptidergic signaling in the central nervous system is a completely wide-open field ready to be explored. If given the opportunity to start a new project from scratch, I would study whether peptides are co-released from neurons throughout the brain and what behavioral consequences that has. More specifically, within midbrain DA neuron subpopulations lie two distinct circuits defined by neuropeptide expression. Through single cell studies[33], two groups of neurons in the VTA have be revealed that express gastrin releasing peptide (GRP) and vasoactive intestinal protein (VIP).

GRP and its receptor GRPR, a G_q coupled GPCR, have a well-documented role in peripheral nervous system itch pathways[260]. In addition, there have been a few studies over the last 2 decades that point to small GRP-GRPR circuits in the amygdala and thalamus[261-263]. GRP causes GRPR-expressing neurons in these regions to increase their resting membrane potential and sometimes drives increases in baseline firing rates[262,263]. In addition, these circuits play a role in inhibiting fear memories in the amygdala[261,262]. VIP and its receptors VIPR1/2 have been even less studied in the central nervous system. Some work has shown that VIP is essential in the maintenance of circadian rhythms in the suprachiasmatic nuclei[264]. In addition, injection of a VIPR2 antagonist into the BNST prevented cocaine use reinstatement following-footshock[265]. Finally, through knockout mouse models, VIP signaling was shown to be excitatory on thalamocortical neurons[266]. Aside from these studies, there has been very little to explore what role VIP plays as a neuropeptide in the central nervous system. This is curious because VIP marks one of the major interneuron cell types[15,191], giving these neurons the potential to have multi-dimensional signaling in addition to GABA release on any neuron that expresses a VIP receptor. Based on preliminary analyses of peptide expressing DA neurons and their projections targets, we have shown that GRP-DA

neurons and VIP-DA neurons are embedded in circuitry that would allow for neuropeptide co-release to play a significant, functional role in brain function.

GRPR neurons in the medial shell

WE and others have shown that DA neurons in the ventromedial VTA and SNc express the neuropeptide gastrin releasing peptide (GRP) (Fig. 1A) [97,177,178,196]. What has yet to be explored is whether DA neurons release GRP, and whether their cognate receptors are present in the striatum. Previous work has shown that GRP-DA neurons project to the DMS and NAc MSh (Fig. 1B)[97]. To follow up on this work, our lab has explored whether the SPNs in the striatum that receive projections from GRP-DA neurons express GRP receptor (GRPR). To this point, we used fluorescent *in situ* hybridization (FISH) to determine whether *Drd1* or *Drd2* expressing SPNs also express *Grpr*. Interestingly, we found evidence for two distinct populations of *Grpr* expressing neurons throughout the striatum (Fig. 1C+F). In a band of D1-SPNs across the ventral DMS there is sparse expression of *Grpr+* neurons (Fig. 1C). In the medial shell, across the anterior to posterior axis, there are high density regions of *Grpr+* D2-SPNs (Fig. 1C+D). Within the medial shell, the highest density is found in the most dorsal regions, where almost 20% of D2-SPNs express *Grpr* (Fig. 1E). These findings were very exciting as there has been no reference to any GRP-GRPR circuits within the basal ganglia and this represented a completely novel finding. In order to move forward, we needed a transgenic mouse line to label *Grpr+* neurons.

Fortunately, there was a mouse model made in 2017. Using this GRPR-Cre mouse[267] crossed with Ai9;tdTom[206], we confirmed the presence of GRPR+ SPNs in the NAc MSh (Fig. 2A). Interestingly, nearly every SPN in the dorsal striatum expresses tdTomato in this line, whereas the NAc MSh showed expression similar to FISH data (Fig. 2A). This is likely caused by off-target recombination and not ubiquitous *Grpr* expression because P0 pups showed no increase *Grpr+* expression in the dorsal striatum (data not shown) and the GRPR-Cre mouse was developed using BAC transgenic methods which historically lead to variable expression. We believe the FISH data represents the true baseline expression of *Grpr*. Because of the over labeling, we don't believe this mouse line will allow the study of *Grpr+* neurons in the dorsal striatum. To determine if the GRPR-Cre+ neurons in the medial shell labeled D2-SPNs specifically, we crossed a GRPR-Cre;Ai9 mouse with a D2-GFP[258] mouse line and looked at co-labeling. 88% of GRPR-Cre+ neurons in the anterodorsal MSh shell expressed D2-GFP, with the ventral MSh showing 79% co-expression (Fig. 2B). The overlap changed, decreasing slightly in the more posterior regions (Fig. 2B). Based on this evidence, we believe the GRPR-Cre+ neurons in the medial shell and core are the D2-GRPR neurons found through FISH. Our next goal was to determine if this subpopulation of D2 neurons had distinct circuitry or response to GRP.

Canonically, D2 SPNs in the medial shell project almost exclusively to the ventral pallidum (VP)[268]. To determine the projection targets of D2-GRPR neurons, we injected an AAV5-Flex-mCherry virus into the medial shell of GRPR-Cre;D2-GFP mice (Fig. 2C). We then took serial sections of the VP to compare the gross projections from D2 neurons to the ventral pallidum labeled with GFP to the GRPR-Cre;mCherry expression. We found that GRPR-Cre+ neurons in the MSh selectively project to the anteromedial VP (Fig. 2D). This implies that D2-GRPR neurons represent a distinct sub-circuit of D2 SPNs. Finally, to determine if GRP affects GRPR-Cre+ neurons in the MSh, we used slice physiology experiments. In GRPR-Cre;Ai9 mice, we made accumbal slice preparations. Slices were bathed in ACSF plus inhibitors. GRPR-Cre;Ai9 neurons then underwent a protocol of stepwise current injections. Following this, 50 nM GRP was washed on. Five minutes following GRP wash on, we repeated the stepwise current injections to compare the excitability of the same cell before and after GRP wash-on. These pilot experiments revealed a cell intrinsic increase in excitability following GRP wash-on (example traces in Fig. 2E).

These data open up an exciting line of questions at varying scales. One, at the smallest scale, is what role does GRP have on D2-GRPR SPN physiology? Does this small population of neurons have opposite or amplified effects if GRP is present? Second, are there functional differences between neighboring neurons that are *Grpr+* and *Grpr-*? It would be worth exploring whether these two populations have different physiological properties, projection targets, and inputs. Finally, is there any relationship between D1-GRPR and D2-GRPR neurons? While they likely project to different regions, it is intriguing that there exists two separate, distinct, and small populations of GRPR neurons in the striatum. Exploring whether they have an opposing, cooperative or no relationship would be of interest.

VIPR2 neurons in the bed nucleus stria terminalis

VIP has been consistently shown to mark a subset of DA neurons in the dorsal raphe nucleus (DRN), peri-aqueductal grey (PAG), and VTA (Figure 3A)[177,178]. Interestingly, these neurons appear to project almost exclusively to a sub-region of the oval of the bed nucleus stria terminalis (BNST), and the central amygdala (Figure 3B)[182]. Interestingly, one of the major receptors for VIP, VIP receptor 2 (VIPR2 or VPAC2) is found in only three regions throughout the brain, the oval of the BNST, the CEA, and the suprachiasmatic nucleus (STN) (Figure 3C-D)[160,269,270]. VIPR2 neurons in the BNST express GABAergic markers with a smaller proportion expressing *Drd2* (Fig. 3E). Thus, while there are dopaminergic projections and neurons with DA receptors in the BNST, there exist neurons that can respond to VIP and may not respond to DA. This is strong evidence that there is a functional circuit that depends on VIP release from VIP-DA

neurons.

Future work to determine the role of neuropeptide-DA co-release

There are a host of basic experiments that need to be done to uncover whether these dopaminergic populations release GRP or VIP. The most vital ones depend on further work washing GRP or VIP onto GRPR neurons in the MSh or VIPR2 neurons in the BNST using slice physiology. This should be done with a cocktail of antagonists for glutamatergic, GABAergic, and dopaminergic receptors to isolate the cell intrinsic responses to the neuropeptide. This is important because there is currently a dearth of neuropeptide reporters which makes it difficult to determine if neuropeptides are released and if they are released by DA neurons. Two pieces of experimental evidence would be sufficient to answer this question. First, electron microscopy in the NAc MSh and BNST with antibody labeling of DA neuron axons, and if possible, GRP or VIP. This would confirm dopaminergic axons contain both DA and neuropeptides. If the neuropeptide antibodies aren't high enough quality, simply confirming the presence of dense-core vesicles[271] which contain neuropeptides would at least verify that dopaminergic axons contain neuropeptides. Following this, physiology experiments could confirm the functional release of neuropeptides. One could activate DA neuron subpopulations that express GRP or VIP using an intersectional labeling in physiology slice preps bathed in a cocktail of antagonists for AMPA/NMDA receptors, GABA receptors, and DA receptors. One would then record from GRPR$^+$ or VIPR$^+$ neurons following GRP-DA or VIP-DA neuron activation to explore whether these neurons respond in a similar way to when the neuropeptide was washed-on. If they do respond in the presence of the cocktail of antagonists, it is likely to be caused by neuropeptide released from DA neurons. This could be confirmed further by abolishing the response with the addition of a neuropeptide receptor blocker. If there is evidence for dense-core vesicles within dopaminergic axons, and GRPR$^+$ or VIPR$^+$ neurons show a response to neuropeptide-DA neuron activation that is abolished with neuropeptide antagonists, this will be sufficient evidence to confirm peptidergic co-release.

If the previous experiments show that there is neuropeptide release and it causes significant changes in cell physiology, further experiments could be used to determine whether peptidergic release causes behavioral changes. In order to address this, cannula infusion of GRP or VIP into the NAc MSh or BNST of awake, behaving mice could help uncover their role. This will require careful consideration of the literature to decide which behavioral tests would be appropriate. In addition, the use of a peptide receptor antagonist as a control would be necessary to ensure this is caused by specific neuropeptide actions. Of course, there is the still the possibility that there are physiological effects of neuropeptide wash-on, but no significant effect of cannula injection on any hypothesized behavior. There are several reasons why this could be.

Considering both GRPR and VIPR2 act via slow GPCRs, and act on long time scales, they may not have a quickly discernable role. In addition, it is possible that their actions are subtle, or involve only small populations of neurons, thus showing no functional role in behavior. It may be a far stretch to assume that there is an entirely parallel signaling system throughout the central nervous system that has only had its surface scratched. Maybe in matters such as these, skepticism is important. However, until the evidence to the contrary is shown, this scientist will continue to believe it is there: strong opinions loosely held.

Figures and Legends
Figure 1

A VTA •*Grp+* SNc

B DLS DMS Grp-DA VTA LSh Core MSh SNc

C ● *D1⁺/GRPR⁺* MSNs ● *D2⁺/GRPR⁺* MSNs

Bregma: 1.42   Bregma: 1.34   Bregma: 1.18

D Medial Shell *Grpr in situ*

Drd1
Drd2
Grpr
10um

E Percent of D2-MSNs that are Grpr⁺

4.5% 18.4%
1.5%
<1% 1.3%
Bregma: 1.42

3.7% 18.6%
<1%
<1% 2.5%
Bregma: 1.34

4.7% 18.1%
<1%
<1% 3.7%
Bregma: 1.18

25% *Grpr+*

<1% *Grpr+*

F *Grpr* MSN identity

Percent

Lateral Shell/ ventromedial striatum   Core   Medial Shell

D1/D2
D1
D2
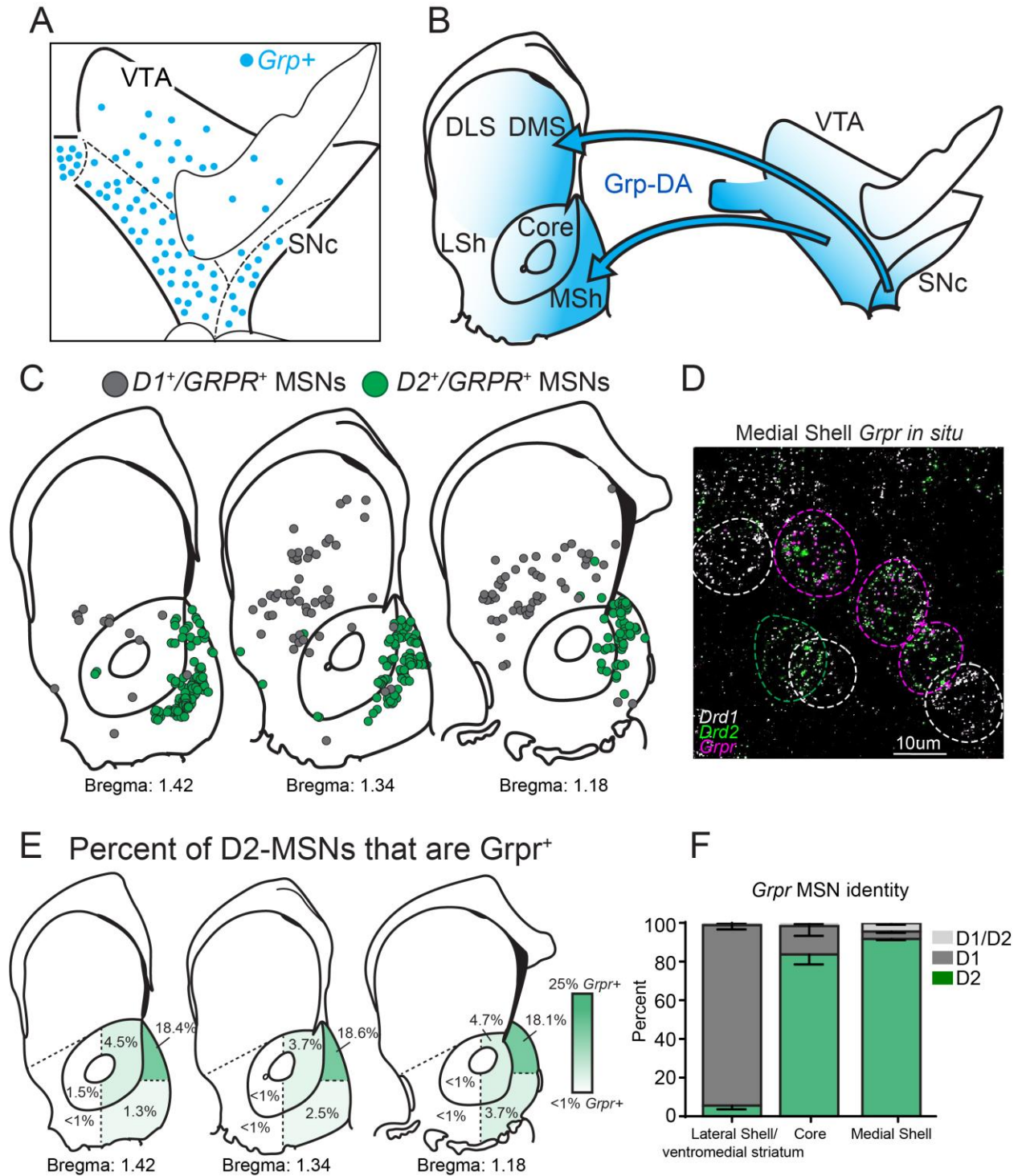
Figure 1. Grp-Grpr circuitry in mesolimbic DA neurons and striatal SPNs. A) Representative *in situ* data for *Grp*/*Th* co-expression in the mouse midbrain**.** Each dot represents a neuron positive for both *Grp* and *Th*. Figure made from previously published data[97]. **B)** Schematic of GRP-DA neurons and their projection targets to the striatum. GRP-DA neurons make strong, strict projections to the dorsal medial striatum (DMS) and nucleus accumbens medial shell (NAc MSh). Figure made from previously published data[97] **C)** Representative *in situ* data for *Grpr* expression in three separate sections of the striatum. Grey dots represent neurons positive for both *Grpr* and dopamine receptor subtype 1 (*Drd1)*. Green dots represent neurons positive for both *Grpr* and *Drd2*. Individual neurons were aligned to their relative location from the Paxinos mouse brain atlas[197]. **D)** Fluorescent *in situ* for *Grpr, Drd1,* and *Drd2* from the medial shell. White circles show *Drd1+* neurons, green circles show *Drd2+* neurons, and magenta circles show *Drd2+/Grpr+* neurons. **E)** Schematic that shows what percent of all *Drd2+* neurons in the given region express *Grpr+*. GRPR-D2 SPNs are heavily enriched in the dorsal medial shell. **F)** Bar graph showing what percent of *Grpr+* neurons in the indicated region are *Drd1+, Drd2+,* or both *Drd1+* and *Drd2+*. *Grpr* expression shows anatomical segregation where they are *Drd1+* in the lateral shell and ventromedial striatum, and *Drd2+* in the nucleus accumbens core and medial shell.

Figure 2

GRPR-Cre;Ai9 expression in the striatum

A — tdTomato — 500 um
I — tdTomato — 100 um
II — tdTomato — 100 um

B — AAV5-Flex-mCherry — GRPR-Cre;D2-Gfp

C — GRPR-Cre;D2-GFP; Flex-mCherry — D2-GFP — mCherry — 250 um

— GRPR-Cre;Flex-mCherry and D2-GFP overlap in the NAc Msh —

mCherry — 50 um
D2-GFP — 50 um
D2-GFP — mCherry — 50 um

D — Percent of GRPR-Cre+ neurons that are D2+

56%   88%
79%
Bregma: 1.34

74%   100% D2+
88%
52%
50% D2+
Bregma: 1.18

E — D2-GRPR projections in the ventral pallidum

level
40
30
20
10
a.u

D
M — L
V

Dorsal Striatum

P
A
VP

F — Current injections
Baseline
50 nM GRP

100 pA
75 pA
50 pA

20 mV
250 ms

Figure 2. GRPR-Cre neuron expression, projections, and physiology. A) Confocal image of GRPR-Cre;Ai9 expression in the striatum. Insets show nearly pan-neuronal expression in the dorsal medial striatum (I), and sparse expression in the NAc MSh (II). **B)** Schematic of injection scheme. AAV5-Flex-mCherry was injected into the MSh of D2-GFP mice. **C)** mCherry expression in GRPR-Cre;D2-GFP mice following injection. Right panels show zoomed image of (C). Green arrows indicate mCherry+/D2-GFP+ neurons and magenta arrows indicate mCherry+/D2-GFP- neurons. **D)** Schematic of overlap between D2-GFP neurons and mCherry neurons. Highest overlap was found in the dorsal MSh (88%) and posterior core (88%). **E)** Projection heat maps of mCherry fibers from the MSh to the ventral pallidum (VP). The highest density of fibers was found in the mediodorsal anterior VP. **F)** Example traces from cell physiology experiments. GRPR-Cre neurons were injected with current steps before and after GRP wash on. GRP wash on caused increases in excitability. There was a higher probability of firing action potentials following the same current injections following GRP wash on.

Figure 3

A ● *Vip+*

v PAG
DRN

B Dorsal Raphe/
Periaqueductal Gray
VIP-DA
BNST

C ● *Gad2+/Vipr2+* neurons
Oval
LD AL A
BNST

D Oval LD AL
Vipr2
Drd2
100 um

E Percent co-labeling with *Vipr2*
Gad2
Drd2
Drd1
0   50   100
Vipr2
Drd2
Gad2
20 um
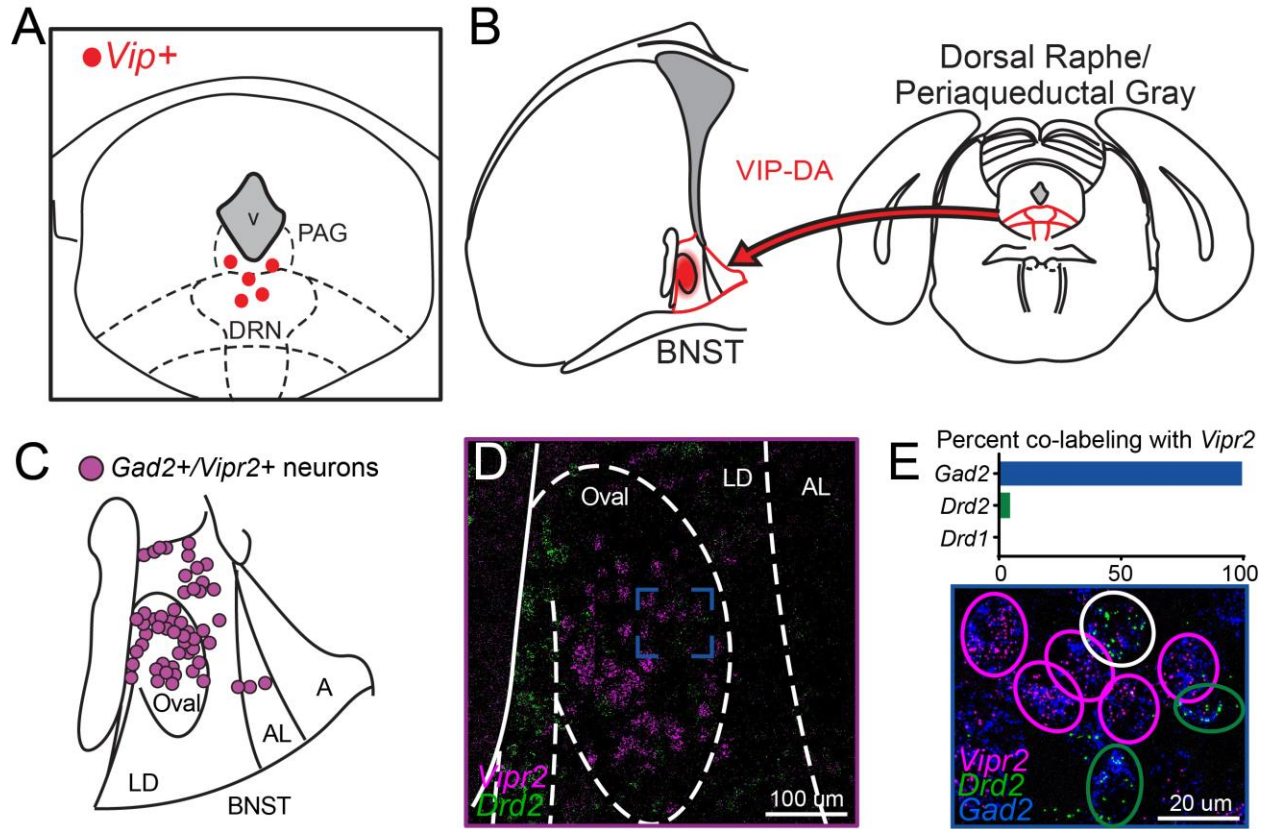
Figure 3. VIP-VIPR2 circuitry in DRN DA neurons and GABAergic BNST oval neurons. A) Representative IHC data for VIP/DAT co-expression in the mouse DRN**.** Each dot represents a neuron positive for both VIP and DAT. **B)** Schematic of VIP-DA neurons and their projection targets to the oval of the bed nucleus of the stria terminalis (BNST). Projection data taken from previously published reports[177]. **C)** Representative *in situ* data for *Vipr2* expression in a single section of the BNST. Magenta dots represent neurons positive for *Vipr2*. Individual neurons were aligned to their relative location from the Paxinos mouse brain atlas[197]. (LD – laterodorsal, LA – lateral anterior, A – Anterior) **D)** Fluorescent *in situ* for *Vipr2* and *Drd2* BNST. **E)** Bar graph of the percent of *Vipr+* neurons that are also *Gad2+, Drd2+,* or *Drd1+.* Image shows a zoom of panel (D). Magenta circles show *Vipr+/Gad2+* neurons*,* white circles show *Drd2+/Gad2+* neurons, and green circles show *Vipr2+/Gad2+/Drd2+* neurons.

References

1 Crick, F. H. C. The impact of molecular biology on neuroscience. *Philosophical transactions of the Royal Society of London. Series B, Biological sciences* **354**, 2021-2025, doi:10.1098/rstb.1999.0541 (1999).

2 Cajal, R. y. The structure and connexions of neurons. *Nobel Lectures*, 220-253 (1906).

3 Golgi, C. The neuron doctrine - theory and facts. *Nobel Lectures*, 189-217 (1906).

4 Eccles, B. J. C., Fatt, P. & Koketsu, K. Cholinergic and inhibitory synapses in a pathway from motor-axon collaterals to motoneurones. *Journal of Physiology* **126**, 524-562 (1954).

5 Dale, H. Pharmacology and Nerve-endings. *Journal of the Royal Society of Medicine* **28**, 319-332, doi:10.1177/003591573502800330 (1935).

6 Vaaga, C. E., Borisovska, M. & Westbrook, G. L. Dual-transmitter neurons: Functional implications of co-release and co-transmission. *Current Opinion in Neurobiology* **29**, 25-32, doi:10.1016/j.conb.2014.04.010 (2014).

7 Carlsson, A. in *Nobel Lectures*   303-322 (2000).

8 Coons, A. H., Creech, H. J., Norman Jones, R. & Berliner, E. The Deomnstration of Pneumococcal Antigens in Tissues by the Use of Fluorescent Antibody. *The Journal of Immunology* **45**, 159-170 (1942).

9 Pardue, M. L. & Gall, J. G. Molecular hybridization of radioactive DNA to the DNA of cytological preparations. *Proceedings of the National Academy of Sciences of the United States of America* **64**, 600-604, doi:10.1073/pnas.64.2.600 (1969).

10 Tessmar-Raible, K. *et al.* Conserved Sensory-Neurosecretory Cell Types in Annelid and Fish Forebrain: Insights into Hypothalamus Evolution. *Cell* **129**, 1389-1400, doi:10.1016/j.cell.2007.04.041 (2007).

11 Arendt, D. The evolution of cell types in animals: Emerging principles from molecular studies. *Nature Reviews Genetics* **9**, 868-882, doi:10.1038/nrg2416 (2008).

12 Stoeckli, E. T. Understanding axon guidance : are we nearly there yet ? , doi:10.1242/dev.151415 (2018).

13 Luo, L., Callaway, E. M. & Svoboda, K. Genetic Dissection of Neural Circuits. *Neuron* **57**, 634-660, doi:10.1016/j.neuron.2008.01.002 (2008).

14 Huang, J. Z. & Zeng, H. Genetic Approaches to Neural Circuits in the Mouse. *Annual Review of Neuroscience* **36**, 183-215, doi:10.1146/annurev-neuro-062012-170307 (2013).

15 Markram, H. *et al.* Interneurons of the neocortical inhibitory system. *Nature Reviews Neuroscience* **5**, 793-807, doi:10.1038/nrn1519 (2004).

16 Nelson, S. B., Sugino, K. & Hempel, C. M. The problem of neuronal cell types: a physiological genomics approach. *Trends in Neurosciences* **29**, 339-345, doi:10.1016/j.tins.2006.05.004 (2006).

17 Mott, D. D. & Dingledine, R. Interneuron Diversity series: Interneuron research - Challenges and strategies. *Trends in Neurosciences* **26**, 484-488, doi:10.1016/S0166-2236(03)00200-5 (2003).

18 Eberwine, J. H. *et al.* Analysis of gene expression in single live neurons. *Proceedings of the National Academy of Sciences* **89**, 3010-3014, doi:10.1016/S0958-1669(99)00036-1 (1992).

19 Phillips, J. & Eberwine, J. H. Antisense RNA amplification: A linear amplification method for analyzing the mRNA population from single living cells. *Methods: A Companion to Methods in Enzymology* **10**, 283-288, doi:10.1006/meth.1996.0104 (1996).

20 Lambolez, B., Audinat, E., Bochet, P., Crépel, F. & Rossier, J. AMPA receptor subunits expressed by single purkinje cells. *Neuron* **9**, 247-258, doi:10.1016/0896-6273(92)90164-9 (1992).

21 Hinkle, D. *et al.* Single neurons as experimental systems in molecular biology. *Progress in Neurobiology* **72**, 129-142, doi:10.1016/j.pneurobio.2004.01.001 (2004).

22   Sheng, H. Z., Lin, P. X. & Nelson, P. G. Analysis of Multiple Heterogeneous mRNAs in Single Cells. *Analytical Biochemistry* **222**, 123-130 (1994).

23   Svensson, V., Vento-tormo, R. & Teichmann, S. A. Exponential scaling of single-cell RNA-seq in the past decade. *Nature Publishing Group* **13**, 599-604, doi:10.1038/nprot.2017.149 (2018).

24   Luo, L. *et al.* Gene expression profiles of laser-captured adjacent neuronal subtypes. *Nature Medicine* **5**, 117-122, doi:10.1038/4806 (1999).

25   Tietjen, I. *et al.* Single-cell transcriptional analysis of neuronal progenitors. *Neuron* **38**, 161-175, doi:10.1016/S0896-6273(03)00229-0 (2003).

26   Kamme, F. *et al.* Single-cell microarray analysis in hippocampus CA1: Demonstration and validation of cellular heterogeneity. *Journal of Neuroscience* **23**, 3607-3615, doi:10.1523/jneurosci.23-09-03607.2003 (2003).

27   Bernard, A., Sorensen, S. A. & Lein, E. S. Shifting the paradigm: new approaches for characterizing and classifying neurons. *Current Opinion in Neurobiology* **19**, 530-536, doi:10.1016/j.conb.2009.09.010 (2009).

28   Wang, Z., Gerstein, M. & Snyder, M. RNA-Seq: a revolutionary tool for transcriptomics. *Nature reviews. Genetics* **10**, 57-63, doi:10.1038/nrg2484 (2009).

29   Shapiro, E., Biezuner, T. & Linnarsson, S. Single-cell sequencing-based technologies will revolutionize whole-organism science. *Nature Reviews Genetics* **14**, 618-630, doi:10.1038/nrg3542 (2013).

30   Macosko, Evan Z. *et al.* Highly Parallel Genome-wide Expression Profiling of Individual Cells Using Nanoliter Droplets. *Cell* **161**, 1202-1214, doi:10.1016/j.cell.2015.05.002 (2015).

31   Vogel, C. & Marcotte, E. M. Insights into the regulation of protein abundance from proteomic and transcriptomic analyses. *Nature Reviews Genetics* **13**, 227-232, doi:10.1038/nrg3185 (2012).

32   Haque, A., Engel, J., Teichmann, S. A. & Lönnberg, T. A practical guide to single-cell RNA-sequencing for biomedical research and clinical applications. *Genome Medicine* **9**, 1-12, doi:10.1186/s13073-017-0467-4 (2017).

33   Poulin, J. F., Gaertner, Z., Moreno-Ramos, O. A. & Awatramani, R. Classification of Midbrain Dopamine Neurons Using Single-Cell Gene Expression Profiling Approaches. *Trends in Neurosciences* **43**, 155-169, doi:10.1016/j.tins.2020.01.004 (2020).

34   Saunders, A. *et al.* Molecular Diversity and Specializations among the Cells of the Adult Mouse Brain. *Cell* **174**, 1015-1030.e1016, doi:10.1016/j.cell.2018.07.028 (2018).

35   Zeisel, A. *et al.* Molecular Architecture of the Mouse Nervous System. *Cell* **174**, 999-1014.e1022, doi:10.1016/j.cell.2018.06.021 (2018).

36   10xGenomics. Chromium Megacell Demonstration. (2018).

37   Brenner, S. Sequences and consequences. *Philosophical Transactions of the Royal Society B: Biological Sciences* **365**, 207-212, doi:10.1098/rstb.2009.0221 (2010).

38   von Bartheld, C., Bahney, J. & Herculano-Houzel, S. The search for true numbers of neurons and glial cells in the human brain: A review of 150 years of cell counting. *Journal of Comparative Neurology2* **524**, 3865-3895, doi:10.1016/j.physbeh.2017.03.040 (2016).

39   Zeng, H. & Sanes, J. R. Neuronal cell-type classification: Challenges, opportunities and the path forward. *Nature Reviews Neuroscience* **18**, 530-546, doi:10.1038/nrn.2017.85 (2017).

40   Bota, M. & Swanson, L. W. The neuron classification problem. *Brain Research Reviews* **56**, 79-88, doi:10.1016/j.brainresrev.2007.05.005 (2007).

41   Migliore, M. & Shepherd, G. M. An integrated approach to classfication neuronal phenotypes. *Nature Reviews Neuroscience* **6**, 810 (2005).

42   Fishell, G. & Heintz, N. The neuron identity problem: Form meets function. *Neuron* **80**, 602-612, doi:10.1016/j.neuron.2013.10.035 (2013).

43   Ronan, T., Qi, Z. & Naegle, K. M. Avoiding common pitfalls when clustering biological data. *Science Signaling* **9**, 1-13, doi:10.1126/scisignal.aad1932 (2016).

44   Ren, J. *et al.* Single-cell transcriptomes and whole-brain projections of serotonin neurons in the mouse dorsal and median raphe nuclei. *eLife* **8**, 1-36, doi:10.7554/eLife.49424 (2019).

45   Shekhar, K. *et al.* Comprehensive Classification of Retinal Bipolar Neurons by Single-Cell Transcriptomics. *Cell* **166**, 1308-1323.e1330, doi:10.1016/j.cell.2016.07.054 (2016).

46   Economo, M. N. *et al.* Distinct descending motor cortex pathways and their roles in movement. *Nature* **563**, 79-84, doi:10.1038/s41586-018-0642-9 (2018).

47   Tasic, B. *et al.* Shared and distinct transcriptomic cell types across neocortical areas. *Nature* **563**, 72-78, doi:10.1038/s41586-018-0654-5 (2018).

48   Stanley, G., Gokce, O., Malenka, R. C., Südhof, T. C. & Quake, S. R. Continuous and Discrete Neuron Types of the Adult Murine Striatum. *Neuron* **105**, 688-699.e688, doi:10.1016/j.neuron.2019.11.004 (2020).

49   Lein, E. S. *et al.* Genome-wide atlas of gene expression in the adult mouse brain. *Nature* **445**, 168-176, doi:10.1038/nature05453 (2007).

50   Cembrowski, M. S. & Menon, V. Continuous Variation within Cell Types of the Nervous System. *Trends in Neurosciences* **41**, 337-348, doi:10.1016/j.tins.2018.02.010 (2018).

51   Harris, K. D. *et al.* Classes and continua of hippocampal CA1 inhibitory neurons revealed by single-cell transcriptomics. *PLoS Biology* **16**, 1-37, doi:10.1371/journal.pbio.2006387 (2018).

52   Tasic, B. *et al.* Adult mouse cortical cell taxonomy revealed by single cell transcriptomics. *Nature Neuroscience* **advance on**, 1-37, doi:10.1038/nn.4216 (2016).

53   Spitzer, N. C. Neurotransmitter Switching? No Surprise. *Neuron* **86**, 1131-1144, doi:10.1016/j.neuron.2015.05.028 (2015).

54   Xiao, L., Priest, M. F., Nasenbeny, J., Lu, T. & Kozorovitskiy, Y. Biased Oxytocinergic Modulation of Midbrain Dopamine Systems. *Neuron* **95**, 368-384.e365, doi:10.1016/j.neuron.2017.06.003 (2017).

55   Woodworth, H. L. *et al.* Neurotensin Receptor-1 Identifies a Subset of Ventral Tegmental Dopamine Neurons that Coordinates Energy Balance. *Cell Reports* **20**, 1881-1892, doi:10.1016/j.celrep.2017.08.001 (2017).

56   German, D. C., Schlusselberg, D. S. & Woodward, D. J. Three-dimensional computer reconstruction of midbrain dopaminergic neuronal populations: from mouse to man. *J Neural Transm* **57**, 243-254 (1983).

57   Herculano-Houzel, S., Mota, B. & Lent, R. How to build a bigger brain: Cellular scaling rules for rodent brains. *Evolution of Nervous Systems* **3**, 155-166, doi:10.1016/B0-12-370878-8/00345-1 (2010).

58   Brichta, L. & Greengard, P. Molecular determinants of selective dopaminergic vulnerability in Parkinson's disease: an update. *Frontiers in Neuroanatomy* **8**, 1-16, doi:10.3389/fnana.2014.00152 (2014).

59   Watabe-Uchida, M., Zhu, L., Ogawa, S. K., Vamanrao, A. & Uchida, N. Whole-Brain Mapping of Direct Inputs to Midbrain Dopamine Neurons. *Neuron* **74**, 858-873, doi:10.1016/j.neuron.2012.03.017 (2012).

60   Björklund, A. & Dunnett, S. B. Dopamine neuron systems in the brain: an update. *Trends in Neurosciences* **30**, 194-202, doi:10.1016/j.tins.2007.03.006 (2007).

61   Morales, M. & Margolis, E. B. Ventral tegmental area: cellular heterogeneity, connectivity and behaviour. *Nature Reviews Neuroscience* **18**, 73-85, doi:10.1038/nrn.2016.165 (2017).

62   Engelhard, B. *et al.* Specialized coding of sensory, motor and cognitive variables in VTA dopamine neurons. *Nature* **570**, 509-513, doi:10.1038/s41586-019-1261-9 (2019).

63   German, D. C., Manaye, K., Smith, W. K., Woodward, D. J. & Saper, C. B. Midbrain dopaminergic cell loss in Parkinson's disease: computer visualization. *Annals of neurology* **26**, 507-514, doi:10.1002/ana.410260403 (1989).

64   Carlsson, A., Lindqvist, M., Magnusson, T. & Waldeck, B. On the Presence of 3-Hydroxytramine in Brain. *Science*, 471 (1958).

65   Carlsson, A. & Waldeck, B. A Fluorimetric Method for the Determination of Dopamine (3-Hydroxytyramine.). *Acta Physiologica Scandinavica* **44**, 293-298, doi:10.1111/j.1748-1716.1958.tb01628.x (1958).

66   Sano, I. *et al.* Distribution of catechol compounds in human brain. *BBA - Biochimica et Biophysica Acta* **32**, 586-587, doi:10.1016/0006-3002(59)90652-3 (1959).

67   Falck, B. Cellular Localization of Monoamines. *Progress in Brain Research* **8**, 28-44, doi:10.1016/S0079-6123(08)60111-9 (1964).

68   Falck, B., Hillarp, N. A., Thieme, G. & Torp, A. Fluorescence of Catechol Amines and Related Compounds Condensed with Formaldehyde. *Journal of Histochemisty and Cytochemisty* **10**, 348-354 (1962).

69   Dahlstrom, A. & Fuxe, K. Evidence for the existence of monoamine neurons in the central nervous system. *Zeitschrift für Zellforschung und Mikroskopische Anatomie* **62** (1965).

70   Chan-Palay, V., Záborszky, L., Köhler, C., Goldstein, M. & Palay, S. L. Distribution of tyrosine-hydroxylase-immunoreactive neurons in the hypothalamus of rats. *Journal of Comparative Neurology* **227**, 467-496, doi:10.1002/cne.902270403 (1984).

71   Donaldson, I., Marsden, C. D., Schneider, S. A. & Bhatia, K. P. in *Book of movement disorders* 159-370 (2012).

72   Calne, D. B., Dubini, A. & Stern, G. Did Leonardo describe Parkinson's diseasE? *New England Journal of Medicine*, 594 (1989).

73   Goetz, C. G. The history of Parkinson's disease: Early clinical descriptions and neurological therapies. *Cold Spring Harbor Perspectives in Medicine* **1**, doi:10.1101/cshperspect.a008862 (2011).

74   Parkinson, J. An essay on the shaking palsy. 1817. *The Journal of neuropsychiatry and clinical neurosciences* **14**, 223-236, doi:10.1176/jnp.14.2.223 (2002).

75   Berg, D. *et al.* Time to redefine PD? Introductory statement of the MDS Task Force on the definition of Parkinson's disease. *Movement Disorders* **29**, 454-462, doi:10.1002/mds.25844 (2014).

76   Damier, P., Hirsch, E. C., Agid, Y. & Graybiel, a. M. The substantia nigra of the human brain: II. Patterns of loss of dopamine-containing neurons in Parkinson's disease. *Brain* **122**, 1437-1448, doi:10.1093/brain/122.8.1437 (1999).

77   Bertler, Å. & Rosengren, E. Occurrence and distribution of dopamine in brain and other tissues. *Experientia* **15**, 10-11, doi:10.1007/BF02157069 (1959).

78   Ehringer, H. & Hornykiewicz, O. Verteilung von noradrenalin und dopamin (3-hydroxytyramin) im gehirn des menschen und ihr verhalten bei erkrankungen des extrapyramidalen systems. *Klinische Wochenschrift* **38**, 1236-1239 (1960).

79   Hirsch, E., Graybiel, a. M. & Agid, Y. a. Melanized dopaminergic neurons are differentially susceptible to degeneration in Parkinson's disease. *Nature* **334**, 345-348, doi:10.1038/334345a0 (1988).

80   Mann, D. M. A. & Yates, P. O. Lipoprotein pigments-their relationship to ageing in the human nervous system: I. The lipofuscin content of nerve cells. *Brain* **97**, 481-488, doi:10.1093/brain/97.1.481 (1974).

81   Jenner, P. Oxidative stress in Parkinson's disease. *Annals of neurology* **53**, S26-S38, doi:10.1007/s12291-009-0017-y (2003).

82   Surmeier, D. J., Obeso, J. A. & Halliday, G. M. Selective neuronal vulnerability in Parkinson disease. *Nature Reviews Neuroscience* **18**, 101-113, doi:10.1038/nrn.2016.178 (2017).

83   Schon, E. a. & Przedborski, S. Mitochondria: The Next (Neurode)Generation. *Neuron* **70**, 1033-1053, doi:10.1016/j.neuron.2011.06.003 (2011).

84   Chuhma, N., Mingote, S., Moore, H. & Rayport, S. Dopamine neurons control striatal cholinergic neurons via regionally heterogeneous dopamine and glutamate signaling. *Neuron* **81**, 901-912, doi:10.1016/j.neuron.2013.12.027 (2014).

85   Testa, C. M., Sherer, T. B. & Greenamyre, J. T. Rotenone induces oxidative stress and dopaminergic neuron damage in organotypic substantia nigra cultures. *Molecular Brain Research*, doi:10.1016/j.molbrainres.2004.11.007 (2005).

86   Höglinger, G. U. *et al.* Dysfunction of mitochondrial complex I and the proteasome: Interactions between two biochemical deficits in a cellular model of Parkinson's disease. *Journal of Neurochemistry*, doi:10.1046/j.1471-4159.2003.01952.x (2003).

87   Moore, D. J., West, A. B., Dawson, V. L. & Dawson, T. M. Molecular Pathophysiology of Parkinson's Disease. *Annual Review of Neuroscience* **28**, 57-87, doi:10.1146/annurev.neuro.28.061604.135718 (2005).

88   Guzman, J. N. *et al.* Oxidant stress evoked by pacemaking in dopaminergic neurons is attenuated by DJ-1. *Nature* **468**, 696-700, doi:10.1038/nature09536 (2010).

89   James Surmeier, D., Guzman, J. N., Sanchez, J. & Schumacker, P. T. Physiological phenotype and vulnerability in Parkinson's disease. *Cold Spring Harbor Perspectives in Medicine* **2**, 1-27, doi:10.1101/cshperspect.a009290 (2012).

90   German, D. C., Manaye, K. F., Sonsalla, P. K. & Brooks, B. a. Midbrain dopaminergic cell loss in Parkinson's disease and MPTP-induced parkinsonism: sparing of calbindin-D28k-containing cells. *Annals of the New York Academy of Sciences* **648**, 42-62, doi:10.1111/j.1749-6632.1992.tb24523.x (1992).

91   Scherman, D. *et al.* Striatal dopamine deficiency in parkinson's disease: Role of aging. *Annals of Neurology* **26**, 551-557, doi:10.1002/ana.410260409 (1989).

92   Liss, B. *et al.* K-ATP channels promote the differential degeneration of dopaminergic midbrain neurons. *Nature Neuroscience* **8**, 1742-1751, doi:10.1038/nn1570 (2005).

93   Duty, S. & Jenner, P. Animal models of Parkinson's disease: A source of novel treatments and clues to the cause of the disease. *British Journal of Pharmacology* **164**, 1357-1391, doi:10.1111/j.1476-5381.2011.01426.x (2011).

94   Kirik, D., Rosenblad, C. & Björklund, a. Characterization of behavioral and neurodegenerative changes following partial lesions of the nigrostriatal dopamine system induced by intrastriatal 6-hydroxydopamine in the rat. *Experimental neurology* **152**, 259-277, doi:10.1006/exnr.1998.6848 (1998).

95   Martin, I., Kim, J. W., Dawson, V. L. & Dawson, T. M. LRRK2 pathobiology in Parkinson's disease. *Journal of Neurochemistry* **131**, 554-565, doi:10.1111/jnc.12949 (2014).

96   Alberico, S. L., Cassell, M. D. & Narayanan, N. S. The Vulnerable Ventral Tegmental Area iin Parkinson's Disease. *Basal Ganglia* **5**, 51-55, doi:10.1016/j.baga.2015.06.001. (2015).

97   Kramer, D. J., Risso, D., Kosillo, P., Ngai, J. & Bateup, H. S. Combinatorial expression of Grp and Neurod6 defines dopamine neuron populations with distinct projection patterns and disease vulnerability. *eNeuro* **5**, doi:10.1523/ENEURO.0152-18.2018 (2018).

98   Baxter, K. K., Uittenbogaard, M. & Chiaramello, A. The neurogenic basic helix-loop-helix transcription factor NeuroD6 enhances mitochondrial biogenesis and bioenergetics to confer tolerance of neuronal PC12-NeuroD6 cells to the mitochondrial stressor rotenone. *Experimental Cell Research* **318**, 2200-2214, doi:10.1016/j.yexcr.2012.07.004 (2012).

99   Uittenbogaard, M., Baxter, K. K. & Chiaramello, A. The neurogenic basic helix-loop-helix transcription factor NeuroD6 confers tolerance to oxidative stress by triggering an antioxidant response and sustaining the mitochondrial biomass. *ASN neuro* **2**, e00034, doi:10.1042/AN20100005 (2010).

100   Lammel, S. *et al.* Unique Properties of Mesoprefrontal Neurons within a Dual Mesocorticolimbic Dopamine System. *Neuron* **57**, 760-773, doi:10.1016/j.neuron.2008.01.022 (2008).

101   Khaliq, Z. M. & Bean, B. P. Pacemaking in dopaminergic ventral tegmental area neurons: Depolarizing drive from background and voltage-dependent sodium conductances. *Journal of Neuroscience* **30**, 7401-7413, doi:10.1523/JNEUROSCI.0143-10.2010 (2010).

102   Grace, A. A. & Bunney, B. S. Nigral dopamine neurons: intracellular recording and identification with L-dopa injection and histofluorescence. *Science* **210**, 654-656, doi:10.1126/science.7433992 (1980).

103   Grace, A. A. & Bunney, B. S. The control of firing pattern in nigral dopamine neurons: Burst firing. *Journal of Neuroscience* **4**, 2877-2890, doi:10.1523/jneurosci.04-11-02877.1984 (1984).

104   Grace, A. A. & Bunney, B. S. The control of firing pattern in nigral dopamine neurons: single spike firing. *Journal of Neuroscience* **4**, 2866-2876, doi:10.1039/CT9140501039 (1984).

105   Neuhoff, H., Neu, A., Liss, B. & Roeper, J. I(h) channels contribute to the different functional properties of identified dopaminergic subpopulations in the midbrain. *The Journal of neuroscience : the official journal of the Society for Neuroscience* **22**, 1290-1302, doi:22/4/1290 [pii] (2002).

106   Shepard, P. D. & German, D. C. A subpopulation of mesocortical dopamine neurons possesses autoreceptors. *European Journal of Pharmacology* **98**, 455-456 (1984).

107   Chiodo, L. A., Bannon, M. J., Grace, A. A., Roth, R. H. & Bunney, B. S. Evidence for the absence of impulse-regulating somatodendritic and synthesis-modulating nerve terminal autoreceptors on subpopulations of mesocortical dopamine neurons. *Neuroscience* **12**, 1-16, doi:10.1016/0306-4522(84)90133-7 (1984).

108   Gariano, R. F., Tepper, J. M., Sawyer, S. F., Young, S. J. & Groves, P. M. Mesocortical dopaminergic neurons. 1. Electrophysiological properties and evidence for soma-dendritic autoreceptors. *Brain Research Bulletin* **22**, 511-516, doi:10.1016/0361-9230(89)90103-2 (1989).

109   Johnson, S. W. & North, R. A. Two types of neurone in the rat ventral tegmental area and their synaptic inputs. *The Journal of Physiology* **450**, 455-468, doi:10.1113/jphysiol.1992.sp019136 (1992).

110   Margolis, E. B., Mitchell, J. M., Ishikawa, J., Hjelmstad, G. O. & Fields, H. L. Midbrain Dopamine Neurons: Projection Target Determines Action Potential Duration and Dopamine D2 Receptor Inhibition. *Journal of Neuroscience* **28**, 8908-8913, doi:10.1523/JNEUROSCI.1526-08.2008 (2008).

111   Ford, C. P., Mark, G. P. & Williams, J. T. Properties and opioid inhibition of mesolimbic dopamine neurons vary according to target location. *Journal of Neuroscience* **26**, 2788-2797, doi:10.1523/JNEUROSCI.4331-05.2006 (2006).

112   Lammel, S., Ion, D. I., Roeper, J. & Malenka, R. C. Projection-Specific Modulation of Dopamine Neuron Synapses by Aversive and Rewarding Stimuli. *Neuron* **70**, 855-862, doi:10.1016/j.neuron.2011.03.025 (2011).

113   Lerner, T. N. *et al.* Intact-Brain Analyses Reveal Distinct Information Carried by SNc Dopamine Subcircuits. *Cell* **162**, 635-647, doi:10.1016/j.cell.2015.07.014 (2015).

114   Margolis, E. B. *et al.* K Opioids Selectivity Control Dopaminergic Neurons Projecting To the Prefrontal Cortex. *Proceedings of the National Academy of Sciences of the United States of America* **103**, 2938-2942, doi:10.1073/pnas.0511159103 (2006).

115   Wolfart, J., Neuhoff, H., Franz, O. & Roeper, J. Differential expression of the small-conductance, calcium-activated potassium channel SK3 is critical for pacemaker control in dopaminergic midbrain neurons. *Journal of Neuroscience* **21**, 3443-3456, doi:10.1523/jneurosci.21-10-03443.2001 (2001).

116   Farassat, N. *et al.* In vivo functional diversity of midbrain dopamine neurons within identified axonal projections. *eLife* **8**, 1-27, doi:10.7554/eLife.48408 (2019).

117   Collins, A. L. & Saunders, B. T. Heterogeneity in striatal dopamine circuits: Form and function in dynamic reward seeking. *Journal of Neuroscience Research*, 1-24, doi:10.1002/jnr.24587 (2020).

118   Beier, K. T. *et al.* Circuit Architecture of VTA Dopamine Neurons Revealed by Systematic Input-Output Mapping. *Cell* **162**, 622-634, doi:10.1016/j.cell.2015.07.015 (2015).

119   Menegas, W. *et al.* Dopamine neurons projecting to the posterior striatum form an anatomically distinct subclass. *eLife* **4**, 1-30, doi:10.7554/eLife.10032 (2015).

120   Dauer, W. & Przedborski, S. Parkinson's Disease: Mechanisms and Models. *Neuron* **39**, 889-909, doi:10.1016/S0896-6273(03)00568-3 (2003).

121   Howe, M. W. & Dombeck, D. A. Rapid signalling in distinct dopaminergic axons during locomotion and reward. *Nature* **535**, doi:10.1038/nature18942 (2016).

122   Schultz, W. Multiple Dopamine Functions at Different Time Courses. *Annual Review of Neuroscience* **30**, 259-288, doi:10.1146/annurev.neuro.28.061604.135722 (2007).

123   Wise, R. & Rompre, P. P. Brain Dopamine And Reward. *Annual Review of Psychology* **40**, 191-225, doi:10.1146/annurev.psych.40.1.191 (1989).

124   Wise, R. A. Intracranial self-stimulation: mapping against the lateral boundaries of the dopaminergic cells of the substantia nigra. *Brain Research* **213**, 190-194, doi:10.1016/0006-8993(81)91260-9 (1981).

125   Corbett, D. & Wise, R. A. Intracranial self-stimulation in relation to the ascending dopaminergic systems of the midbrain: A moveable electrode mapping study. *Brain Research* **185**, 1-15, doi:10.1016/0006-8993(80)90666-6 (1980).

126   Fibiger, H. C., LePiane, F. G., Jakubovic, A. & Phillips, A. G. The role of dopamine in intracranial self-stimulation of the ventral tegmental area. *Journal of Neuroscience* **7**, 3888-3896, doi:10.1523/jneurosci.07-12-03888.1987 (1987).

127   Schultz, W., Dayan, P. & Montague, P. R. A neural substrate of prediction and reward. *Science* **275**, 1593-1599, doi:10.1126/science.275.5306.1593 (1997).

128   Schultz, W. Behavioral dopamine signals. *Trends in Neurosciences* **30**, 203-210, doi:10.1016/j.tins.2007.03.007 (2007).

129   Hollerman, J. R. & Schultz, W. Dopamine neurons report an error in the temporal prediction of reward during learning. *Nature Neuroscience* **1**, 304-309, doi:10.1038/1124 (1998).

130   Fiorillo, C. D., Tobler, P. N. & Schultz, W. Discrete Coding of Reward Dopamine Neurons. *Science* **299**, 1898-1902, doi:10.1126/science.1077349 (2003).

131   Witten, I. B. *et al.* Recombinase-driver rat lines: Tools, techniques, and optogenetic application to dopamine-mediated reinforcement. *Neuron* **72**, 721-733, doi:10.1016/j.neuron.2011.10.028 (2011).

132   Steinberg, E. E. *et al.* A causal link between prediction errors, dopamine neurons and learning. *Nature Neuroscience* **16**, 966-973, doi:10.1038/nn.3413 (2013).

133   Thierry, A.-M., Tassin, J.-P., Blanc, G. & Glowinski, J. Selective activation of the mesocortical DA system by stress. *Nature* **263**, 242-244, doi:10.1038/263242a0 (1976).

134   Mantz, J., Thierry, A. M. & Glowinski, J. Effect of noxious tail pinch on the discharge rate of mesocortical and mesolimbic dopamine neurons: selective activation of the mesocortical system. *Brain Research* **476**, 377-381, doi:10.1016/0006-8993(89)91263-8 (1989).

135   Abercrombie, E. D., Keefe, K. A., DiFrischia, D. S. & Zigmond, M. J. Differential Effect of Stress on In Vivo Dopamine Release in Striatum, Nucleus Accumbens, and Medial Frontal Cortex. *Journal of Neurochemistry* **52**, 1655-1658, doi:10.1111/j.1471-4159.1989.tb09224.x (1989).

136   Chiodo, L. A., Antelman, S. M., Caggiula, A. R. & Lineberry, C. G. Sensory stimuli alter discharge rate of dopamine (DA) neurons: evidence for two functional types of DA cells in the substantia nigra. *Brain Research* **189**, 544-549, doi:10.1016/0006-8993(80)90366-2 (1980).

137   Salamone, J. D. The involvement of nucleus accumbens dopamine in appetitive and aversive motivation. *Behavioural Brain Research* **61**, 117-133, doi:10.1016/0166-4328(94)90153-8 (1994).

138   Bertolucci-D'Angio, M., Serrano, A. & Scatton, B. Mesocorticolimbic dopaminergic systems and emotional states. *Journal of Neuroscience Methods* **34**, 135-142, doi:10.1016/0165-0270(90)90051-G (1990).

139   Dunn, A. J. Stress-Related Activation of Cerebral Dopaminergic Systems. *Annals of the New York Academy of Sciences* **537**, 188-205, doi:10.1111/j.1749-6632.1988.tb42106.x (1988).

140   Young, A. M. J. Increased extracellular dopamine in nucleus accumbens in response to unconditioned and conditioned aversive stimuli: Studies using 1 min microdialysis in rats. *Journal of Neuroscience Methods* **138**, 57-63, doi:10.1016/j.jneumeth.2004.03.003 (2004).

141   Bromberg-Martin, E. S., Matsumoto, M. & Hikosaka, O. Dopamine in Motivational Control: Rewarding, Aversive, and Alerting. *Neuron* **68**, 815-834, doi:10.1016/j.neuron.2010.11.022 (2010).

142   Brischoux, F., Chakraborty, S., Brierley, D. I. & Ungless, M. a. Phasic excitation of dopamine neurons in ventral VTA by noxious stimuli. *Proceedings of the National Academy of Sciences of the United States of America* **106**, 4894-4899, doi:10.1073/pnas.0811507106 (2009).

143   Matsumoto, M. & Hikosaka, O. Two types of dopamine neuron distinctly convey positive and negative motivational signals. *Nature* **459**, 837-841, doi:10.1038/nature08028 (2009).

144   Stamatakis, A. M. & Stuber, G. D. Activation of lateral habenula inputs to the ventral midbrain promotes behavioral avoidance. *Nature Neuroscience* **15**, 1105-1107, doi:10.1038/nn.3145 (2012).

145   Lammel, S. *et al.* Input-specific control of reward and aversion in the ventral tegmental area. *Nature* **491**, 212-217, doi:10.1038/nature11527 (2012).

146   de Jong, J. W. *et al.* A Neural Circuit Mechanism for Encoding Aversive Stimuli in the Mesolimbic Dopamine System. *Neuron* **101**, 133-151.e137, doi:10.1016/j.neuron.2018.11.005 (2019).

147   Lammel, S., Lim, B. K. & Malenka, R. C. Reward and aversion in a heterogeneous midbrain dopamine system. *Neuropharmacology* **76**, 351-359, doi:10.1016/j.neuropharm.2013.03.019 (2014).

148   Bassareo, V., De Luca, M. A. & Di Chiara, G. Differential Expression of Motivational Stimulus Properties by Dopamine in Nucleus Accumbens Shell versus Core and Prefrontal Cortex. *Journal of Neuroscience* **22**, 4709-4719, doi:10.1523/jneurosci.22-11-04709.2002 (2002).

149   Kalivas, P. W. & Duffy, P. selective activation of dopamine transmission in the shell of the nucleus accumbens by stress. *Brain Research1*, 325-328, doi:10.1038/nn.2219 (1995).

150   Rocchetti, J. *et al.* Presynaptic D2 dopamine receptors control long-term depression expression and memory processes in the temporal hippocampus. *Biological Psychiatry* **77**, 513-525, doi:10.1016/j.biopsych.2014.03.013 (2015).

151   Kempadoo, K. A., Mosharov, E. V., Choi, S. J., Sulzer, D. & Kandel, E. R. Dopamine release from the locus coeruleus to the dorsal hippocampus promotes spatial learning and memory. *Proceedings of the National Academy of Sciences of the United States of America* **113**, 14835-14840, doi:10.1073/pnas.1616515114 (2016).

152   Edelmann, E. & Lessmann, V. Dopaminergic innervation and modulation of hippocampal networks. *Cell and Tissue Research* **373**, 711-727, doi:10.1007/s00441-018-2800-7 (2018).

153   Duszkiewicz, A. J., McNamara, C. G., Takeuchi, T. & Genzel, L. Novelty and Dopaminergic Modulation of Memory Persistence: A Tale of Two Systems. *Trends in Neurosciences* **42**, 102-114, doi:10.1016/j.tins.2018.10.002 (2019).

154   Takeuchi, T. *et al.* Locus coeruleus and dopaminergic consolidation of everyday memory. *Nature* **537**, 357-362, doi:10.1038/nature19325 (2016).

155   Lee, J. H., Lee, S. & Kim, J. H. Amygdala Circuits for Fear Memory: A Key Role for Dopamine Regulation. *Neuroscientist* **23**, 542-553, doi:10.1177/1073858416679936 (2017).

156   de Oliveira, A. R. *et al.* Conditioned fear is modulated by D2 receptor pathway connecting the ventral tegmental area and basolateral amygdala. *Neurobiology of Learning and Memory* **95**, 37-45, doi:10.1016/j.nlm.2010.10.005 (2011).

157   Wang, S., Hu, S. H., Shi, Y. & Li, B. M. The roles of the anterior cingulate cortex and its dopamine receptors in self-paced cost–benefit decision making in rats. *Learning and Behavior* **45**, 89-99, doi:10.3758/s13420-016-0243-0 (2017).

158   Aly-Mahmoud, M. *et al.* Role of anterior cingulate cortex in instrumental learning: Blockade of dopamine D1 receptors suppresses overt but not covert learning. *Frontiers in Behavioral Neuroscience* **11**, 1-14, doi:10.3389/fnbeh.2017.00082 (2017).

159   Elston, T. W., Croy, E. & Bilkey, D. K. Communication between the Anterior Cingulate Cortex and Ventral Tegmental Area during a Cost-Benefit Reversal Task. *Cell Reports* **26**, 2353-2361.e2353, doi:10.1016/j.celrep.2019.01.113 (2019).

160   Ng, L. *et al.* An anatomic gene expression atlas of the adult mouse brain. *Nature neuroscience* **12**, 356-362, doi:10.1038/nn.2281 (2009).

161   Yamaguchi, T., Qi, J., Wang, H. L., Zhang, S. & Morales, M. Glutamatergic and dopaminergic neurons in the mouse ventral tegmental area. *European Journal of Neuroscience* **41**, 760-772, doi:10.1111/ejn.12818 (2015).

162   Lammel, S. *et al.* Diversity of transgenic mouse models for selective targeting of midbrain dopamine neurons. *Neuron* **85**, 429-438, doi:10.1016/j.neuron.2014.12.036 (2015).

163   Pristerà, A. *et al.* Transcription factors FOXA1 and FOXA2 maintain dopaminergic neuronal properties and control feeding behavior in adult mice. *Proceedings of the National Academy of Sciences of the United States of America* **112**, E4929-E4938, doi:10.1073/pnas.1503911112 (2015).

164   Metzakopian, E. *et al.* Genome-wide characterization of Foxa2 targets reveals upregulation of floor plate genes and repression of ventrolateral genes in midbrain dopaminergic progenitors. *Development (Cambridge)* **139**, 2625-2634, doi:10.1242/dev.081034 (2012).

165   Yan, C. H., Levesque, M., Claxton, S., Johnson, R. L. & Ang, S. L. Lmx1a and Lmx1b function cooperatively to regulate proliferation, specification, and differentiation of midbrain dopaminergic progenitors. *Journal of Neuroscience* **31**, 12413-12425, doi:10.1523/JNEUROSCI.1077-11.2011 (2011).

166   Wever, I., Largo-Barrientos, P., Hoekstra, E. J. & Smidt, M. P. Lmx1b influences correct post-mitotic coding of mesodiencephalic dopaminergic neurons. *Frontiers in Molecular Neuroscience* **12**, 1-16, doi:10.3389/fnmol.2019.00062 (2019).

167   Andersson, E. K. I., Irvin, D. K., Ahlsiö, J. & Parmar, M. Ngn2 and Nurr1 act in synergy to induce midbrain dopaminergic neurons from expanded neural stem and progenitor cells. *Experimental Cell Research* **313**, 1172-1180, doi:10.1016/j.yexcr.2006.12.014 (2007).

168   Arenas, E., Denham, M. & Villaescusa, J. C. How to make a midbrain dopaminergic neuron. *Development (Cambridge, England)* **142**, 1918-1936, doi:10.1242/dev.097394 (2015).

169   Kee, N. *et al.* Single-Cell Analysis Reveals a Close Relationship between Differentiating Dopamine and Subthalamic Nucleus Neuronal Lineages. *Cell Stem Cell* **20**, 29-40, doi:10.1016/j.stem.2016.10.003 (2017).

170   Nouri, N. & Awatramani, R. A novel floor plate boundary defined by adjacent En1 and Dbx1 microdomains distinguishes midbrain dopamine and hypothalamic neurons. *Development (Cambridge)* **144**, 916-927, doi:10.1242/dev.144949 (2017).

171   Grimm, J., Mueller, A., Hefti, F. & Rosenthal, A. Molecular basis for catecholaminergic neuron diversity. *Proceedings of the National Academy of Sciences of the United States of America* **101**, 13891-13896, doi:10.1073/pnas.0405340101 (2004).

172   Joksimovic, M. *et al.* Spatiotemporally separable Shh domains in the midbrain define distinct dopaminergic progenitor pools. *Proceedings of the National Academy of Sciences of the United States of America* **106**, 19185-19190, doi:10.1073/pnas.0904285106 (2009).

173   Bodea, G. O. & Blaess, S. Establishing diversity in the dopaminergic system. *FEBS Letters* **589**, 3773-3785, doi:10.1016/j.febslet.2015.09.016 (2015).

174   Chung, C. Y. *et al.* Cell type-specific gene expression of midbrain dopaminergic neurons reveals molecules involved in their vulnerability and protection. *Human Molecular Genetics* **14**, 1709-1725, doi:10.1093/hmg/ddi178 (2005).

175   Greene, J. G., Dingledine, R. & Greenamyre, J. T. Gene expression profiling of rat midbrain dopamine neurons: Implications for selective vulnerability in parkinsonism. *Neurobiology of Disease* **18**, 19-31, doi:10.1016/j.nbd.2004.10.003 (2005).

176   Brichta, L. *et al.* Identification of neurodegenerative factors using translatome-regulatory network analysis. *Nature neuroscience* **18**, 1325-1333, doi:10.1038/nn.4070 (2015).

177   Poulin, J. F. *et al.* Defining midbrain dopaminergic neuron diversity by single-cell gene expression profiling. *Cell Reports* **9**, 930-943, doi:10.1016/j.celrep.2014.10.008 (2014).

178   La Manno, G. *et al.* Molecular Diversity of Midbrain Development in Mouse, Human, and Stem Cells. *Cell* **167**, 566-580.e519, doi:10.1016/j.cell.2016.09.027 (2016).

179   Hook, P. W. *et al.* Single-Cell RNA-Seq of Mouse Dopaminergic Neurons Informs Candidate Gene Selection for Sporadic Parkinson Disease. *American Journal of Human Genetics* **102**, 427-446, doi:10.1016/j.ajhg.2018.02.001 (2018).

180   Tiklová, K. *et al.* Single-cell RNA sequencing reveals midbrain dopamine neuron diversity emerging during mouse brain development. *Nature communications* **10**, 581, doi:10.1038/s41467-019-08453-1 (2019).

181   Bimpisidis, Z. *et al.* The NeuroD6 subtype of VTA neurons contributes to psychostimulant sensitization and behavioral reinforcement. *eNeuro* **6**, doi:10.1523/ENEURO.0066-19.2019 (2019).

182   Poulin, J.-F. *et al.* Mapping projections of molecularly defined dopamine neuron subtypes using intersectional genetic approaches. *Nature Neuroscience* **21**, doi:10.1038/s41593-018-0203-4 (2018).

183   Stuber, G. D., Hnasko, T. S., Britt, J. P., Edwards, R. H. & Bonci, a. Dopaminergic Terminals in the Nucleus Accumbens But Not the Dorsal Striatum Corelease Glutamate. *Journal of Neuroscience* **30**, 8229-8233, doi:10.1523/JNEUROSCI.1754-10.2010 (2010).

184   Adrover, M. F., Shin, J. H. & Alvarez, V. a. Glutamate and Dopamine Transmission from Midbrain Dopamine Neurons Share Similar Release Properties But Are Differentially Affected by Cocaine. *Journal of Neuroscience* **34**, 3183-3192, doi:10.1523/JNEUROSCI.4958-13.2014 (2014).

185   Hnasko, T. S. *et al.* Vesicular Glutamate Transport Promotes Dopamine Storage and Glutamate Corelease In Vivo. *Neuron* **65**, 643-656, doi:10.1016/j.neuron.2010.02.012 (2010).

186   Tritsch, N. X., Granger, A. J. & Sabatini, B. L. Mechanisms and functions of GABA co - release. *Nature Publishing Group* **17**, 139-145, doi:10.1038/nrn.2015.21 (2016).

187   Tritsch, N. X., Oh, W. J., Gu, C. & Sabatini, B. L. Midbrain dopamine neurons sustain inhibitory transmission using plasma membrane uptake of GABA, not synthesis. *eLife* **2014**, 1-20, doi:10.7554/eLife.01936 (2014).

188   Tritsch, N. X., Ding, J. B. & Sabatini, B. L. Dopaminergic neurons inhibit striatal output through non-canonical release of GABA. *Nature* **490**, 262-266, doi:10.1038/nature11466 (2012).

189   Kim, J.-I. *et al.* Aldehyde dehydrogenase 1a1 mediates a GABA synthesis pathway in midbrain dopaminergic neurons. *Science (New York, N.Y.)* **350**, 102-106, doi:10.1126/science.aac4690 (2015).

190   Elphick, M. R., Mirabeau, O. & Larhammar, D. Evolution of neuropeptide signalling systems. *Journal of Experimental Biology* **221**, 1-15, doi:10.1242/jeb.193342 (2018).

191   Baraban, S. C. & Tallent, M. K. Interneuron Diversity series: Interneuronal neuropeptides - Endogenous regulators of neuronal excitability. *Trends in Neurosciences* **27**, 135-142, doi:10.1016/j.tins.2004.01.008 (2004).

192   Smith, S. J. *et al.* Single-cell transcriptomic evidence for dense intracortical neuropeptide networks. *eLife* **8**, 1-35, doi:10.7554/eLife.47889 (2019).

193   Herkenham, M. Mismatches between neurotransmitter and receptor localizations in brain: observations and implications. *Neuroscience* **23**, 1-38, doi:10.1016/0306-4522(87)90268-5 (1987).

194   Nusbaum, M. P., Blitz, D. M. & Marder, E. Functional consequences of neuropeptide and small-molecule co-transmission. *Nature Reviews Neuroscience* **18**, 389-403, doi:10.1038/nrn.2017.56 (2017).

195   van den Pol, A. N. Neuropeptide Transmission in Brain Circuits. *Neuron* **76**, 98-115, doi:10.1016/j.neuron.2012.09.014 (2012).

196   Viereckel, T. *et al.* Midbrain Gene Screening Identifies a New Mesoaccumbal Glutamatergic Pathway and a Marker for Dopamine Cells Neuroprotected in Parkinson's Disease. *Scientific Reports* **6**, 35203, doi:10.1038/srep35203 (2016).

197   Paxinos, G. & Franklin, K. B. J. The Mouse Brain in Stereotaxic Coordinates. (2004).

198   Blesa, J. & Przedborski, S. Parkinson's disease: animal models and dopaminergic cell vulnerability. *Frontiers in neuroanatomy* **8**, 155, doi:10.3389/fnana.2014.00155 (2014).

199   Di Salvio, M. *et al.* Otx2 controls neuron subtype identity in ventral tegmental area and antagonizes vulnerability to MPTP. *Nat Neurosci* **13**, 1481-1488, doi:10.1038/nn.2661 (2010).

200   Poulin, J.-F., Tasic, B., Hjerling-Leffler, J., Trimarchi, J. M. & Awatramani, R. Disentangling neural cell diversity using single-cell transcriptomics. *Nature Neuroscience* **19**, 1131-1141, doi:10.1038/nn.4366 (2016).

201   Vogt Weisenhorn, D. M., Giesert, F. & Wurst, W. Diversity matters - heterogeneity of dopaminergic neurons in the ventral mesencephalon and its relation to Parkinson's Disease. *Journal of Neurochemistry* **139**, 8-26, doi:10.1111/jnc.13670 (2016).

202   Chan, C. S. *et al.* 'Rejuvenation' protects neurons in mouse models of Parkinson's disease. *Nature* **447**, 1081-1086, doi:10.1038/nature05865 (2007).

203   Liu, G. *et al.* Aldehyde dehydrogenase 1 defines and protects a nigrostriatal dopaminergic neuron subpopulation. *Journal of Clinical Investigation* **124**, 3032-3046, doi:10.1172/JCI72176 (2014).

204   Khan, S. *et al.* Survival of a novel subset of midbrain dopaminergic neurons projecting to the lateral septum is dependent on NeuroD proteins. *Journal of Neuroscience*, doi:10.1523/JNEUROSCI.2414-16.2016 (2017).

205   Backman, C. M. *et al.* Characterization of a Mouse Strain Expressing CreRecombinase From the 3' Untranslated Regionof the Dopamine Transporter Locus. *Genesis* **45**, 383-390, doi:10.1002/dvg (2006).

206   Madisen, L. *et al.* A robust and high-throughput Cre reporting and characterization system for the whole mouse brain. *Nature neuroscience* **13**, 133-140, doi:10.1038/nn.2467 (2010).

207   Goebbels, S. *et al.* Genetic Targeting of Principal Neurons in Neocortex and Hippocampus of NEX-Cre Mice. *Genesis (New York, N.Y. : 2000)* **44**, 611-621, doi:10.1002/dvg (2006).

208   Kim, D. *et al.* TopHat2: accurate alignment of transcriptomes in the presence of insertions, deletions and gene fusions. *Genome Biology* **14**, R36, doi:10.1186/gb-2013-14-4-r36 (2013).

209   Bolger, A. M., Lohse, M. & Usadel, B. Trimmomatic: A flexible trimmer for Illumina sequence data. *Bioinformatics* **30**, 2114-2120, doi:10.1093/bioinformatics/btu170 (2014).

210   Liao, Y., Smyth, G. K. & Shi, W. FeatureCounts: An efficient general purpose program for assigning sequence reads to genomic features. *Bioinformatics* **30**, 923-930, doi:10.1093/bioinformatics/btt656 (2014).

211   Fletcher, R. B. *et al.* Deconstructing Olfactory Stem Cell Trajectories at Single-Cell Resolution. *Cell Stem Cell* **20**, 817-830.e818, doi:10.1016/j.stem.2017.04.003 (2016).

212   Cole, M. B. *et al.* Performance Assessment and Selection of Normalization Procedures for Single-Cell RNA-Seq. *BioRxiv*, 1-30, doi:10.1101/235382 (2017).

213   Bolstad, B. M., Irizarry, R. a., Astrand, M. & Speed, T. P. A comparison of normalization methods for high density oligonucleotide array data based on variance and bias. *Bioinformatics (Oxford, England)* **19**, 185-193, doi:10.1093/bioinformatics/19.2.185 (2003).

214   Bullard, J. H., Purdom, E., Hansen, K. D. & Dudoit, S. Evaluation of Statistical Methods for Normalization and Differential Expression in mRNA-Seq Experiments Evaluation of Statistical Methods for Normalization and Differential Expression in mRNA-Seq Experiments. *U.C. Berkeley Div. Biostat. Pap. Ser.* **11**, 94, doi:10.1186/1471-2105-11-94 (2009).

215   Risso, D., Perraudeau, F., Gribkova, S., Dudoit, S. & Vert, J.-p. A general and flexible method for signal extraction from single-cell RNA-seq data. *Nature Communications* **9**, 1-17, doi:10.1038/s41467-017-02554-5 (2018).

216   Law, C. W., Chen, Y., Shi, W. & Smyth, G. K. voom: precision weights unlock linear model analysis tools for RNA-seq read counts. *Genome Biology* **15**, R29, doi:10.1186/gb-2014-15-2-r29 (2014).

217   Bateup, H. S. *et al.* Excitatory/Inhibitory Synaptic Imbalance Leads to Hippocampal Hyperexcitability in Mouse Models of Tuberous Sclerosis. *Neuron* **78**, 510-522, doi:10.1016/j.neuron.2013.03.017 (2013).

218   Thiele, S. L., Warre, R. & Nash, J. E. Development of a Unilaterally-lesioned 6-OHDA Mouse Model of Parkinson's Disease. *Journal of Visualized Experiments*, 1-10, doi:10.3791/3234 (2012).

219   Romanov, R. a. *et al.* Molecular interrogation of hypothalamic organization reveals distinct dopamine neuronal subtypes. *Nature Neuroscience* **20**, doi:10.1038/nn.4462 (2016).

220   Roeper, J. Dissecting the diversity of midbrain dopamine neurons. *Trends in Neurosciences* **36**, 336-342, doi:10.1016/j.tins.2013.03.003 (2013).

221   Uittenbogaard, M. & Chiaramello, A. The basic helix-loop-helix transcription factor Nex-1/Math-2 promotes neuronal survival of PC12 cells by modulating the dynamic expression of anti-apoptotic and cell cycle regulators. *Journal of Neurochemistry* **92**, 585-596, doi:10.1111/j.1471-4159.2004.02886.x (2005).

222   Nutt, D. J., Lingford-Hughes, A., Erritzoe, D. & Stokes, P. R. a. The dopamine theory of addiction: 40 years of highs and lows. *Nature Reviews Neuroscience* **16**, 305-312, doi:10.1038/nrn3939 (2015).

223   Roesler, R. & Schwartsmann, G. Gastrin-releasing peptide receptors in the central nervous system: Role in brain function and as a drug target. *Frontiers in Endocrinology* **3**, 1-12, doi:10.3389/fendo.2012.00159 (2012).

224   Ekstrand, M. I. *et al.* Molecular profiling of neurons based on connectivity. *Cell* **157**, 1230-1242, doi:10.1016/j.cell.2014.03.059 (2014).

225 Ikemoto, S. Dopamine reward circuitry: Two projection systems from the ventral midbrain to the nucleus accumbens-olfactory tubercle complex. *Brain Research Reviews* **56**, 27-78, doi:10.1016/j.brainresrev.2007.05.004 (2007).

226 Yun, I. a. The Ventral Tegmental Area Is Required for the Behavioral and Nucleus Accumbens Neuronal Firing Responses to Incentive Cues. *Journal of Neuroscience* **24**, 2923-2933, doi:10.1523/JNEUROSCI.5282-03.2004 (2004).

227 Beckstead, R. M., Domesick, V. B. & Nauta, W. J. H. Efferent connections of the substantia nigra and ventral tegmental area in the rat. *Brain Research* **175**, 191-217, doi:10.1016/0006-8993(79)91001-1 (1979).

228 Swanson, L. W. The projections of the ventral tegmental area and adjacent regions: A combined fluorescent retrograde tracer and immunofluorescence study in the rat. *Brain Research Bulletin* **9**, 321-353, doi:10.1016/0361-9230(82)90145-9 (1982).

229 Henny, P. *et al.* Structural correlates of heterogeneous in vivo activity of midbrain dopaminergic neurons. *Nature Neuroscience* **15**, 613-619, doi:10.1038/nn.3048 (2012).

230 Fenno, L. E. *et al.* Targeting cells with single vectors using multiple-feature Boolean logic. *Nature methods* **11**, 763-772, doi:10.1038/nmeth.2996 (2014).

231 Luo, L., Callaway, E. M. & Svoboda, K. Genetic Dissection of Neural Circuits: A Decade of Progress. *Neuron* **98**, 256-281, doi:10.1016/j.neuron.2018.03.040 (2018).

232 Sawamoto, K. *et al.* Visualization, direct isolation, and transplantation of midbrain dopaminergic neurons. *Proceedings of the National Academy of Sciences of the United States of America* **98**, 6423-6428, doi:10.1073/pnas.111152398 (2001).

233 Savitt, J. M., Jang, S. S., Mu, W., Dawson, V. L. & Dawson, T. M. Bcl-x is required for proper development of the mouse: Substantia nigra. *Journal of Neuroscience* **25**, 6721-6728, doi:10.1523/JNEUROSCI.0760-05.2005 (2005).

234 Lindeberg, J. *et al.* Transgenic expression of Cre recombinase from the tyrosine hydroxylase locus. *Genesis* **40**, 67-73, doi:10.1002/gene.20065 (2004).

235 Roostalu, U. *et al.* Quantitative whole-brain 3D imaging of tyrosine hydroxylase-labeled neuron architecture in the mouse MPTP model of Parkinson's disease. *DMM Disease Models and Mechanisms* **12**, 1-13, doi:10.1242/dmm.042200 (2019).

236 Chi, J., Crane, A., Wu, Z. & Cohen, P. Adipo-clear: A tissue clearing method for three-dimensional imaging of adipose tissue. *Journal of Visualized Experiments* **2018**, 1-9, doi:10.3791/58271 (2018).

237 Sousa, V. H., Miyoshi, G., Hjerling-Leffler, J., Karayannis, T. & Fishell, G. Characterization of Nkx6-2-derived neocortical interneuron lineages. *Cerebral Cortex* **19**, 1-10, doi:10.1093/cercor/bhp038 (2009).

238 Madisen, L. *et al.* Transgenic mice for intersectional targeting of neural sensors and effectors with high specificity and performance. *Neuron* **85**, 942-958, doi:10.1016/j.neuron.2015.02.022 (2015).

239 Agarwal, A. *et al.* In vivo imaging and noninvasive ablation of pyramidal neurons in adult NEX-CreERT2 mice. *Cerebral Cortex* **22**, 1473-1486, doi:10.1093/cercor/bhr214 (2012).

240 Kim, J. H. *et al.* High cleavage efficiency of a 2A peptide derived from porcine teschovirus-1 in human cell lines, zebrafish and mice. *PLoS ONE* **6**, 1-8, doi:10.1371/journal.pone.0018556 (2011).

241 Raymond, C. S. & Soriano, P. High-efficiency FLP and ΦC31 site-specific recombination in mammalian cells. *PLoS ONE* **2**, 1-4, doi:10.1371/journal.pone.0000162 (2007).

242 Cong, L. *et al.* Multiplex Genome Engineering Using CRISPR/Cas Systems. *Science* **339**, 819-824, doi:10.1126/science.1231143 (2013).

243   Gertsenstein, M. *et al.* Efficient generation of germ line transmitting chimeras from C57BL/6N ES cells by aggregation with outbred host embryos. *PLoS ONE* **5**, 1-8, doi:10.1371/journal.pone.0011260 (2010).

244   Friedmann, D. *et al.* Mapping mesoscale axonal projections in the mouse brain using a 3D convolutional network. *Proceedings of the National Academy of Sciences*, 201918465, doi:10.1073/pnas.1918465117 (2020).

245   O'Neill, B., Patel, J. C. & Rice, M. E. Characterization of Optically and Electrically Evoked Dopamine Release in Striatal Slices from Digenic Knock-in Mice with DAT-Driven Expression of Channelrhodopsin. *ACS Chemical Neuroscience* **8**, 310-319, doi:10.1021/acschemneuro.6b00300 (2017).

246   Zaborszky, L. & Vadasz, C. The midbrain dopaminergic system: Anatomy and genetic variation in dopamine neuron number of inbred mouse strains. *Behavior Genetics* **31**, 47-59, doi:10.1023/A:1010257808945 (2001).

247   Ingram, D. K. & Corfman, T. P. An overview of neurobiological comparisons in mouse strains. *Neuroscience and Biobehavioral Reviews* **4**, 421-435, doi:10.1016/0149-7634(80)90032-9 (1980).

248   Anderzhanova, E. A. *et al.* Strain differences in profiles of dopaminergic neurotransmission in the prefrontal cortex of the BALB/C vs. C57Bl/6 mice: Consequences of stress and afobazole. *European Journal of Pharmacology* **708**, 95-104, doi:10.1016/j.ejphar.2013.03.015 (2013).

249   Renier, N. *et al.* IDISCO: A simple, rapid method to immunolabel large tissue samples for volume imaging. *Cell* **159**, 896-910, doi:10.1016/j.cell.2014.10.010 (2014).

250   Friedmann, D. *et al.* Mapping mesoscale axonal projections in the mouse brain using a 3D convolutional network. *Proceedings of the National Academy of Sciences*, 1-8, doi:10.1073/pnas.1918465117 (2020).

251   Bateup, H. S. *et al.* Cell type-specific regulation of DARPP-32 phosphorylation by psychostimulant and antipsychotic drugs. *Nature Neuroscience* **11**, 932-939, doi:10.1038/nn.2153 (2008).

252   Bateup, H. S. *et al.* Distinct subclasses of medium spiny neurons differentially regulate striatal motor behaviors. *Proceedings of the National Academy of Sciences of the United States of America* **107**, 14845-14850, doi:10.1073/pnas.1009874107 (2010).

253   Kravitz, A. V. *et al.* Regulation of parkinsonian motor behaviours by optogenetic control of basal ganglia circuitry. *Nature* **466**, 622-626, doi:10.1038/nature09159 (2010).

254   Yang, H. *et al.* Nucleus Accumbens Subnuclei Regulate Motivated Behavior via Direct Inhibition and Disinhibition of VTA Dopamine Subpopulations. *Neuron* **97**, 434-449.e434, doi:10.1016/j.neuron.2017.12.022 (2018).

255   Mohebi, A. *et al.* Dissociable dopamine dynamics for learning and motivation. *Nature* **570**, 65-70, doi:10.1038/s41586-019-1235-y (2019).

256   Sulzer, D., Cragg, S. J. & Rice, M. E. Striatal dopamine neurotransmission: regulation of release and uptake. *Basal Ganglia* **6**, 123-148, doi:10.1016/j.baga.2016.02.001.Striatal (2016).

257   Daigle, T. L. *et al.* A Suite of Transgenic Driver and Reporter Mouse Lines with Enhanced Brain-Cell-Type Targeting and Functionality. *Cell* **174**, 465-480.e422, doi:10.1016/j.cell.2018.06.035 (2018).

258   Heintz, N. Gene Expression Nervous System Atlas (GENSAT). *Nature Neuroscience* **7**, 483, doi:10.1038/nn0504-483 (2004).

259   Arts, M. P. M. & Cools, A. R. Bilateral 6-hydroxidopamine lesion in the dopaminergic A8 cell group produces Long-Lasting deficits in motor programming of cats. *Behavioral Neuroscience* **112**, 102-115, doi:10.1037/0735-7044.112.1.102 (1998).

260   Pereira, P. J. S. *et al.* GRPR/PI3K : Partners in Central Transmission of Itch. *Journal of Neuroscience* **35**, 16272-16281, doi:10.1523/JNEUROSCI.2310-15.2015 (2015).

261   Chaperon, F. *et al.* Gastrin-releasing peptide signaling plays a limited and subtle role in amygdala physiology and aversive memory. *PLoS ONE* **7**, doi:10.1371/journal.pone.0034963 (2012).
262   Shumyatsky, G. P. *et al.* Identification of a signaling network in lateral nucleus of amygdala important for inhibiting memory specifically related to learned fear. *Cell* **111**, 905-918, doi:10.1016/S0092-8674(02)01116-9 (2002).
263   Hermes, M. L. H. J., Kolaj, M., Coderre, E. M. & Renaud, L. P. Gastrin-releasing peptide acts via postsynaptic BB2 receptors to modulate inward rectifier K+ and TRPV1-like conductances in rat paraventricular thalamic neurons. *Journal of Physiology* **591**, 1823-1839, doi:10.1113/jphysiol.2012.249227 (2013).
264   Harmar, A. J. *et al.* The VPAC2 receptor is essential for circadian function in the mouse suprachiasmatic nuclei. *Cell* **109**, 497-508, doi:10.1016/S0092-8674(02)00736-5 (2002).
265   Miles, O. W. *et al.* Pituitary Adenylate Cyclase-Activating Peptide in the Bed Nucleus of the Stria Terminalis Mediates Stress-Induced Reinstatement of Cocaine Seeking in Rats. *Neuropsychopharmacology* **43**, 978-986, doi:10.1038/npp.2017.135 (2018).
266   Lee, S.-H. & Cox, C. L. Excitatory Actions of Vasoactive Intestinal Peptide on Mouse Thalamocortical Neurons Are Mediated by VPAC2 Receptors. *Journal of Neurophysiology* **96**, 858-871, doi:10.1152/jn.01115.2005 (2006).
267   Aresh, B. *et al.* Spinal cord interneurons expressing the gastrin-releasing peptide receptor convey itch through VGLUT2-mediated signaling. *Pain* **158**, 945-961, doi:10.1097/j.pain.0000000000000861 (2017).
268   Kupchik, Y. M. *et al.* Coding the direct/indirect pathways by D1 and D2 receptors is not valid for accumbens projections. *Nature neuroscience* **18**, doi:10.1038/nn.4068 (2015).
269   Usdin, T. B., Bonner, T. I. & Mezey, E. Two receptors for vasoactive intestinal with similar and complementary. *Endocrinology* **135**, 2662-2680, doi:10.1210/endo.135.6.7988457 (1994).
270   Sheward, W. J., Lutz, E. M. & Harmar, A. J. The distribution of vasoactive intestinal peptide2 receptor messenger RNA in the rat brain and pituitary gland as assessed by in situ hybridization. *Neuroscience* **67**, 409-418, doi:10.1016/0306-4522(95)00048-N (1995).
271   Russo, A. F. Overview of Neuropeptides: Awakening the Senses? *Headache* **57**, 37-46, doi:10.1111/head.13084 (2017).